

**MODELLING THE ORIGIN OF ASTROPHYSICAL OUTFLOWS FROM
GALACTIC AND EXTRA-GALACTIC SOURCES POWERED
BY ACCRETING COMPACT OBJECTS**

**THESIS SUBMITTED FOR THE DEGREE OF
DOCTOR OF PHILOSOPHY (SCIENCE)
OF
JADAVPUR UNIVERSITY
2000**

TAPAS KUMAR DAS

**S. N. BOSE NATIONAL CENTRE FOR BASIC SCIENCES
BLOCK JD SECTOR III SALT LAKE
CALCUTTA-700 091
WEST BENGAL
INDIA**

**Modelling the Origin of Astrophysical Outflows from Galactic
and Extra-galactic Sources Powered by Accreting Compact
Objects**

*Thesis Submitted for the Degree of
Doctor of Philosophy (Science) of Jadavpur University,
2000.*

Tapas Kumar Das
S. N. Bose National Centre for Basic Sciences
Block JD Sector III Salt Lake
Calcutta 700 091 West Bengal India

CERTIFICATE FROM THE SUPERVISOR

This is to certify that the thesis entitled "Modelling the Origin of Astrophysical Outflows from Galactic and Extra-galactic Sources Powered by Compact Objects" submitted by Sri Tapas Kumar Das who got his name registered on 24th August, 1998 for the award of Ph.D. (Science) degree of Jadavpur University, is absolutely based upon his own work under my supervision; and that neither this thesis nor any part of its has been submitted for any degree/diploma or any other academic award anywhere before.

PROFESSOR SANDIP CHAKRABARTI



Prof. Sandip K. Chakrabarti

Dated: 19.04.2000

S. N. Bose National Centre For Basic Sciences
Block JD Sector III Calcutta 700 091
India

S.N Bose National Centre for
Basic Sciences

To my parents who spontaneously sacrificed everything to raise me.....

Acknowledgements

It is a great pleasure to thank my thesis supervisor Prof. Sandip K. Chakrabarti for introducing me to the fascinating field of astrophysical jet, and to all present and former members of the astrophysics group of my Institute for time to time constructive interactions. During the three year span of my Ph. D. carrier, I have been greatly benefitted from valuable discussions with several faculty members, Post Doctoral fellows and Ph. D. students of Department of Astrophysics, University of Oxford, Institute für Astrophysic, Universität zu Bonn, Max-Planck Institut für Radioastronomie (MPIfR), Bonn, Nicolaus Copernicus Astronomical Center (CAMK), Warsaw, Inter University Centre for Astronomy and Astrophysics (IUCAA), Puna, Department of Astronomy and Astrophysics, Tata Institute of Fundamental Research (TIFR), Bombay and Theoretical Astrophysics Division, Indian Institute of Astrophysics (IIAP), Bangalore, during my visits to these Institutes to present colloquia and seminars, and with some of the participants of 19th Texas Symposium of Relativistic Astrophysics and Cosmology (held in Paris in 1998) during my participation.

Among all the persons I interacted for academic purpose since my post M.Sc. days, my sincerest gratitude goes to Prof. Utpal Sarkar of Physical Resaerch Laboratory, Ahmedabad, for generously extending his helping hand whenever I had been in trouble. All my family members are gratefully acknowledged for providing the best possible supports (sometimes even by going beyond their capacity) throughout. My wife Atashi deserves special thanks for doing the tedious and thankless job of correcting the typos in my thesis (though the responsibility for errors still existing are solely mine) and for being with me in every bits and pieces of my agony and ecstasy since the day we met.

Table of Contents

Chapter I:	
Motivation and Introduction.	1
<i>Chapter 1.1:</i>	
<i>Expulsive and Propulsive: What are They?</i>	<i>1</i>
<i>Chapter 1.2:</i>	
<i>Basic Accretion Processes.</i>	<i>7</i>
<i>Chapter 1.3:</i>	
<i>The Jet, the Disk, and the Hole:</i>	
<i>A Co-existing Trio at the Heart of Active Galaxies.</i>	<i>17</i>
<i>Chapter 1.4:</i>	
<i>Brief Overview of Existing Disk-Wind Models.</i>	<i>36</i>
Chapter II:	
The Disk-Outflow System.	58
<i>Chapter 2.1:</i>	
<i>Global Transonic Advective Accretion:</i>	
<i>The Complete Prescription for Diving onto the Hole.</i>	<i>58</i>
<i>Chapter 2.2:</i>	
<i>Lifting the Face from the Disk: The Outflow Model.</i>	<i>78</i>
Chapter III:	
Outflows From Spherical Accretion.	107
Chapter IV:	
Concluding Remarks.	134
Bibliography.	143

Expulsive and Propulsive: What Are They?

Chapter 1.1

SUMMARY

Though widely observed to be emanating out from a variety of galactic and extra-galactic sources, the underlying physical mechanism behind the formation of the cosmic jets and outflows are wrapped around by the veil of mystery till date. They (jets) are physical conduits along which mass, momentum, energy and magnetic flux are channelled from the stellar, galactic and extra-galactic objects to the outer medium. Geometrically these jets are narrow (small opening angle) conical or cylindrical/semi-cylindrical protrusions covering an astonishing range in size. While the jets associated with young stars are typically 10^{17} cm in length, jets from some giant extra-galactic sources have an overall extent in excess of 10^{24} cm (De-Young, 1991). Thus the jet phenomenon is seen on scales that cover more than seven orders of magnitude and some of the extra-galactic radio jets are considered to be the largest single coherent structures found in the universe. Though it is now a well-known fact that a variety of celestial objects, spanning from stars (having all masses) during their formation (Young Stellar Objects) to Active Galactic Nuclei (and possibly sources of γ ray bursts also (Mészáros & Rees, 1997)) suffer mass loss through jets, the detailed nature of the formation of the extragalactic jets is not quite clear due to the lack of proper understanding of the underlying physical mechanism responsible for jet production. Neither the amount of matter contained in these jets could accurately be calculated by any definitive method. We illustrate what motivates us to formulate a simultaneous inflow-outflow solution for explaining the hydrodynamic origin of astrophysical outflows from sources powered by accreting compact objects and to compute the mass outflow rate only in terms of accretion parameters.

One of the most prominent signatures of activities around the Active Galactic Nuclei

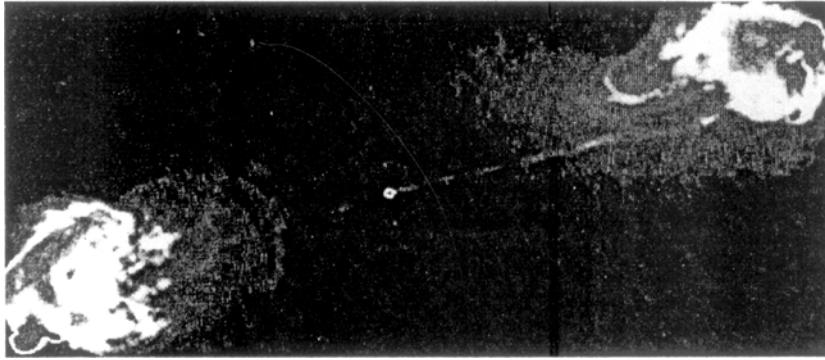


Fig. 1.1.1:

VLA radio image of Cygnus A after repeated correction from atmospheric effects and calibration errors (Observation by R. H. Perley and J. W. Dreher). The bright spot in the center is the core of the galaxy. Two bright patches on either side of the core (one at the top right and the other at the lower left corner of the image) represent the radio emitting lobes while the thin band connecting the central spot with the top right patch is the jet shooting out from the core (Reproduced with kind permission from R. H. Perley and J. W. Dreher).

(AGN) ^{*} is the presence of mass outflows and jets. AGNs produce cosmic jets through which immense amount of matter and energy are ejected out of the cores of the galaxies (Begelman, Blandford & Rees, 1984, BBR84 from now onwards). The structure of these jets can reach sizes of several million light years and extent way beyond their host galaxies into the vastness of intergalactic space. Similarly, micro quasars [†] have also been very recently discovered where the mass outflows are formed from stellar mass black hole candidates (Mirabel & Rodriguez, 1998).

Looking back at the era of infancy of radio observations of the extragalactic sources, one sees that in 1953, Jenison and Dasgupta (1953) discovered that the radio emission from Cygnus A was originating from two amorphous blobs straddling symmetrically the associated optical galaxy rather than the galaxy itself (Figure 1.1.1.). Subsequent observations of other powerful radio emitting sources revealed the fact that this is rather a general phe-

^{*} 'Active' galaxies are distinguished from ordinary galaxies in that they show indications of having energy output not related to ordinary stellar processes (standard thermonuclear evolution of energy). Their 'activity' is centered in a small nuclear region ($R \ll 1$ pc $\sim 3.1 \times 10^{18}$ cm) and are associated with strong emission lines. Their power outputs are dramatically enormous ($\sim 10^{46}$ ergs s^{-1}) and equal the mass - energy equivalent to several solar masses per year (BBR84). The nucleus of such galaxies are named "Active Galactic Nuclei"(AGN).

[†] Microquasars are stellar-mass black holes in our galaxy which mimic, in a smaller scale, of the phenomena seen in quasars. Unlike the AGN and Quasar jets (where the extent of the jets may reach several million of light years), the double sided jets coming out of these objects can have sizes upto a few light years only (Mirabel & Rodriguez, 1998 and references therein).

nomenon. Initially it was thought that these radio emitting blobs had been directly shot out of the core of the galaxy, however, this idea created some dynamical problems (adiabatic loss problem, as for example, see BBR84 for detail) which prompted theoreticians to propose a “black box model” to explain the phenomenon. In early theoretical contributions, what people put forward was basically a black box sitting at the dynamical center of the galaxy which is doing something interesting so that these radio emitting lobes are continuously fuelled by the process of channelling matter and energy emanating from the galactic center. There is no need to go into the history of subsequent discussion (and there is no scope to do so either due to the limitation of space, interested readers may have a look at BBR84, Bridle & Perley, 1984, Huges, 1991, Blandford, 1993, Burgarella et al, 1993, Ferrari, 1998), suffice it to say that from the present status of observational evidences, we are in a strong position to say that these channels of matter and energy, or “jets”, (as it was first named by Baade and Minkowski in 1954 (Baade & Minkowski, 1954)) are the ubiquitous feature of the AGNs †, Young Stellar Objects (YSOs) and of some small scale prototype of AGNs, SS433 for example, which is believed to harbour a neutron star at its center. (For a detail discussion of SS433 jet, see Margon, 1984. and Vermulen, 1993). Although since the first theoretical contribution to this black box model approach (Rees, 1971), much work has been done on how such jets interact with their surrounding and on how such interactions may convey the informations about the morphology of different extragalactic radio sources, the fundamental problem of what *exactly* is happening inside the black box still remains unresolved.

From the observational point of view, probably the most attractive feature of these astrophysical jets is that they are the most prominent and visible signatures of the AGNs. Hence, studying the jets has been one of the most exhaustive part of the research carried out by the observational astrophysicists over many years, and a huge “zoo” of different jet species has emerged.

On the other hand, from the theoretical front, the non-stellar activities around the AGNs

† Surely one of the most debatable issues in the realm of astrophysical jets is the ubiquity of AGN jets. How common are they? For reasons which are not clearly understood, fewer than 10% of all QSOs are apparently observed to produce strong radio jets yet the multicomponent spectral characteristics (in optical, UV and X-ray band) of radio loud and radio quiet QSOs are remarkably similar which prompted the majority of workers in this field to speculate the universality of AGN jet production. Line of argument for this belief is as follows: as the radio emission is observed on smaller scales, we are able to detect only the powerfull radio sources. Thus it is possible that incipient jets form in most (if not all) AGNs, but are quenched before reaching the scale on which they could be observed (Begelman, 1993).

are thought to be produced by a powerful engine sitting at the dynamical center of the galaxy (BBR84, Rees, 1984, Rees, 1997, Kormendy & Richstone, 1995 (KR95 from now onwards), Ho, 1998, Ford et al, 1998, Celotti, et al. 1999: also see Chapter 1.3 for detail discussion). Because of the fact that the high luminosity produced by the AGNs are concentrated in a very small volume, it has been strongly argued that these engines are basically powered by the accretion onto massive black holes. This “black hole hypothesis”, namely that essentially all AGNs contain $\sim 10^6 - 10^9 M_{\odot}$ black holes (Rees, 1984) and that these objects together with their orbiting accretion disks are the prime movers for most of the powerful activities of AGNs including the formation of bipolar outflows and relativistic jets (see Chapter 1.3 for detail) are further supported by the recent observational evidences, where the signature of the so called “jet disk symbiosis” is supposed to be detected (see Chapter 1.3 for detail, also see Madejski, 1998. and KR95). That means, for most (if not all) AGNs and microquasars, the jets and the accretion disks around the central compact objects are symbiotically related (see Chapter 1.3 for detail). Probably this has to be the case in reality because in the absence of any binary companion, jet is supposed to be the only outlet for the intrinsic angular momentum of the interstellar/ intergalactic matter accreting onto an isolated compact object. So the accretion powered outflows are not merely an incidental by-product of the mass flow through the disk but, in fact, are a necessary ingredient in the accretion process, in that they constitute the main mechanism for removing excess angular momentum of the inflowing matter. Hence, it is quite logical to conclude that the jet formation and accretion onto isolated black holes are not two different issues to be studied disjointedly, rather they must be strongly correlated and it is *necessary* to study the accretion and jet within the same framework. On the other hand, the major difference between the ordinary stellar outflows and the outflows/jets from the vicinity of a black hole or a neutron star, is that they do not have their own atmospheres and outflows/jets in this case *have to be generated from the inflowing materials only*.

Keeping these basic facts in the back of our mind, our aim was to theoretically study the mass outflow from galactic/ extragalactic sources more realistically than what has been attempted so far. The existing models which study the origin, acceleration and collimation of mass outflow in the form of jets from AGNs and Quasars are roughly of three types (see Chapter 1.4 for detail). From the analytical front, though the wind type and accretion type solutions come out from the same set of governing equations (Königl, 1989,

Chakrabarti & Bhaskaran, 1992), till today there was no attempt to obtain the estimation of outflow rate from the inflow rate. We proposed a theoretical model, which, for the first time we believe, can compute (semi analytically and semi numerically) the absolute value of mass outflow rate (fraction of inflowing material which is being ‘kicked out’ as outflows) from the matter accreting onto galactic and extra-galactic black holes using combinations of exact transonic accretion and wind topologies which form a self-consistent inflow-outflow system. The simplicity of black holes and neutron stars lie in the fact that they do not have atmospheres. But the inflowing matter surrounding them have, and similar method as employed in stellar atmospheres should be applicable to the accreting matter surrounding them. The approach in our model is precisely this. We first determine the properties of the inflow and outflow and identify solutions to connect them. In this manner we self-consistently determine what fraction of the matter accreting onto these compact objects is coming out as outflows/jets.

If \dot{M}_{in} is the time rate of accretion onto a compact object (the amount of matter *falling in* per unit time) and \dot{M}_{out} be the time rate of outflow (the amount of matter being ‘kicked out’ per unit time as *wind*), the ratio $\left(\frac{\dot{M}_{out}}{\dot{M}_{in}}\right)$ we call the ‘Mass Outflow Rate’ and denote it by R_m . Thus R_m is a measure of the ratio of the outflow rate to the inflow rate of matter. The major aim of our work is to compute the absolute value of R_m in terms of the inflow parameters and to study the dependence of R_m on those parameters. For matter accreting with considerable intrinsic angular momentum (formation of accretion disks), we establish that the bulk of the outflow is from the CENtrifugal pressure dominated BOundary Layer. We find (Das, 1998 (D98 from now onwards), Das & Chakrabarti, 1999 (DC99 from now onwards)) that R_m varies anywhere from a few percent to even close to a hundred percent depending on the initial parameters of the inflow, the degree of compression of matter near the CENBOL and the polytropic index of the flow (see Chapter 2.2). Our model thus, not only provides a sufficiently plausible estimation of R_m , but is also able to study the variation of this rate as a function of various parameters governing the flow.

We have also studied the mass outflow from spherical accretion with zero intrinsic angular momentum (Das, 1999a, 1999b, 1999c, 2000). It has been shown that a self-supported relativistic hadronic interaction mediated spherical standing shock may be produced even for accretion with zero angular momentum. We have taken this shock surface as the generating surface of mass outflow for spherical inflow and have compared the re-

sults with that of obtained for outflows from disk-outflow system (see Chapter 3.).

Before presenting the technical details of any particular work, it is always better to describe the individual building blocks of the model as well as to explain various concepts and facts related to that work: a brief review of others contributions in the same field is also necessary as we believe. We do these in next subchapters. In Chapter 1.2, fundamentals of the accretion phenomena (spherical as well as disk accretion) are provided, Chapter 1.3 illustrates the well accepted belief that the generators of AGN powerhouses are accreting super-massive black holes (the so called 'black hole hypothesis') which may be responsible for production of large scale jets and outflows which emphasises the fact that it is unavoidable to extract outflows from accreting materials *only*. Finally, in Chapter 1.4, we provide a brief outline of other jet models and argue that contributions due to others, though excellent in explaining a number of fundamental aspects of formation, dynamics and collimation of astrophysical jets from sources powered by accreting compact objects, is insufficient to self-consistently connect the accretion and wind solutions and to compute the barionic matter content in jets *only* in terms of inflow parameters which has been successfully achieved in our work.

Basic Accretion Processes

Chapter 1.2

SUMMARY

Fundamentals of accretion process on massive compact objects are briefly discussed. Indicating the necessity for switching over to disk accretion from spherical accretion, elementary properties of standard thin disk and thick disks are highlighted.

1 BASICS OF THE BASIC:

The process by which any gravitating astrophysical object captures interstellar/ intergalactic matter is called accretion. The rate at which matter dives onto the gravitating object is known as accretion rate and usually is measured in units of gms^{-1} . Throughout this work, accretion rate will be denoted by \dot{M} and will be measured in geometric unit. However, other units may also be used while referring other literatures. In those cases, necessary conversion factors will be provided in appropriate places. For non-steady accretion, \dot{M} will be a function of the radial distance from the central gravitating objects (in the unit of Schwarzschild radius $\frac{2GM}{c^2}$) e.g., $\dot{M} = \dot{M}(r_g)$ where r_g denotes the Schwarzschild radius. However, for steady accretion (on which this work will be focussed), the rate would be fixed for all radii.

Accretion is served as a source of energy in a variety of astrophysical objects starting from different type of binary systems to the enormous energy output of AGNs which is believed to harbour accreting supermassive black holes (SMBHs) at its centre. The most fundamental difference between accretion onto black holes and onto other stellar bodies (including neutron stars) is that while for stars, accretion ends by a collision either directly with the hard surface of the stars or with the outer boundary of a magnetosphere (for strongly magnetized stars) resulting the release of heat energy in the form of ra-

diation (due to the transformation of gravitational energy of accreting matter) *from the surface*, for the black hole accretion, as matter passes through event horizon from where no radiation can escape classically, unlike the previous case *all* luminosity is formed *on the way* to it. The efficiency of accretion is not known from the beginning, contrary to the accretion onto stars, and depends strongly on many factors like energy, angular momentum of the accreting matter, or magnetic field embedded onto it and on various boundary conditions.

As it is absolutely impossible to provide a detail discussion of a topic as vast and diverse as accretion onto various astrophysical objects here in such a small span, this section will mention only a few topic and will concentrate on fewer still related only to accretion onto black hole. For details of various aspects of accretion processes onto compact objects, recent reviews like Chakrabarti, 1996a, Wiita, 1998, Lin & Papaloizou, 1996, Blandford, 1999, Rees, 1997, Bisnovayati-Kogan, 1998, Abramowicz et al, 1998, will be of great help. Accretion processes onto black holes may be broadly classified into two different categories. When accreting material does not have any intrinsic angular momentum, flow is spherically symmetric and any parameters governing the accretion will be a function of radial distance only. On the other hand, for matter accreting with considerable intrinsic angular momentum, * flow geometry is not that much trivial. Usually the specific angular momentum (which will be denoted by λ throughout this work) of interstellar/intergalactic medium is of the order of $10^{30} \text{cm}^2 \text{s}^{-1}$ which is far larger than the maximal spin angular momentum of the accreting black hole ($\sim 5 \times 10^{23} M_8 \text{cm}^2 \text{s}^{-1}$ (Blandford, 1993)) which generates a centrifugal force that will become significant before infalling matter plunges through the event horizon and accreting fluid will be thrown into circular orbits around the hole, moving inward only when viscous stress in the fluid have transported away the excess amount of angular momentum. This outward viscous transport of angular momentum of the accreting matter leads to the formation of accretion disk around the hole. The structure and radiation spectrum of these disks depends on various physical parameters governing the flow and on some specific boundary conditions which will be discussed in more detail in subsequent sections.

* It happens when matter falling onto the black holes comes from the neighbouring stellar companion in the binary, or when the matter appears as a result of a tidal disruption of stars whose trajectory approaches sufficiently close to the hole so that self-gravity could be overcome. The first situation is observed in many galactic X-ray sources containing a stellar mass black hole and the second one happens in Quasars and AGNs if the central supermassive hole there is surrounded by a dense stellar cluster.

2 SOME PARAMETERS OF OUR INTEREST:

There are several fiducial parameters associated with the scale of accretion (Blandford, 1993, Chakrabarti, 1998). Some of those of related interest are presented in order:

(i) *Length Scale*: Physical quantities around black holes are expected to have variations in not too smaller than a length scale called Schwarzschild radius denoted by r_g ($r_g = \frac{2GM}{C^2}$; G = Universal Gravitational Constant, M = mass of the black hole). Similarly, if there are perturbations on accretion disks, the size of the perturbations are also of similar length. A rough estimation gives:

$$r_g \sim 3 \times 10^5 \frac{M_{BH}}{M_\odot}$$

(ii) *Time Scale*: The shortest possible time scale of variation of quantities close to the black hole horizon is regarded as the associated time scale and denoted by t_g :

$$t_g = \frac{r_g}{c} \sim 3 \times 10^{-5} \frac{M_{BH}}{M_\odot} \text{Sec.}$$

(iii) *Specific Angular Momentum*: The angular momentum per unit mass of the accreting matter is defined as specific angular momentum and will be denoted by λ throughout this thesis. The unit of λ would be $\frac{2GM}{c}$ in the system of unit used in this work hence λ would be equal to cr_g .

(iv) *Eddington Luminosity and Eddington Rate*: There is a critical luminosity called Eddington luminosity (and denoted by L_{Edd}) which exerts a radiation pressure on an electron-proton pair that just balances the attractive force of gravity:

$$L_{Edd} = \frac{4\pi M m_p}{\sigma_T} \sim 10^{46} M_8 \text{ergs}^{-1}.$$

Associated with this is an Eddington accretion rate, would be able to sustain an Eddington luminosity with unit efficiency η for conversion of mass into radiant energy:

$$\dot{M}_{Edd} = L_{Edd} \sim 10^{25} M_8 \text{gs}^{-1} \sim 0.2 M_8 M_\odot \text{yr}^{-1}$$

$$\dot{M}_{Edd} = 1.44 \times 10^{17} \frac{M_{BH}}{M_\odot} \text{gms}^{-1}$$

It is to be noted that \dot{M}_{Edd} is an upper limit of accretion rate and is strictly valid for spher-

ical accretion in Newtonian space-time when the Thompson scattering is dominant.

A mass-dependent Eddington time (the e-folding time for the mass of a black hole accretion at the Eddington rate) may be defined as:

$$t_{Edd} = \frac{M}{\dot{M}_{Edd}} \sim 4 \times 10^8 yr$$

along with an associated Eddington particle density (characteristic of the particle density near the horizon when the hole accretes at the Eddington rate)

$$\rho_{Edd} = \frac{\dot{M}}{4\pi m^2 m_p} \sim 10^{-13} M_8^{-1} cm^{-3}$$

For completeness, Eddington temperature T_{Edd} and Eddington magnetic field strength B_{Edd} may be defined as

$$T_{Edd} = \left(\frac{L_{Edd}}{4\pi m^2 \sigma_{SB}} \right)^{\frac{1}{4}} = 5 \times 10^5 M_8^{-\frac{1}{4}} K$$

$$B_{Edd} = \left(\frac{L_E}{m^2} \right)^{\frac{1}{2}} = 4 \times 10^4 M_8^{-\frac{1}{2}} Gauss.$$

Before we delve into the technical detail of various basic accretion processes, it is worth discussing the idea of “transonicity” in the context of accretion flows in brief. (For an thorough discussion on transonic accretion flows, see Chakrabarti, 1990): Let the instantaneous dynamical velocity and local acoustic velocity of a compressible fluid moving along a space curve parametrized by r be $u(r)$ and $a(r)$ respectively. Local Mach number $M(r)$ of the fluid would be then $\frac{u(r)}{a(r)}$. The flow will be locally subsonic or supersonic according to $M(r) < 1$ or > 1 , i.e., according to $u(r) < a(r)$ or $u(r) > a(r)$. The flow is transonic if at any moment it crosses $M = 1$. This happens when subsonic to supersonic or supersonic to subsonic transition takes place either continuously or discontinuously. The points where such crossing continuously takes place are called *sonic points* and where such crossing takes place discontinuously are called *shocks* or discontinuities. Such discontinuities or shocks will be discussed in greater details later in §3 of Chapter 2.1 and §1 - 3 of Chapter 3.

3 SPHERICAL ACCRETION:

Hoyel and Lyttleton (1939) were the first to initiate the study of accretion process of interstellar gas on a moving Newtonian star. They considered the dynamical effects only without taking account the pressure effects. Subsequently, pressure was included and analysis

of Newtonian spherical accretion for simple polytropic gas was presented in the seminal paper by Bondi (1952). Michel (1972) extended the analysis to the relativistic cases so that the solution could be applied to the compact objects also (namely to the black holes) Shapiro (1973, 1973a) and recently Malec (1996, 1999) have investigated spherical accretion in fully general relativistic framework. Due to the fact that black holes lack its own hard surface, the outgoing radiation is produced by the accreting gas *in flight* and the radiation spectrum is determined by various radiative processes. Svartzman (1971a, 1971b) and Shapiro (1973a, 1973b) considered the effects of the radiation cooling in the optically thin, nearly adiabatic flow onto the black hole. Meszaros (1975) found that under the equipartition assumption, the plausible dissipation mechanism, e.g., turbulent motions and magnetic field reconnections etc. could increase the efficiency by a few order of magnitude over the nearly adiabatic case but the detail accounting of different dissipative mechanism could not be done.

Accretions considered in above cases were optically thin and the effects of radiation on the dynamics were minimal. In general the optically thick accretions have much lower gas temperature compared to the optically thin flow and the radiation spectrum essentially peaks in the UV region as for a massive star (Blondin, 1986, Flammang, 1982, 1984). Soffel (1982) studied spherical accretion for both sub and super Eddington luminosities for stellar mass holes ignoring compton heating.

The effects of the outgoing radiation on the infalling matter was first considered by Mestel (1954) for accretion onto normal stars. Shvartzman (1971a, 1971b) considered the same problem for neutron stars. Buff and Mc.Cray (1974) constructed models which are in thermal equilibrium and found that X-ray Compton heating can break the steady inflow. Ostriker et. al (1976) were the first to realize the importance of pre-heating. Cowie et al. (1978) extended the analysis by introducing a time dependent hydrodynamic model. Later on, Chang and Ostriker studied high-efficiency, high-luminosity flows and formulated stationary solutions with standing shock. Shocks generated in spherical accretion will be discussed in detail in Chapter 3.

4 BREAKING THE SPHERICAL SYMMETRY; DISK ACCRETION:

For spherically accretion discussed above, the infall velocity (radial) is very high hence emission from such a rapidly falling matter was not found to be strong enough to ex-

plain the high luminosity of Quasars and AGNs. Introducing the idea of magnetic dissipation, efforts were made to improve luminosity (Shvartsman, 1971a, 1971b, Shapiro, 1973a, 1973b). Indeed, efforts to improve luminosities of a spherical flows are on even in recent days (see Chapter 3). Meanwhile, possible disk-like structures around one of the binary components were found (Kraft, 1963) and some tentative suggestions that matter should accrete in the form of disks were put forward (Burbidge & Pendergest, 1968, Lynden-Bell, 1969).

Theoretically, accretion disks around black holes were first envisaged to occur within a binary stellar system where one of the components is compact object (i.e., white dwarfs, neutron stars or a black hole) and the secondary would feed matter onto the primary either through an wind or through Roche lobe overflow. In either case, the accreted matter would clearly possess substantial intrinsic angular momentum with respect to the compact object (a black hole, for our discussion). A flow with that much angular momentum will have much smaller infall velocity and much higher density compared to the spherical accretion. The infall time being higher, viscosity within the fluid, presumably produced by turbulence or magnetic field, would have time to dissipate angular momentum (except in regions very close to the black holes, cases which will be discussed in detail in §1 of Chapter 2.2) and energy. As matter loses angular momentum, it sinks deeper into the gravitational potential well and radiate more efficiently. The flow encircles the compact accretor and forms a quasi-stationary disk like structure around the compact object and preferably in the orbital plane of it. Clear evidences for such accretion disks around white dwarfs in binaries was provided by analysis of Cataclysmic variable (Robinson, 1976).

Accretion forming a Keplerian disk around a Schwarzschild black hole produces efficiencies of $\eta \sim 0.057$ and accretion onto a maximally rotating Kerr black hole is even more efficient, yielding $\eta \sim 0.42$. However, the actual efficiencies depends on quantities such as viscosity parameters and the cooling process inside the disk (see Wiita, 1998 and references therein). This energy is released in the entire electromagnetic spectrum and the success of a disc model depends on its ability to describe the way this energy is distributed in various frequency band.

In case of binary systems, where one of the components is a compact object like white dwarfs, neutron star or a black hole, the companion is stripped off its matter due to the tidal effects. The stripped off matter, with angular momentum equal to that of the companion, gradually falls towards the central compact object (a black hole, for our case) as

the angular momentum is removed by viscosity. As the flow possesses a considerable angular momentum to begin with, it is reasonable to assume that the disk will form and the viscosity would transport angular momentum from inner part of the disk radially to the outer part which allows matter to further fall onto the compact body. This situation could be described properly by standard thin accretion disk Keplerian in nature. On the other hand, in the case of active galaxies and quasars, the situation could be somewhat different. The supermassive ($M_{BH} \gtrsim 10^6 M_\odot$) central black hole is immersed in a dense cloud of intergalactic matter. In absence of any binary companion, matter is supplied to the central black hole very intermittently, and the angular momentum of the accreting matter at the outer edge of the disk may be sub-Keplerian. This low angular momentum flow departs the disk from Keplerian in nature and a ‘thick disk’ is more appropriate to describe the behaviour instead of standard thin, Keplerian Shakura Sunyaev (Shakura & Sunyaev, 1973: SS73 from now onwards) disk. Below we describe the basic features of both of the thin and thick disk respectively.

4.1 Standard Thin Disk:

In standard thin disk model (SS73, Novikov & Thorne, 1973), originally conceived to describe Roche lobe accretion in a binary system, the local height $H(r)$ of the disk is assumed to be small enough compared to the local radius of the disk r , i.e., the ‘thinness’ condition is dictated by the fact that $H(r) \ll r$ always. Accretion in this case is assumed to possess substantial value of \dot{M} but the luminosity is sub-Eddington. Pressure is neglected so that the radial force balance equations dictates the specific angular momentum distribution to become Keplerian and the radial velocity is negligible compared to the azimuthal velocity ($v_r \ll v_\phi$). Unlike the spherical accretion, temperature distribution is far below than virial and the ‘cold’ accretion in this case is highly non-adiabatic. Under the above mentioned set of assumptions, radial equations of steady state disk structure could be decoupled from the vertical ones and could be solved independantly. The complete solutions (which defines the steady state disk structure) can be obtained by solving four relativistic conservation equations namely; the conservation of rest mass, specific angular momentum, specific energy and vertical momentum balance condition. In addition, a viscosity law must be specified which should transport angular momentum outwards allowing matter to fall in. On the top of it, in standard thin disk model, the shear is approximated

as proportional to the pressure of the disk with proportionality constant α ($\alpha \rightarrow$ viscosity parameter being $\alpha < 1$ always). With this simplified assumption, the solution is obtained by expressing the vertically averaged mass density $\Sigma(r)$, flux radiated from upper disk surface $F(r)$, half local disk thickness $h(r)$ and local disk temperature $T(r)$ as an algebraic function of basic accretion parameters like r , M_{BH} , \dot{M} , a (Kerr parameter) and α . While $F(R)$ is essentially independent of shear prescription, (thus on α), $h(r)$, $\Sigma(r)$ and $T(r)$ all do depend on α . The Newtonian approximation shows that the total luminosity emerging from both surfaces of the disk is one-half of the maximum total luminosity contained in the infalling matter.

A standard thin disk described above are usually considered to be divided into three somewhat distinct regions, they are (see Wiita, 1998 and references therein):

(i) *The outer region:* At a distance of about $\left(\frac{r}{M_{BH}}\right) > 100$, the gas pressure becomes much greater compared to the radiation pressure and the opacity is mostly free-free.

(ii) *Middle region:* In between $100 < \left(\frac{r}{M_{BH}}\right) < 4$. Most of the luminosity of the disk arise from this region. Gas pressure dominates, but not with as much intensity as what was in outer region. Opacity is mostly due to electron scattering.

(iii) *Inner region:* Typically at $\left(\frac{r}{M_{BH}}\right) < 4$. This region is determined by radiation pressure and electron scattering.

High uncertainty remains in investigating the exact nature of the viscosity inside a thin accretion disk (see Wiita, 1998 and references therein). One of the major problems is to explain the origin of sufficiently large viscosity that seems to be present inside accretion disks in the binary system. Unfortunately, under nearly all astrophysically relevant circumstances, all of the well understood microscopic transverse momentum transport mechanism such as ionic, molecular and radiative viscosity are extremely small. Observations with direct relevance to the nature and strength of the macroscopic viscosity mechanism are very difficult to make; the only fairly direct observational evidence for the strength of disk viscosity comes from the dwarf novae system. For a black hole as compact accretor, such observational evidences is far from reality till date. Therefore advances in understanding the disk viscosity is largely based on the oretical analysis and numerical techniques. Usually accepted view is that the viscosity may be due to magnetic transport of angular momentum or due to small scale turbulent dissipation. Over the past several years an explanation of viscosity in terms of Velikhov-Chandrasekhar-Balbus-Hawley in-

stability (linear magnetic instability) has been investigated intensively. The net effect causes the transport with an effective $\alpha \sim 0.01$. With the increase of \dot{M} , viscous instability starts generating inside the disk. A time dependent behaviour of a thin disk resulting out of this which has been found to be of particular importance in explaining the dwarf novae outburst is called a 'limit cycle behaviour' (Meyer & Meyer-Hofmeister, 1988). Such a behaviour is found to be present even when one considers accretion disks around super-massive black holes (Lin & Shields, 1986; Cannizo, 1992). Of course, self gravity and of the disk might play an important role in active galaxies so that the simple dwarf-novae type computations need not hold in practice.

4.2 Thick Disk:

The assumptions implying accretion disks are always thin can break down in the innermost region when careful consideration of the effects of general relativity show that the flow must go supersonically through a cusp. For super-Eddington accretion rate ($\dot{M} \gg \dot{M}_{Edd}$), radiation emitted by the in-falling matter exerts a significant pressure on the gas. The radiation pressure inflates the disk, and make it geometrically thick ($H(r) \sim r$, at least for the inner $10 - 100r_g$), which is often otherwise known as accretion torus (Wiita, 1998 and references therein). This considerable amount of radiation pressure must be incorporated to find the dynamical structure of the disk and in determining the thermodynamical quantities inside the disk. Incorporation of the radiation pressure term in Euler equation dictates the angular momentum deviation from that of the Keplerian; the angular momentum distribution is super (sub) Keplerian if the pressure gradient is positive (negative). It was pointed out (Lynden-Bell, 1978) that as matter with considerable angular momentum refuses to come close to the rotation axis of the disk, a funnel wall would be produced along the spinning axis of the BH in which high radiation pressure could possibly drive matter outward in the form of collimated outflows or jets. All these were very exciting, since the origin and formation of jets were real problem, the funnel wall with its super-Eddington luminosity seems to be helpful to drive matter outward.

Introducing a pseudo-Newtonian [†] potential of the form $\Phi_{PN} = -\frac{GM}{(r-2r_g)}$ in lieu of the

[†] This potential, now widely used and known as PW potential, can mimic the space time around Schwarzschild metric very nicely. It perfectly produces the correct values of $r_{ms} = 6r_g$ and $r_{mb} = 4r_g$ and closely approximates the efficiency with $\eta(r_{ms}) = 0.0625$.

usual $\Phi_N = -\frac{GM}{r}$, Paczyński and Wiita (1980, PW80 from now onwards) provided the first thick disk model which joins with the standard thin disk at large radius without any discontinuity and pointed out several important features of these configuration. It has been shown that the structure of thick disk in inner region is nearly independent of the viscosity and efficiency of accretion drops dramatically. More sophisticated model of radiation supported thick disk including self-gravity of the disk with full general relativistic treatment was introduced later (Wiita, 1982, Chakrabarti, 1988, Lanza, 1992). The spectra emitted from thick disks are almost similar to those of the thin disks in the optical but not in other wavebands. Thick disks produces more radiation at high frequencies (EUV and Soft X-rays) if viewed essentially face-on but the spectra becomes softer and weaker if viewed at high inclination angle (see Wiita, 1998 and references therein).

Despite having a couple of interesting features such as production of supercritical luminosity, possible ability to collimate jets, magnetic activity in the funnel as the explanation of rapid variability in BL-Lacs, sometimes a better fitting spectra than that of thin disks etc, standard thick accretion disk model suffers from some limitations for which its study fell from favour in the late '80s. Firstly, the strong anisotropic nature of the emission properties of the disk has been a major disadvantage. Secondly, a non-accreting thick disk is found to be dynamically and globally unstable to non-axisymmetric perturbations. However, an ideal 'classical thick disk', if modified to incorporate high accretion rates involving both low angular momentum and radial infall velocity self-consistently, may remain viable. These goals could be achieved by self-consistently introducing the shock waves and a sub-Keplerian inner disk in an initially thin disk. Inside the shock wave, flow is likely to be hotter and to puff up and resembles the standard thick disk model. This is the subject of the 'advective accretion disk model' on which our disk-outflow system. Details of this issue will be discussed in Chapter 2.1.

The Jet, the Disk, and the Hole: A Co-existing Trio at the Heart of Active Galaxies

Chapter 1.3

SUMMARY

In this section, we provide a number of compelling arguments in favour of the accreting super-massive black holes (SMBH) to be the best choices for the prime movers of the energetic activities manifested around AGNs. We also highlight some of the observational results obtained for some specific active galaxies indicating the existence of SMBHs with dust discs and radio jets at their centres thus establishing the evidence for co-existence of jet disk and hole at the dynamical centres of AGNs.

1 ARE ACCRETING SUPER-MASSIVE BLACK HOLES THE PRIME MOVERS FOR AGNS?

Most of the phenomenologies associated with AGNs require the presence of a deep gravitational potential well in which mass-energy can be converted and radiated with high efficiency. The discovery of Quasars in the early '60s quickly spurred the idea that their dramatically enormous energy output ($\gtrsim 10^{46} \text{ erg s}^{-1}$) was essentially gravitational in origin since all known atomic and nuclear processes are just too inefficient to feed these cosmic power houses. A variety of scenarios were advented to explain their energy generation mechanism which includes relativistic stars, star clusters, spinors, magnetoids or supermassive disk (see BBR84 for a detail discussion) but the proposal (first put forward in mid'60s(Zeldovicch & Novikov, 1964, Salpeter, 1964, Lynden-Bell, 1969)) that QSOs are basically powered by accreting supermassive black holes (SMBHs) sitting at their dynamical centres became the most viable and attractive paradigm (Rees, 1984, BBR84, Blandford, 1993, Rees, 1997). Evidences have been progressively mounting since last three decades in support of this paradigm by aggregating a number of individual incidences indicating the existence of a powerful central engine relatively compact and dynamically

stable compared to other alternative sources already mentioned. It is important to note in this context that this so called 'black hole hypothesis' largely stands on the implausibility of alternative explanations rather than having any rigorously justified empirical basis (Kormendy & Richstone, 1995, KR95 from now onwards, Ho, 1998). Also to be mentioned here that not only the AGNs, rather a number of relatively anonymous galaxies that show no sign of nuclear activity (the so called 'normal' galaxies) also show evidences for harbouring accreting massive compact objects thus suggesting that SMBHs are an integral components of galactic structures at least in elliptical and bulge-dominated galaxies (Ho, 1998).

Below we briefly focus on two phenomena associated with AGNs reinforcing the belief that their 'prime movers' are associated with some relativistic potentials and that all these prime movers are essentially equivalent in all active nuclei are further supported from the fact that despite significant phenomenological differences, the fundamental properties of AGNs seem to be remarkably similar over a luminosity range of more than six orders of magnitude (Celloti et al, 1999).

- *High efficiency conversion factor:* Efficiencies of conversion of matter to radiation of the order of at least a few percentages are mandatory in order to satisfy the observational constraints on both the amount of available fuel in the host galaxy as well as on the expected residual mass for AGNs. Above mentioned efficiency greatly exceeds that of any available mass-energy conversion process takes place in nature. The tight constraint on the size of the dynamical centre, the long term stabilities of such core masses, the quite coherent structure and lack of periodicities in the observed variabilities, all argue against it being produced by clustering of individual 'fragments' or bodies rather these evidences strongly favour of the case for the observed luminosities originating from the extraction of gravitational energy from matter in the potential wells of a single, coherent, stable dark mass in the range $10^6 \sim 10^9 M_{\odot}$ (Rees, 1984, BBR84).

- *Production of outflows and jets:* Most of the (if not all) AGNs appear to be associated with expulsion of matter and energy in two oppositely directed collimated structure (astrophysical jets (Ferrari, 1998, Bridle & Perley, 1984, Blandford, 1993)). Bulk kinetic energies of these 'jets' can be of the same order as the total luminosities and the jets appear to reasonably aligned. The jet phenomena thus requires the presence of a deep potential well and a stable preferred axis over the long time scale.

For both the issues addressed above, the crucial information, which, almost invariably identifies the prime movers of central activity with accreting SMBHs, is the presence of a large, dark and stable mass concentration within a radius small enough, such that the inferred gravitational potential cannot in any case ascribe to aggregates of any sort of astrophysical objects (any sort of 'clusters', so to say). Constraints on the presence of clusters came from the requirement that the time scale for cluster evaporation and/or collapse into a single object should be larger than the age of the system. In any case, two general lines of arguments used to infer the existence of the presence of SMBHs in AGNs are (Medejski, 1998):

(i) To measure the total mass of the central gravitating object within a volume and to argue that no other form besides a SMBH can sustain with this parameter set; either via estimating the central volume by variability data and mass from the luminosity or via measuring the velocity of stars nearby to the central objects at a specified distance from galactic centre using essentially Keplers law.

(ii) To study the distortion of the emission lineshapes caused by the strong gravity resulting from the presence of SMBH at galactic centre as the prime mover.

Evidences against stellar processes mounted as some individual outbursts were found to have energies in excess of stellar rest masses and variability time scales shorter than those normally associated with supernova. It also proved hard to account for compact radio jets in the context of the star cluster model. The arguments against supermassive stars and spinors were essentially theoretical. They were argued to be either dynamically unstable or at least relatively short lived. Although they may possibly be identified with certain classes of AGNs, they were thought unlikely to account for the majority (see BBR84 and Blandford, 1993 for a detail discussion).

Observationally, the hunt for SMBHs has been frustrated by two principal limitations (Ho, 1998). Firstly, typical ground based observations are severely hampered by atmospheric seeing and only the heftiest dark masses in the closest galaxies could be detected. However, the situation has been largely improved with the advent of the Hubble Space Telescope and radio VLBI techniques. The more subtle complications involve the actual modelling of stellar kinematics data.

2 EVIDENCES INDICATING THE PRESENCE OF ACCRETING SMBHS:

2.1 Indirect Clues from Relatively Early works:

Many of the brighter flat spectrum radio sources have been shown to exhibit expansions at upto ten or more times the speed of light which is known as 'superluminal motions' (Pearson, et al, 1987, Zensus, 1997). Initially these superluminal motions attracted special attentions for appearing to violate the rules of special relativity and it was argued that quasars cannot be as remote as are believed, and that the use of redshifts and Hubble expansion law in determining their distances was not fully justified. Although the exact and detailed physical interpretation of this kind of motion remains uncertain, the line of argument to explain this phenomena follows:

superluminal expansion, as apparently possess dynamical velocity $> c$, is expected to originate from relativistic fluid motion in a source region and such a relativistic speed attained is to be expected because of the presence of a extremely deep potential well tightly packed at the centres of the corresponding galaxies; measuremental volume of which (compactness) provides enough support to infer it due to an accreting SMBH.

Another strong radio astronomical evidence emerges from the persistence of radio source axes directionally fixed in space for times no shorter than 10 million years for some cases (Bridle & Perley, 1984). A Kerr black hole, acting as a compact gyroscope is a natural way to accomplish this (Blandford, 1993).

In this context it is worth mentioning that early clues from photometric signature alone, though initially came with a promising prospect of finding SMBHs in Globular Clusters by investigating the local distribution of stars resulting from the adiabatic growth of an accreting SMBH in per-existing stellar environment, ultimately remained inefficient to uniquely predict the presence of SMBHs at galactic centres and a more arduous task to obtain a more self-consistent approach was concieved (Ho, 1998).

2.2 Evidences from Rapid Variability of Observed Radiation:

Variability studies are very important in identifying the physical processes and the size of the region in which the radiation in a given wavelength range is produced. If variability is obscured on a time scale of $\Delta\tau$ in the source frame, then the radiation must be produced in a region with size constrained by $R \lesssim c\Delta\tau$, c being the velocity of propagation

of radiation (Kembhavi & Narlikar, 1999).

If the source is bigger than this limit, different part of the source would not be causally connected and they would not be varying in phase with each other. This would lead to reduction of amplitudes for variation. When different variability time scales are found in a source at the same frequency, the most rapid variability is taken to be indicative of the source size, after allowing for redshift and relativistic beaming effects. The slower variations are likely to be due to slow changes in the source structure and other effects such as different radiative heating and cooling processes.

The variability of active galaxies generally shows the highest amplitude and the shortest time scales in the X-ray and γ -ray bands, which happen to be clearly separated from the optical/UV bands by the strong absorption of the interstellar medium in our Galaxy (Madejski, 1998 and references therein).

This rapid variability and some other concrete arguments indicate that the X-ray/ γ -rays comes from a region very close to the hole and in many cases, is the primary source of energy in the active galaxies. While the total bolometric luminosities of Quasars is often dominated by the optical and UV flux, the bulk of this flux probably arises in more distant region from the central objects compared to the production of X and γ -rays. The optical and UV radiation coming from the innermost regions, however, are believed to originate as a result of reprocessing of the X ray/ γ -ray photons (Ulrich et al, 1997 and references therein).

It should be mentioned in this context that Blazars as a class are found to have rapid and large amplitude variability, which distinguishes them from other classes of AGNs. Blazars have been found to vary at all wavelengths from the radio to X-rays and at all time scales from days or less to years (Impey & Neugebauer, 1988). A large sample of Blazars observed with the IAU has been analyzed for UV variabilities by different workers (Edelson, 1992 and references therein). It has been found that the UV variability is correlated with optical polarization as well as with the observed UV luminosity. However, when several AGNs, observed contemporaneously in the optical band and with the IAU are examined, it has been observed that the fluxes in the optical and UV bands vary in phase, with no measurable delay. For optical variability observations, some indication are there in the literature (Hook. et al, 1994, Kembhavi & Narlikar, 1999) which tells that the degree of optical variability in quasars depends on their luminosity and redshift. At optical wavelengths, variability has been observed on an wide timescale, starting from as

short as days to as long as years. Observations in the optical region are usually available only over a limited number of epochs spaced non-uniformly, which makes it difficult to apply the usual methods of time series analysis to the study of the variability time scales. Comparing optical and near infra red variations, it is found that the two occur together or with a delay of one day at most, on the other hand, in the radio domain, variations are observed in compact sources on time scales of weeks to months, the shorter time scales being observed at the higher frequencies. The time scales of variations are of the order of years in the 0.1 - 1 GHz range, months to years in the 1 - 10 GHz range and weeks to months in the 40 - 100 GHz range (Bregman, 1990 and references therein).

The shortest time scales for variability have been found at high energies, but the time scale accessible at any wavelength depends upon the frequencies of observations and the signal to noise ratio. At X-ray wavelengths, the best data is available from EXOSAT, which has good sensitivity and a highly eccentric orbit, and therefore reduced occultations of sources by the Earth (Kembhavi & Narlikar, 1999, Madejski, 1998 and references therein). This allows the continuous observations of a source for several days at a time. The capability of EXOSAT were particularly well suited to the study of time variations and a somewhat clearer picture is now available. Contrary to the earlier observations, X-ray flux variations have been found on different time scales and it has been shown that short term variability is common to all AGNs (Madejski, 1998, McHardy 1989). The X-ray variability of AGNs, in general, was found to be aperiodic (Kembhavi & Narlikar, 1999 and references therein). While a measurement of periodic variability would give us a clue to the circumnuclear environment and thus the nature of the black hole, no clue for periodic variability is available (Madejski, 1998). There was much excitement when periodic variability was observed in the low luminosity Seyfert 1 galaxy NGC 6814 (Mushotzsky, et al, 1993). However, observations with ROSAT showed the periodicity was due to another X-ray sources ~ 37 arcminutes away, just outside the field of view, which has contaminated the flux from NGC 6814 (Madejski, et al, 1994).

Two cases of quasi-periodic (QP) variation of flux have been reported for NGC 5548 (Papadakis, 1993) and NGC 4051 (Papadakis, 1995) inferred for the EXOSAT data. Another example of QP variability, weak enough as because have been inferred from only a few cycles, is IRAS 18325-5926 (Iwasawa, 1998).

Nevertheless, from the standard causality arguments ^{*}, all the above mentioned cases of rapid variability imply a compact source size powering the AGNs in general. Even the earlier X-ray data provided the clue that the innermost region of the Quasars are very compact (Madejski, 1998 and references therein). However, it is worth mentioning here that, though the set of variability data provide one of the most concrete evidences in favour of the compactness of central power emitting regions of AGNs (and that the prime movers for the AGNs are nothing but SMBHs because of their intense compactness), are unable to account for their exact size, since the observed emission may well be anisotropic, yielding an underestimate of the emitting volume, as is almost certainly the case for Blazars (Madejski, 1998).

2.3 Evidences from Stellar and Gas Dynamics:

One very useful method of hunting SMBHs at galactic centres is to assess the distribution of matter in the few central parsecs of the galaxy. Assuming that strong gravity produced by the central object is the major dominant force, the motion of the stars and gas in the vicinity of the putative galactic centres offers a robust method for accomplishing the challenging task of identifying the accreting SMBHs with the central engine of AGNs and quasars by revealing the mass interior to the radius of the objects studied (KR95, Ho, 1998, Celloti, et al, 1999). Though use of both stellar and gas dynamics provide interesting advantages and simplification for modelling, gas dynamics, as because gas is highly responsive to non-gravitational forces, can in principle be influenced by forces other than gravity like various radiative forces and pressure gradients. Hence it is expected that among the two categories of evidences (observations from stellar kinematics and gas kinematics), more definitive search are based on stellar kinematics. However, since internal energy can quite easily be dissipated but the intrinsic angular momentum can not, gas is expected to settle down in a relatively cold disk-like structures with its bulk motion component dominating their dynamics. This may simplify the difficulties associated with the de-projection of velocity field (KR95). For some cases, gas dynamical measures have thus provided less ambiguous evidences for the presence of a central massive dark mass and of more accute measurements of how much matter is there. Stellar dynamical

^{*} No stationary sources of isotropic radiation can vary faster than the time it takes for light to cross it.

black hole search is an extremely vast and wide subject, and we won't touch it here in detail. An excellent detail review on this topic is due to Kormendy and Richstone (KR95). However, the basic principle of this method is as follows:

The motion of the stars at the galactic centre is directly affected by the potential well of the galaxy and the central mass concentration. Stars thus basically dynamically behave like point masses in ballistic motion under the influences of the central potential well. The velocity field can be significantly anisotropic since encounters between stars are negligible and the relaxation time for the stellar system exceeds the other relevant timescales and, in fact, suitable stellar distributions are known to mimic the presence of a central massive object. Therefore the results obtained from stellar dynamics are significantly dependent on modelling.

2.3.1 *Method Based on Gas Dynamics:*

Determination of the dynamics within the inner $\sim 10^2$ parsecs of some nearby galaxies have been obtained using HST observations. In some cases, the emission from ionized gas in certain spectral lines is sufficiently bright which is a strong evidence for the orbital motion of a gas in quasi flat and relatively cold disk like structures (the Dusty Disk (KR95, Ho, 1998))

In this context, M87 demands special attention because it was the first object for which the nuclear gas disk was used to determine the central massive object which is now known to be $M_{central} \sim 3.2 \times 10^9 M_{\odot}$ and the compactness ($\lesssim 3.5 pc$) of the volume in which it is concentrated tells of no other possibilities other than it to be a SMBH (KR85). We shall come to this example in little more detail in §3.2 Like M87, similar spectroscopic observations done with HST support the existence of a compact dark massive core in other objects, the mildly active nucleus of NGC 4261 and radio galaxy Arp 102B (Ho, 1998 and references therein), for example. Not only for AGNs, the hearts of a number of 'normal' galaxies also are being revealed in this fashion (KR95). The high velocities of gas observed in the innermost regions of these objects can not be explained in any other ways besides invoking the presence of SMBHs at their dynamical centres. AGNs are thus probably only the tip of the iceberg in this 'big game hunting', i.e., the search for SMBHs at galactic centres.

One of the strongest possible techniques to infer the presence of accreting SMBHs at the heart of active galaxies till today is the investigation of gas dynamics by means of the maser-emission line of water at the wavelength of 1.3 cm. MASER (Microwave Amplification by Stimulated Emission of Radiation) is a phenomenon physics of which is almost fundamentally same as LASER except the fact that unlike LASER, powerful Radio waves are emitted in MASER instead of optical radiation. Maser phenomena are commonly found in the molecular gases in the environment of a variety of celestial bodies under the condition of population inversion (first astronomical maser was detected as the 18cm radio emission from hydroxyl radical (Weaver, et al, 1965, Gundermann, 1965)) and these astronomical masers, because of their high brightness and spot like features, are supposed to be excellent probes of the position and proper movements of the masing objects. The term ‘megamaser’s are assigned to the extremely powerful maser emission having isotropic luminosity of the order of $10^3 L_{\odot}$.Extra-galactic maser usually found at the core of the AGNs and was first detected as broad OH maser emission observed in IC 4553 (Bann, et al, 1982). 22-GHz emission from extragalactic water masers are preferentially detected in galaxies with active nuclei, where physical conditions, possibly realized in a circumnuclear disk favours this form of maser emission (Miyoshi, 1998 and references therein). Not only it is one of the surest proof of existence SMBH at galactic centres, but also provides the most elegant observations showing the presence a disk like structure of accreting material around the central compact object and is capable of measuring the mass of the hole independently of the otherwise uncertain estimations. Although several maser-emitting discs have now been discovered, the most convincing and robust case remains that of the nucleus of spiral seyfert 2 galaxy NGC 4258 (Miyoshi et al, 1994,1995) situated at a distance of 6.8 Mpc away from us, probably because of the fact that the emitting disk is observed edge-on (see §3.2 for a detail discussion). The measured mass of the central compact mass is $M_{compact} \sim 3.6 \times 10^7 M_{\odot}$ confined within a region of the size $r_{compact} \sim 0.012$ parsec having mean density $\rho_{compact} = 4.9 \times 10^{12} M_{\odot} pc^{-3}$. The other modest examples are Seyfert Nucleus NGC 1068 (the second best example) with $M_{compact} = 1.7 \times M_{\odot}$, $r_{compact} = 0.65$ parsec, $\rho_{compact} = 1.5 \times 10^7 M_{\odot} pc^{-3}$ and 14.4 Mpc away from us, NGC 4945 with $M_{compact} \sim 1.4 \times 10^6 M_{\odot}$, $r_{compact} \sim 0.012$ parsec, $\rho_{compact} = 1.2 \times 10^7 M_{\odot} pc^3$ and 5.2 Mpc away from us and NGC 3079 with $M_{compact} \sim 1.3 \times 10^6 M_{\odot}$, $r_{compact} \sim 0.64$ parsec, $\rho_{compact} = 1.2 \times 10^6 M_{\odot} pc^{-3}$ and 20.4 Mpc away from us. NGC 4945 demands spe-

cial attention in this context because this Galaxy expected to be bulgless. If the dark mass in its centre is trully in the form of an accreting SMBH, then even galaxies without a bulge can also harbour a SMBH (Ho, 1998).

2.4 Evidences from Gravitationally Redshifted Emission:

Among various observational signatures of accreting SMBHs at centres of the active galaxies, parhabs the most direct source of information about the strong gravitational field (produced by the central compact object) comes from the analysis of X-ray spectroscopic data. Evidences from gas dynamics, though excellent are probes for the search of SMBHs, suffers from the limitation that, as the gas studied lies usually beyond $\sim 30000 r_g$, the major characteristic signatures of presence of SMBHs, the relativistic effects due to the strong gravitational field produced by them is not explicitly manifested for gas dynamical incidences not occurring in the near vicinity of the SMBHs. X-ray spectroscopy, on the other hand, provides a better approach to analyze the relativistic effects (as x-rays are produced much closer to the hole) in particular, by investigating the energy shifts in spectral lines due to strong gravitational fields which have been performed by the recent detection of the broad Fe $K\alpha$ line at 6.4 KeV in AGNs (Tanaka et al, 1995). This line has been known for quite some time to be a common feature in the hard X-ray spectra of Seyfert 1 AGNs (Pounds, et al. 1990). Fe $K\alpha$ lines, along with an additional hard continuum component imprinted on the primary, are thought to be produced via fluorescence and back-scattering from optically thick material covering half of the field of spanned by the primary continuum source (Nandra & Pounds, 1994, Guilbert & Rees, 1994, Lightman & White, 1988). Since the line arises from matter in motion, its profile is a trace of the velocity field of the accreting material. The observations of these lines, though can not assess the geometry of the distribution of emitting matter unambiguously, is highly consistent with an geometrically thin but optically thick irradiated accretion disk around SMBH. The emission lines from the X-ray illuminated inner part of the accretion disks, being produced from a region very close to the hole, are supposed to be very broad because of the large Doppler and gravitational shifts. Clear evidence for significant broadening consistently compatible with standard accretion disk model (the best fitted disk shows an inner radius of $6r_g$) have been seen from ASCA satellite observations of the X-ray bright Seyfert Galaxy MCG-6-30-15 where the Fe $K\alpha$ line exhibits Doppler motions approaching

relativistic velocities (~ 0.3 pc) as well as an asymmetric red wing consistent with gravitational redshift (Tanaka, et al, 1995). The strongest lines, showing a profile skewed to the red, are produced in a face on geometry where gravitational and transverse Doppler effects dominate. On the other hand, the blue side of the profile becomes more prominent for edge-on disks. A detailed spectral fitting of the line shape indicates that the emitted energy of the discussed Fe $K\alpha$ line is indeed 6.4 KeV and the bulk of its flux comes from a region $< 10r_g$, indicates the presence of quasi-neutral material close to the hole. Analysis of a number of Seyfert spectra from the ASCA archive shows that the relativistic Fe $K\alpha$ line is a characteristic feature of a large number of sources (Nandra, et al, 1997 and references therein).

However, it is difficult to explain very large equivalent width of this line. This problem may be circumvented if the lines are assumed to be produced from outflowing winds suggesting that the stretched wing is due to down-scattered emission lines (Chakrabarti & Titarchuk, 1995, Oosterbroeck, et al, 1996, Murray & Chiang, 1997, 1998).

X-ray spectroscopy thus offers an unique opportunity to investigate the innermost region in the immediate vicinity of the central compact object situated at the dynamical centre of the AGNs in general. Currently available data set, as described already, suggests that the observed X-ray spectra contains a significant contribution from accreting matter and detailed modelling of the line asymmetry has even the potential to measure the spin of the hole, however, results are still not completely conclusive due to uncertainties in the modelling itself (Reynolds & Begelman, 1997) and to complex response of X-ray instruments, which confuses the iron line profile with both the iron edge and the underlying continuum. The progress in this very important field is expected to result from new X-ray observations of future age like AXAF, Astro-E, XMM and Constellation-X for example.

2.5 Holes and Disks from Radio Observations:

The radio structure of a typical extragalactic radio sources essentially shows two lobes of radio emission with steep non-thermal spectra and a stationary compact nuclear core with high surface-brightness and a flat and complex radio-spectrum which is the unresolved base of the jets (Bridle & Perley, 1984, BBR84, Saikia, 1984, 1998, Hardee, Bridle & Zensus, 1996). Observations of the nuclei of radio cores by VLBI techniques have led to significant advancement in our understanding of the energy generation mechanism

of AGNs and provides evidences in favour of the canonical scenario of black holes and disks, which are intimately related to the source of energy. Below we describe a few direct observational evidences showing the co-existence of holes and disks and jet originating from the hole-disk set up.

2.5.1 Seyfert Galaxy NGC 4151:

The radio continuum structure of NGC 4151 (resides 20.3 Mpc away from us) shows elongated structure with several knot like discontinuities which clearly indicate the presence of collimated outflows (radio jets) (Pedlar et al, 1993). High resolution HI absorption line study (with MERLIN radio telescope using 0.15 arcsecond angular resolution) shows that only the component close to the nuclear core produces significant absorption which suggest the presence of disk (with a maximum extension of 50 pc) at the centre of the galaxy. Reverberation mapping of the $H\beta$ line measures the mass of the central SMBH as $M_{center} = 1.6 \times 10^7 M_{\odot}$ (Mundell, et al. 1995 and references therein).

2.5.2 Elliptical Radio Galaxy Cen A (NGC 5728):

The giant elliptical galaxy nearest to us is the Cen A (NGC 5728) which is a powerful radio source. Among other extensive studies at a number of wavebands, observations of $^{12}CO(2\rightarrow 1)$ emission from the dynamical centre of the galaxy suggests that the emission comes from an edge-on circumnuclear ring of radius 100 pc with a velocity of 220 km s^{-1} . This ring, being orthogonal to the radio jet produced by the galaxy, indicates that an accretion disk is supposed to be there associated with a central massive black hole from which the jet is being launched (Rydbeck, et al 1993). The mass of the hole has been inferred to be $1.4 \times 10^9 M_{\odot}$.

3 BRINGING THE WHOLE PICTURE INTO FOCUS; SOME ILLUSTRATIVE EXAMPLES:

Here we will discuss some specific examples which are believed to harbour accreting SMBHs along with disks of accreting matter (dust disk/accretion disk) and radio/optical jets oriented perpendicular/nearly perpendicular to the plane of the disk. These examples indicate that the 'coupled accretion-jet' picture, i.e., that the jets and accretion onto

SMBH at the dynamical centres of the AGNs are symbiotically related, is supposed to be a valid assumption.

3.1 M87 (NGC 4486):

M87 is a giant elliptical galaxy near the centre of Virgo cluster, being one of the two dominant galaxies in the cluster (the other one is NGC 4472, Biretta, 1993). The associated radio source (Virgo A, 3C 274, 1228+127) is classified as FR I source based on its low luminosity and edge-darkened morphology. Its distance has been measured to be 15.9 Mpc using a redshift independent technique. M87 drew attention long back (since 1918: for nearly 82 years!) when observation by H. D. Curtis (Curtis, 1918) marked the first discovery of an extragalactic jet, though its physical nature, as well as that of its host nebulae, would remain obscure for several more decades. Radio interferometric images revealed the bright radio lobes and the optical jets itself and the jet was detected at X-ray frequencies also. While several hundred jets have now been discovered from different sources, the prototypical AGN galaxy M87 remains one of the best example to study the extra-galactic jet phenomena as well as to test the BH paradigm for AGNs. The optical synchrotron jet, nonthermal radio source and large velocities of ionized gas in the nucleus singled out M87 as one of the earliest examples of a galaxy with an active nucleus. At the host of the powerful radio source Virgo A, this has been a favourite target in search for massive black hole because a central SMBH would provide a plausible source of energy to power the relativistic jet in M87, and its proximity provides a good scale for seeing the interaction of the hole with its surrounding galaxies which made M87 a terrific laboratory for seeking further evidences that AGNs have central SMBH fed by a surrounding disk. In fact, M87 is the first object for which the nuclear gas disk was used to determine the mass of the central SMBH (see KR95 and references therein).

3.1.1 *The Hole and The Disk:*

Decades back, using CCD photometry (M87 was the first elliptical galaxy to be investigated with CCD), it was found that it has a cuspy core and its velocity dispersion was shown to rise inside the core radius from 278 km s^{-1} at $r = 10''$ to 350 km s^{-1} at $r = 1.5''$. These observations could be fitted with isotropic dynamical model only if M87 could

contain a central compact object of mass $M_{compact} = 3 \times 10^9 M_{\odot}$. Also the non-thermal point source and the nuclear cusp in the stellar light distribution have been investigated. From the analysis of the deconvoluted surface brightness profile of M87 using spherically aberrated Wide Field/Planetary Camera 1 (WFPC1) images (Lauer et al, 1992), it has been concluded that there is a massive dark object at the centre of the galaxy having mass $M_{compact} = 2.6 \times 10^9 M_{\odot}$ but this solution was not unique without enough additional kinematical evidences which were yet to be obtained (Ford et al. 1994 and references therein). Although the observations and arguments described thus far provided compelling reasons to think that there is a massive black hole in the centre of M87, they have not been definitive for several reasons. Foremost is the fact that ground based observations makes it difficult to resolve features close enough to the centre to see the unmistakable gravitational signature of a massive black hole and simultaneously avoid dilution of the spectrum by light from the nonthermal sources in the nucleus. A second problem is that the mass derived from the stellar kinematics is model dependent, making it possible to explain the observed velocity dispersion by being suitably clever with velocity anisotropy. The apparent light cusp resulting from stars collecting in the deep potential surrounding a massive black hole is highly suggestive, but cuspy cores are not enough to uniquely discover SMBHs at the centres of the active galaxies. It has been argued that stellar dynamical black hole searches was not too efficient to reveal the hearts of AGNs.

Gas, on the other hand, tells a clearer story. That there might be some hope of detecting a central BH by spectroscopy of emission lines from ionized gas in the nuclear region of M87 was indicated almost at the same time that of the CCD observations of the galactic core (see KR95 and references therein). Eventually, the signature of a single, coherent and supermassive compact object comes, however, from a disk of ionized gas located at the galactic centre and orbiting in a plane perpendicular to its well known jet. Spectroscopic observation of ionized gas in circular motion close to the core of the galaxy can provide powerful and straightforward way to look for the Keplarian rotation curve which would be signature of a massive black hole. Consequently, Wide Field/Planetary Camera 2 (WFPC2) taken narrow band images of M87 was investigated to look for organized structure in the ionized gas (Ford et al, 1994 and references therein). These images suggest that the ionized gas in the nucleus has settled into a rotating disk. The rotation velocity in the disk, with a massive object at its centre, will rise towards the center rather than decrease to zero as in a galaxy with no central dark mass; this is indeed observed in reality.

Using HST FOS spectroscopy observations, the radial velocity at its diametrically opposite positions along the major axis on either side of the nucleus have been measured. The measurements of radial velocity at $r = \pm 19 \text{ pc}$ show that one side of disk is approaching at $500 \pm 50 \text{ km s}^{-1}$ and the other side of the disk is receding at $500 \pm 50 \text{ km s}^{-1}$. Absorption associated with the disk and sense of rotation imply that the apparent spiral arms trail the rotation. The observed radial velocity connected for a 42° inclination of the disk imply rotation of $\pm 720 \text{ km s}^{-1}$. The estimated total mass of the central compact object as $M_{compact} \sim 2.4 \times 10^9 M_\odot$ within 18 pc of the nucleus which must be a black hole because no other form of mass concentration can fit the bill of having such a stable and coherent high density profile. It has also been argued that the optical and radio luminosity would depend on the mass of the central SMBH and the rate at which it is being fuelled. The case for a central SMBH in M87 has been considerably strengthened through more recent observations with HST using long-slit mode of the Faint Object Camera to obtain higher quality spectra extends upto $r = 3.5 \text{ pc}$ (Harms, et al. 1994). The velocity fit for the inner few tenth of an arc second are well fitted by a model of thin disk in Keplerian motion. X-ray data reveal hot gas pervading M87 itself, as well as in the surrounding cluster. If there were a huge central hole, then some of this gas would inevitably be swirling into it, at a rate that could be estimated, and this accretion would give rise to more conspicuous activity than can be seen in a normal galaxy without any central accretor. The radio and X-ray emission from the vicinity of M87 is indeed fully consistent with accretion at the expected rate, so the observed non-stellar output from M87 actually corroborates the evidence for harbouring an accreting SMBH (Rees, 1997, Fabian & Rees, 1995).

3.1.2 *Jets from M87:*

As already mentioned, M87 is well known for its radio and optical jet. High resolution optical and spectroscopic observations show that the jet is well collimated on scales from about 1 to 1000 pc, with collimation extending down to scales $\sim 0.01 \text{ pc}$. Beyond 1 Kpc, the jet passes through shock like discontinuities, became unstable and poorly collimated, but yet continues to scales $\sim 35 \text{ Kpc}$. The recent discovery of an continuum hot spot opposite to the jet strongly suggest a counter-jet is present (Sparks, et al, 1992). The optical and X-ray morphologies of the jet are remarkably similar to the radio (Biretta, 1993). Throughout the jet the radio spectral index is ~ 0.5 . The relativistic jet is perpendicular to

the disk structure with a bulk Lorentz factor of $\Gamma_{Jet} = 4$. From the jet morphology, it has been argued that M87 is probably nothing but a Blazar with the jet oriented at an angle $\sim 40^\circ$ to the line of sight (Madjeski, 1998 and references therein).

3.2 NGC 4258:

The spiral low luminosity ($\sim 10^{42} \text{erg sec}^{-1}$) sub-Eddington ($\frac{L}{L_E} \sim 3 \times 10^{-4}$) spiral Seyfert 2 Galaxy NGC 4258, lies at a distance of about 6.4 ± 0.9 Mpc away from us, has an AGN of modest power and its optical spectrum shows a low-luminosity nuclear emission-line region (LINER) with a weak broad-line component. Between its normal spiral arms, it shows some 'anomalous' arms seen in $H\alpha$, radio synchrotron [†] and in X-ray among which the $H\alpha$ arms consist of braided components. The standard explanation of this 'anomaly' is that the core of this galaxy has a gas disk and produces a radio jet, interaction of which with the gas of the disk produces the anomalous arm emission (Miyoshi, 1998 and references therein).

3.2.1 The Hole and the Disk:

An extremely powerful SMBH probe is provided by the detection of H_2O maser emission in 4258. There are three groups of MASER lines, one is at the systemic velocity of the galaxy (476 km s^{-1}) while the others are strongly redshifted (with intensities of about one half or one third of the main features) and weaker blueshifted (with intensities of about one tenth of the main features) with high velocity feature offset from the systemic velocity by $\sim \pm 900 \text{ km s}^{-1}$ (Miyoshi, et al. 1994, 1995, Miyoshi 1998 and references therein). This maser spectrum of NGC 4258 can be interpreted as arising from a thin Keplerian disk, rapidly rotating around an extremely compact massive object. Greenhill et al (1995a, 1995b) showed that the systemic velocity source consists of many masers along a line $0''.00026 \times 0''.00005 = 0.009 \times 0.002 \text{ pc}$ in extent that is perpendicular to the inner radio jet where the velocities are tightly correlated with position. It has been suggested that the masers are in a thin annulus of radius 0.1 pc with individual velocity drift $\sim 9 \text{ km s}^{-1} \text{ yr}^{-1}$ implying a rotation velocity of 900 km s^{-1} and a central mass $M_{compact} = 2 \times 10^7 M_\odot$.

The robust proof of disk picture (rotating disk around SMBH at the Galactic centre) come

[†] Radio continuum image at 1.4 GHz shows that the anomalous arms are brightest in non-thermal synchrotron emission

from the important high resolution ($\Delta\theta = 0''.0006 \times 0''.0003$; $\Delta v = 0.2 \text{ km s}^{-1}$) VLBA observations due to Miyoshi et al (1995). They confirmed that the high velocity masers are located $0''.005$ to $0''.025$ on either side of the central line of sources and the maser spots trace a thin ($< 0.003 \text{ pc}$) nearly edge-on annulus with inner and outer radius of 0.13 and 0.26 pc respectively. The masing activity can only be observed along a line of sight where the velocity gradient is zero so either the maser spots are located between the observer and the source or at perpendicular/nearly perpendicular to the line of sight. The spectral resolution in the microwave lines high enough to pin down the velocities with accuracy of 1 km s^{-1} and VLBA achieves an angular resolution better than 0.5 milliarc second (100 times better than the HST, as well as for finer spectral resolution of velocities). These observations have revealed, right in the Galactic core, a slightly warped disk (position angle 86° ; inclination angle 83°) with high rotational speed (1080 km s^{-1} for the inner edge) following a Keplerian rotation curve [†] with very high accuracy ($\lesssim 1\%$). The implied binding mass within 0.13 pc is $3.6 \times 10^7 M_\odot$ which corresponds to a density of $> 4 \times 10^9 M_\odot \text{ pc}^{-3}$ which is impossible to circumscribe by a stable and long lived star clusters because it is highly unlikely that such a high density cluster could be stable for a long time. Even Globular Clusters have stellar densities of $< 10^5 M_\odot \text{ pc}^{-3}$. For instance, if the mass at the centre of NGC 4258 were composed of stars of $1 M_\odot$, the mean stellar separation would be only 100 AU , and the collision time would be very small and collisions would disrupt the cluster instantly (Miyoshi, 1998 and references therein). So a cluster of distinct, dark masses would never be responsible for producing such a steady gravitational potential because then at least some of the objects would escape on a relatively short time scale, and would form a departure of the megamaser emitting material from pure Keplerian motion. So the only possibility is that the central mass must be due to a single SMBH (if not due to something more exotic!).

3.2.2 Signature of Bipolar Jets from Galactic Centre:

Figure 1.3.1 (adopted from Herrnstein et al, 1999 with kind permission) shows the mapping of continuum emission about 3 mJy detected near the water masers in NGC 4258. The strongest emission is located at about 0.025 pc at the north of the dynamical centre

[†] Keplerian because both of the red and blue shifted wings are offset from the systemic features in a nearly planar (slightly warped) structure and the plane of sight velocity decreases with distance from centre as $r^{-0.5}$.

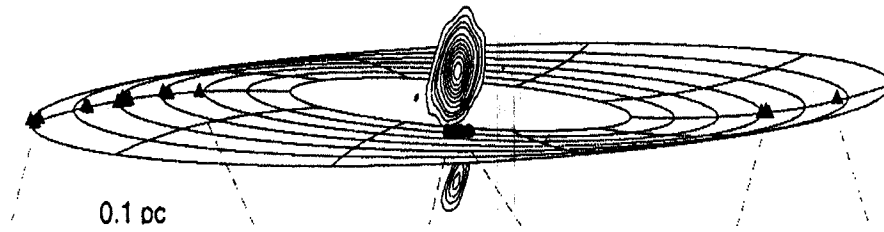


Fig. 1.3.1:

The warped disk model superposed on actual maser positions as measured by the VLBA of NRAO, with top as North. The filled triangles show the positions of the high velocity masers with VLBA continuum images are included as contours. The dot at the centre is the dynamical centre of the disk which is offset from continuum emission. The 22 GHz radio emission traces a sub-parsec scale jet elongated along the rotation axis of the disk well-aligned with a luminous Kpc-scale jet (Herrnstein, et al, 1999)

of the disk whereas another continuum emission, moderately strong, was found at 0.03 pc south of the centre. These continuum peaks are believed to be two oppositely oriented radio jets emanating from the core of the Galaxy. Another strong evidence for bipolar outflow comes from the X-ray observation due to Pietsh et al (1994). A pair of X-ray sources were found around the core of the Galaxy. Both of the X-ray blobs are 9 minutes apart from the Galactic centre and the line connecting them clearly passes through the nuclear core. It is believed that those X-ray blobs are due to matter ejected from the core.

3.3 What's Special About the Above Choice?

The origin of collimated emission is of particular interest for understanding the nature of active galaxies. We purposely chose the above two examples (NGC 4258 and M87) to argue for the viability of the black hole paradigm and to illustrate the fact that extragalactic radio jets are basically accretion powered. Nuclear disks might be a common denominator in active galaxies and these disks might supply fuels for the SMBHs located at the dynamical galactic centres, and determine the direction of the collimated jets and ionizing radiations geometrically and via the angular momentum in the gas disk, which in turn feeds the accretion disks. The gas in the nuclear disks is thought to come either from the capture of small galaxies or tidal disruption of nearby stars or as the result of a cooling flow. All these ideas are very exciting and bears the signature of highly innovative minds; *but*, have we *discovered* accreting SMBHs at hearts of active galaxies (or even more loosely, in *any* galaxy) *at all*? Unfortunately, rigorously speaking, we *have not*. Though we *have* rigorously *shown* that centres of active galaxies (and in general, other normal galaxies with a bulge) *do* harbour a massive dark object (MDO) in general, any

direct observational evidences to show that these MDOs are indeed accreting SMBHs are still far from reality and we more or less rely on indirect arguments (KR95). So the most fundamental challenge is to show that MDOs are *indeed* SMBHs and this seeks to identify some observational features that might be taken as a fingerprint of the physical processes uniquely associated with the environment of a BH. This is why M87 and NGC 4258 results are so welcome (also the results from MCG-6-30-15, see §2.4). M87 epistemized the AGN paradigm (the BH paradigm as well, so to say). Now the detection of a nuclear gas disk perpendicular to the jet and with velocities implying a BH of just the *right* mass is indeed the first direct contact between BH searches and the rest of the paradigm (the connectivity of Jet, Disk and Hole as well). Along with M87, the apparent detection of a Keplerian rotation curve in NGC 4258 already increases our confidence in the belief that it is *nothing but the accreting SMBHs*, which is indeed the dynamo of AGN power-houses and the progenitor of extragalactic jet phenomena seen from a wide variety of AGNs.

Brief Overview of Existing Disk-Wind Models

Chapter 1.4

SUMMARY

The existing models dealing with outflows from accretion disks/torii around an accreting black holes are briefly outlined. Analytical/semianalytical as well as numerical simulation works of three different categories, viz, thermally driven, hydrodynamically driven and hydromagnetically driven disk-winds are discussed.

Study of galactic/ extra-galactic jets in a holistic approach apparently involves investigation of two barely overlapping domains. Firstly, the jet formation zone, out of which, by courtesy of the jet-theorists, emerges a well-collimated jet. Secondly we have the rest of the Universe where the jet interacts with its surrounding and consists of two major subdomains of interest, namely, the confinement/ collimation property of jets along with its dynamics, and the nature of various radiative processes involved which provide indications of how and in which form energy carried out by jets is being dissipated. It seems from the present status of investigation of above aspects that surely the most tantalising issue among all is the formation of jets and the main challenge to jet-theorists is to answer the question *“How and why the jets are formed?”* Though progress in understanding the exact physics of jet formation has been severely handicapped by inadequacy of our knowledge about microphysics of underlying mechanism of jet formation, from the informations provided in Chapter 1.1 as well as in Chapter 1.3, the basic ingredients of theoretical models attempting to explain the origin and formation of jets seems to be reasonably well agreed upon. They are: first, a deep central potential well provided by an accreting SMBH in case of jets from AGNs and QSOs and a stellar mass black hole in case of jet from microquasars, and, second, the matter accreting onto the central accretor in order to provide the energy for continuous throttling of the jets and for providing the required symmetry for jet formation. The invariable association of astrophysical jets/

outflows with an accretion disk thus reinforce the belief that probing the jet production mechanism ultimately boils down to theoretical investigation of how do the accretion disks around black holes launch jets.

In this chapter we attempt to provide a sketchy outline of some important works already present in the literature which deals outflows/ jets generated from accretion disks. As it is absolutely impossible in this limited space to do justice to the voluminous and impressive amount of work that has been carried out in this field, we, by no means, claim this chapter to be a comprehensive review in this subject and in advance apologize for unwanted omission of any important reference related to this field.

Works on jet formation present in literature may be broadly classified into three distinct categories which are in order:

(i) *Thermally Driven Winds*; where the radiation pressure due to photons of the accretion disk (thick or thin) imparts its momentum to the accreting gas to drive outflows.

(ii) *Hydrodynamic Winds*; where a fluid with internal energy per particle greater than its rest mass, accelerates upon its expansion by converting its internal energy into directed motion.

(iii) *Magnetocentrifugally Driven winds*; where the energy associated with the poyinting flux due to the twisting of magnetic field by the rotation of the accretion disk is converted into directed motion at large distance from the central compact object.

In §1, we describe various models of thermally driven winds, §2 provides a variety of works dealing with hydrodynamic wind while §3, (largely based upon two excellent review articles by Ferrari (1998) and Heyvaerts (1999)) is devoted to models describing magnetohydrodynamic winds. Finally in §4, we illustrate the important differences between all the existing models and model presented in our work for explaining the formation of jet.

1 THERMALLY DRIVEN WINDS:

Some classes of Active Galactic Nuclei (Quasars are the best examples) are extremely luminous objects close to their Eddington limit, intense pressure of radiation field acting on electron-proton pairs could be sufficient to overcome gravitational attraction of the central accretor along some certain direction. Usually two categories of thermally driven disk

winds are of investigation: winds from the deep funnels of thick accretion disk replenished by UV photons from its walls; and, in a variant on this mechanism, outflows from corona over a thin accretion disk. While an independent confining mechanism would, in any case, be required if the jet is accelerated by UV photons from thin disk, a thick disk generated funnel can naturally provide the initial collimation mechanism.

Various mechanisms are supported to drive thermal disk winds, the most important of which are the irradiation of the accretion disk by the central sources as outlined above, and the two-temperature hot accretion disk. In the former case, the irradiation is dominant in the outer edge of the disk and the disk temperature varies as $T_{disk} \propto r^{-\frac{3}{7}}$. In later case, gas is heated to a relativistic temperature in the inner region of the accretion disk. Bellow we describe two major works related to thermal winds.

Eggum et al (1985, 1988) presented nonrelativistic radiation-hydrodynamics calculation of axisymmetric supercritical (super-Eddington) accretion disk using Newtonian mechanics accomplishing the radiative transport using a single-group flux-limited diffusion algorithm in cylindrical co-ordinates, assuming both azimuthal symmetry and reflection symmetry about the disk midplane. The inner part of the disk was investigated where radiation provides the vertical support and the opacity is accurately given by Gray-Thompson scattering opacity and flux limited diffusion. Anisotropic and isotropic constant kinematic viscosity models were used. The accretion flow was assumed to be driven by a macroscopic shear stress tensor of the form:

$$\Pi^{ij} = A(i, j)\Gamma^{ij}$$

$$\Gamma^i_j = -\mu\rho(v^i_{,j} + v^i_j, -\frac{2}{3}\delta^i_j v^k_{,k})$$

v^i being fluid velocity, ρ is fluid density and a comma denotes covariant differentiation; $\mu = 1.5 \times 10^{15} \text{ cm}^2 \text{ s}^{-1}$ with characteristics Reynolds number $R_e = \left(\frac{rv_e}{\mu}\right)$. They numerically investigated the domain of accretion rate as $1.1 \lesssim \dot{M} \lesssim 10$ and the form for viscosity used in their work led to disk structure subject to no instabilities other than the convective instability. Their numerical simulation investigations were divided into four different structural zones: a convective core, an accretion zone, a photosphere (more properly described as a photocone) and a jet. The accretion was modelled to be in between the active connective core and the photosphere and jet zones, so that it partially shields the latter from fluctuations in the former and has no effective mechanism for converting kinetic energy to radiation so that the gravitational potential energy of the

material which enters the accretion zone makes little contribution to the disk luminosity. The super-Eddington numerical solutions produced radiation pressure driven jets which appears as soon as radiative equilibrium was established in the inner disk and shows variability. The mass efflux is apparently the consequences of the finite scale height of the disk and its photocone, which lofts matter onto the accelerating radiation field within the vortex. However, the opening angle of their jets was large enough which conflicts with the observational results. The inner region of the convective core provided a significant effect on the variability of the jet mass flowrate as well as accretion rate. It was proposed that their calculations might be scaled to conditions appropriate to AGNs and Quasars by suggesting that extragalactic relativistic jets might contain a core of thermal plasma.

Ferrari et al (1985) discussed the quasi-2-D hydrodynamic problem of relativistic equilibrium flows for given profiles of the propagating channels. Considering orbiting thick disk around the central compact accretor, and adopting the following assumptions:

- a) The flow is optically thin.
- b) The radiation field can be collimated geometrically along the funnel by radiation-wall interactions and the radiation flux scales with the cross-sectional area of the funnel and normalized to the total luminosity of the funnel which is assumed to be proportional to the Eddington luminosity.

They presented transonic wind-type solutions of the relativistic quasi-2-D Navier Stokes fluid equations, which was assumed to govern the initial acceleration of plasma inside the funnel of the disk. Their solution depends on geometrical parameters characterizing the shape and height of the funnel and on radiation parameters characterizing luminosity and collimation of the radiation field inside the funnel. They showed that straight forward hydrodynamical effects led to effective acceleration close to the nucleus. Their model was analogous to twin-exhaust model of hydrodynamic wind due to Blandford & Rees (Blandford & Rees, 1974, BR74 from now onwards) with the extra momentum deposition added by the radiation pressure inside the funnel and the rapid expansion of the gas at the exit of the funnel brings the critical point inward along the axis. Unlike Chakrabarti (1984a, 1984b), (where the direct influence of the central object on the collimating object was investigated) in their model, the central accretor affects the beam collimation only indirectly through the formation of the steep accretion funnels. Moments of the radiation field inside the funnel are determined by the wall's emissivity, the physical conditions and absorption coefficients of the gas and the interaction of the flow with the

funnel's walls. Their solution exhibits many critical points and the jet thrust is not constant but decreases in the subsonic regions and increases in the supersonic regime. The surface of the jet is not parallel to the flow, and this corresponds to a consistent external pressure force acting on the field. Flow accelerates (retardes) where the channel widens (becomes narrow). Stationary shocks were found near the exit of the funnels boared in thick accretion disk. Magnetic fields and rotation were not taken care of in their work.

By consistently solving the radiation transport equations in the funnel, Nobilli et al (1998) extended the results to the optically thick flow. It is to be noted that in all models related to acceleration by radiation pressure, the critically limited factor is the Compton drag by the same radiation.

The usual works dealing with radiation pressure driven accelerations normally suffers from the following limitations:

- a) Many sources with powerful extragalactic jets have luminosities well below the conventional Eddington luminosity-and consequently is insufficient for acceleration, even when more efficient absorption processes are considered.
- b) Radiation fields in the funnel is not too anisotropic and a mildly relativistic Lorentz transformation reduced its net momentum density to zero. It is therefore only possible to accelerate the outflowing gas to mildly relativistic speeds, much less than those usually invoked to account for superluminal motions. However, somewhat larger outflow speeds are possible for radiation driven outflows from the corona over thin disks, although the collimation in this case would be much poorer.
- c) It is very difficult to impart a large fraction of the photon field momentum to a gas whose inertia is dominated by protons; the situation is relatively easier for plasmas consisting of e^+e^- pairs but even this case requires that the photon field responsible for the acceleration be rather finely tuned (Contopoulos & Kazanas, 1995). In order that the high Lorentz factor are attained the photon field has to be rather carefully arranged. Whether this takes place in reality is a debatable issue so far.

2 HYDRODYNAMIC WINDS:

2.1 Analytical Works:

Hot tenuous fluid in plasma form at the surface of an accretion disk rotating around a compact accretor can be accelerated outword against the gravitational attraction of the

central compact body hydrodynamically through internal heating or irradiation. An adiabatic fluid propagating in an external medium with decreasing pressure, provides a relatively simple and direct way of achieving hydrodynamical self-collimation and acceleration due to the requirement for the fluid to pass through the sonic point. This idea was first applied to jet acceleration by Blandford and Rees (1974) in their twin-exhaust model whose physics is essentially derived from the stellar wind theory. Before that, significant contribution was also due to Longair et al (1973) and by Scheuer (1974) where some important fluid dynamical aspects of beam models were discussed consistently. An essential feature of the BR74 model is that active galactic nuclei contain dense thermal gas in addition to the central compact object right at the galactic centre. This gas is assumed to be relatively condensed and possibly magnetized which is confined by the gravitational potential well at the centre of the galaxy and the scale height is assumed to be comparable with the dimensions of the galactic centre so that its pressure is much more compared to that of general extragalactic medium. It has also been assumed that the thermal gas density in the central 10-1000 pc is sufficiently high ($T_{Gas} \sim 10^8$ K). In twin-exhaust model, an equilibrium flow was considered in which fast (probably relativistic) plasma, possibly pervaded by electromagnetic fields (generated in the region very close to the central accretor) escapes along two oppositely-directed channels or 'exhausts'. At all points on the boundary of these channels, the pressure of this relativistic and magnetized plasma must balance the pressure of the static thermal gas cloud. The outflow attains its sonic velocity where the channels cross section reaches the minimum value. The channel is then shown to widen again as the external pressure drops still further, and, as in a de Laval nozzle, the flow becomes supersonic. The expanding fluid is anticipated to be an uncertain mixture of the static magnetic field, hot and relativistic plasma and perhaps a variety of low frequency wave modes. The model deals with ultra-relativistic (polytropic index $\gamma = \frac{4}{3}$) gas with isentropic flow and except very close to the nucleus, the flow has been approximated as one-dimensional. It has also been suggested there that though BR74 deals with fully relativistic fluid, important qualitative features are, however, unchanged if the internal sound speed is non-relativistic.

It has been shown that pressure distribution in the gas cloud, is axisymmetric rather than strictly spherically symmetric and that is why the jets would be expected to emerge along the axis of symmetry, any oblique orientation would not be an equilibrium and it was argued that a flow pattern with a single jet is not an equilibrium situation- a second

jet would invariably develop antiparallel to the first. It has been suggested (though suggestion is quite weak and not at all conclusive) that the flow is freed from the effect of Rayleigh-Taylor and Kelvin-Helmholtz instabilities. Wiita (1978a) attempted to incorporate the Rayleigh - Taylor instability in this context but the Kelvin - Helmholtz instability had been ignored in his work.

However, the twin-exhaust model, though explains some aspects of jet formations nicely, is over simplified and according to this model, the gas that would be required to continuously throttle the most powerful extragalactic jets would radiate an X-ray flux for larger than has been observed. The twin-exhaust model could be appropriate only for low power ($L \lesssim 10^{43} \text{ erg s}^{-1}$, see Blandford, 1993) jets.

Wiita (1978b) refined the BP74 model by taking a more compact central cloud, while keeping the one-dimensional flow approximation. Smith et al (1983) proposed the non-relativistic (speeds of 0.1 c has been used without relativistic corrections) version to the BP74 model to produce steady flows. The magnetic field was assumed to be too weak to affect the dynamics.

Among the many other subsequent papers on hydrodynamic winds from rotating thin accretion disks, contribution due to Fukue and Okada (1989) demands some special attention due to its ability of studying the stability of solution, and capacity of bringing the first critical point very close to the core and immediately making the jet supersonic as is observed. Using cylindrical geometry, they provided a self-consistent complete axisymmetric solution (for inviscid polytropic flow with no magnetic field resulting conversion of specific angular momentum along streamlines) of the balance equations along and perpendicular to streamlines (Bernoulli and Grad-Shafranov equations, respectively) including the effect of centrifugal force generated by the rotating accretion disk (Model without disk rotation was presented in Fukue, 1989) but self-gravity of the disk was neglected. Multiplicity of critical points was found which was argued to be occurred due to a deviation in the shape of the gravitational potential along the streamlines from that of a spherical wind. Energy is injected into each streamline at the base of the disk and a flow pattern is set up that crosses transonic surface to produce a supersonic wind. Depending on the temperature distribution on the disk surface, the fate of the accreting gas may be threefold:

a) When the local temperature distribution is flatter than the inverse of the local equatorial distance, gas on the inner part of the disk is gravitationally bound to form a corona

while the gas in outer region can escape to infinity as hollow cylindrical jet.

b) If the temperature changes exactly as the inverse of the equatorial distance, the entire region of the disk is windy or bound.

c) If the distribution is steeper than $\frac{1}{r_e}$ (r_e being equatorial distance), situation is just reverse of (a), that is, while the outer region gas is bound, the inner region gas can escape to infinity which corresponds to the well-collimated jet.

The link between the jet and the disk is only through the injection of energy at the base of streamlines, there is no back reaction from the jets to the disk.

Proposing the presence of a population of relativistic hadrons in the close vicinity of the central object, Contopoulos & Kazanas (1995) investigated the HD origin of relativistic outflows in AGNs by arguing that the associated neutron production would suffice to produce outflows which could achieve relativistic speed. Adiabatic index of the expanding outflows and detail evolution scheme of the bulk Lorentz factor were claimed to be explained. The role of large scale magnetic field in confining these outflows at large scale was also examined.

Recently it has been proposed that for accretion with insufficient radiative loss of energy due to too low density or with long diffusion timescales, energy may be extracted from the flow mechanically/electromagnetically through winds.

2.2 Numerical Simulation Works:

Hydrodynamic wind has been investigated through numerical simulation by a number of workers. Wilson (1972) initiated the hydrodynamical simulation of gas accreting onto a black hole. His work was followed by other authors also. Hawley et al (1984, 1984a, 1985) while investigating numerical simulation of accretion flows onto black holes, noticed outflows. Considering thick accretion disk around a Kerr black hole, the outflow was shown to be hollow and along the outer edge of the accretion disk. As in their model the accreting gas was supposed to possess considerable intrinsic angular momentum, a strong centrifugal force is produced near the z axis and the gas density becomes very low along the axis. Dealing with to some extent same flow pattern as that of Hawley et al (1984, 1985) (gas with large angular momentum having very small viscosity near z axis) outflow has been investigated using Smoothed Particle Hydrodynamics (SPH) (Molteni et al, 1994). Mass ejection rate has been found to quite considerable in their work. An-

other good work worth refereeing here on fully time dependent analysis of HD outflow is due to Ryu et al, 1997. They studied outflow from disk using Total Variation Diminishing (TVD) method. Taking account the viscosity in the flow, Yokosawa (1995) studied HD disk wind. In his model, viscosity transfers angular momentum from gas concentrated in midplane and fills the polar region with low angular momentum gas. One limitation of this work is that the shock formation and jet acceleration is not properly taken care of. Very recently, using TVD scheme, Nobuta and Hanwa (1999) considered accretion of hot gas with low specific angular momentum with cold dense gas having high specific angular momentum. The former accretes continuously while the later highly intermitently as blobs. The dense gas cloud was assumed to form by some unknown instability or by disruption of a larger cloud. Instead of full general relativistic treatment, the whole work was done using PW80 potential. The high specific angular momentum gas blobs bounce at the centrifugal barrier and creates shock waves. The low specific angular momentum gas is heated at the shock fronts and escape along the rotation axis and eventually evolves into pressure-driven jets; jet acceleration lasts until the shock fade out. One major achievement of their work is they could correlate the jet with time variability of a class of AGNs, also their shock computation was without numerical oscillation. The co-existence of strong shock waves (which accelerates the jet) and jets in their model has been argued to give an explanation of simultaneous X-ray and γ -rays flares and of relativistic jet ejection in accretion powered AGNs and X-ray binaries. It is to be noted here that the pioneering work in this field due to Wilson (1972) could also find the kind of shock proposed here but was unable to find correlated outflows. Another recent work on HD simulation of disk wind is due to Stone et al (1999). They suggested that the net mass accretion rate increases roughly linearly with radius, though, in the absence of a rapid source of dissipation, the surplus mass escapes as a subsonic breeze rather than a supersonic wind. Plewa et al (1997) presented HD simulation of relativistic jets propagating through a nonuniform medium and studied the bending of jets propagating obliquely to the vector of the density gradient. They applied their results of simulation to NGC 4258 and their predicted direction of bending seems to be consistent with the observation. Though HD winds models are simpler than MHD model to deal with (added complications in MHD models are due to introduction of Maxwell's equations which increases the number of characteristics in the fluid system and to make numerical simulation more unstable), are major disadvantages of HD model are that the origin of acceleration and

collimation goes back to ad hoc mechanism, which may be eliminated in MHD model by self-consistent introduction of ordered large scale magnetic field. So in the next section we will discuss MHD wind elaborately. Also the hydrodynamic mechanism has the drawback that the boundary conditions necessary for achieving bulk relativistic outflows are thought to be difficult to obtain naturally. Even though there are mechanisms which could potentially accelerate individual particles to very high energies (see Chapter 3. for detail), the fluid approximation of HD cares only about the mean energy per particle, which, from energy conservation, will have a strict upper limit set by the local depth of the gravitational potential well of the central accretor causing the outflow to possess sub-relativistic velocity with significantly low Γ .

3 MAGNETOHYDRODYNAMIC WINDS:

Large scale magnetic fields are widely believed to be present threading conducting accretion disks and/or the central black hole. This anchoring field may be of external origin or have its source in either of the disk/hole (or both); possibly by dynamo action in the accretor or in the accretion disk. Thus inclusion of contribution of ordered magnetic field, especially when they are dynamically important, is of immense importance while studying launching of astrophysical jets from rotating accretion disk around a SMBH and in investigating their confinement and collimation mechanism (Celloti, et al, 1999, Blandford, 2000, Heyvaerts, 1999, Ferrari, 1998, Lovelace, et al, 1999, BBR84). Magnetohydrodynamic (MDH) winds are an important (and essential too) source of advection losses from magnetized conducting accretion disk. In the presence of a poloidal magnetic field anchored in the accreting material that is wound up by rotation of the disk and generates a collimating toroidal field. The twisting of the magnetic induction field by rotation of the disk drives the jet by mechanically extracting matter, angular momentum and energy from the accretion disk. The power can be extracted from (and symmetry provide by) the rotation of either/both an accretion disk (giving rise to and MHD wind over a large range in radii) or/and being limited to the inner radii - a spinning black hole threaded by a large scale magnetic field.

However, besides the standard hydromagnetic winds where the energy is collimated by both the electromagnetic field and the kinetic flux of matter, a "Poynting flux jet model" has also been suggested (Blandford, 1976, Lovelace, 1976, Lovelace, et al, 1987, Colgate

& Li, 1998) where the energy outflow from the disk is carried mainly by electromagnetic field while the energy carried by the matter is sufficiently small. In these regime of works, rotation of a Keplarian disk twists a poloidal field threading the disk resulting outflows out of the disk extracting angular momentum (in the twist of the field) and energy (in the poynting flux) away from the disk which indirectly facilitates the accretion. We will discuss this case in slightly greater detail later (§JaNI NA).

3.1 Basic Scheme for Solving the Problem:

Standard steady MHD winds are governed by the following set of nonlinear partial differential equations(Ferrari, 1998):

$$\vec{\nabla} \cdot \vec{B} = 0 \quad (1a)$$

$$\vec{\nabla} \times (\vec{v} \times \vec{B}) = 0 \quad (1b)$$

$$\rho(\vec{v} \cdot \vec{\nabla})\vec{v} - (\vec{B} \cdot \vec{\nabla})\frac{\vec{B}}{4\pi} = -\vec{\nabla} \left\{ (P + \frac{B^2}{4\pi}) + \vec{\nabla} \phi \right\} \quad (1c)$$

$$\rho\vec{v} \cdot (\vec{\nabla} \mu - \frac{1}{\rho} \vec{\nabla} P) = \rho\sigma \quad (1d)$$

μ being the specific enthalpy and σ the specific heating and cooling rate.

Only axisymmtric steady solutions for full 2-D cases are available. The set of MHD equations are thus reduced to two coupled equations fully describing the jet dynamics along and across streamlines respectively: they are Bernoulli and Grad-Shafranov (transfield) equations. Adapting *SI* unit in cylindrical co-ordinates $\{r, \phi, z\}$, the unit vectors may be defined as \hat{e}_r , \hat{e}_ϕ and \hat{e}_z . Under axisymmetric assumptions, any vector for this case is the sum of an azimuthal part (toroidal) and a part in the meridional plane (poloidal). The poloidal magnetic field, usually denoted by B_P in literature, may conveniently be represented in terms of a flux function $a(r, z)$ as:

$$\vec{B}_P = \frac{1}{r}(\vec{\nabla} a \times \hat{e}_\phi)$$

Surfaces of constant $a(r, z)$ are called the 'magnetic surfaces' which are basically the surfaces generated by the space rotation of different field lines about the axis. Stationary axisymmetric MHD winds gives a number of conserved quantities along the flow. Defin-

ing α and Ω to be two quantities constant on a particular magnetic surface \star (but which take different values on different magnetic surfaces), the integration of the azimuthal component of the equation of motion gives:

$$rv_\phi - \frac{rB_\phi}{\mu_0\alpha} = L(a) \quad (2a)$$

$L(a)$ being the conserved specific angular momentum (specific angular momentum L_{Matter} of propelling wind + specific angular momentum L_{Field} of the magnetic field associated) on a particular magnetic surface. \dagger Defining $Q(a)$ to be the conserved specific entropy along the flow, the assumption that the bulk flow pressure is given by a polytropic equation of index γ is made; i.e.,

$$P = Q(a)\rho^\gamma$$

The total specific energy conservation equation (obtained by integrating the component of equation of motion along the poloidal field assuming the gravitating body to be a point mass) can then be written as:

$$\frac{1}{2}(v_p^2 + v_\phi^2) + \frac{\gamma Q \rho^{\gamma-1}}{\gamma-1} - \frac{GM_{BH}}{r} - \frac{r\Omega B_\phi}{\mu_0\alpha} = \mathcal{E}(a) \quad (2b)$$

The magnetic part of the constant total specific energy ($\frac{r\Omega B_\phi}{\mu_0\alpha}$) is basically the ratio of the Poynting energy flux to the mass flux. The fluid velocity can be expressed as

$$\vec{v} = \frac{1}{\rho} \{ \alpha(a)\vec{B} + \rho r \Omega(a) \hat{e}_\phi \} \quad (2c)$$

Equations 2(a - c) express in integrated form all MHD equations but for the components of the equation of motion normal to magnetic surfaces (Heyvaerts, 1999). For polytropic MHD flow, the constants of motion (for a particular magnetic surface, of course) are thus the set $\{\alpha, \Omega, L, Q, \mathcal{E}\}$. As unknown quantities can be expressed in terms of only the flux function and local fluid density, solution of MHD problem thus boils down in finding the values of $\rho(r, z)$ and $a(r, z)$ supplemented by determination of $\{\alpha(a), L(a), \mathcal{E}(a)\}$, which, unfortunately, unlike $Q(a)$ and $\Omega(a)$ are not given by boundary conditions at the origin of the wind. The set $\{a(r, z), \rho(r, z)\}$ is shown to satisfy the system consists of the Bernoulli

\star The definition of α and Ω comes from viewing the flow as if infinitesimal flux tubes were pipes entrained in rotation with angular velocity Ω , in which plasma flows with a mass flux to magnetic flux ratio α thus implying the flow surfaces to be magnetic surfaces

\dagger Due to torques exerted by MHD forces, the angular momentum of *only* the fluid is not conserved in the motion but the sum total of the ($L_{Matter} + L_{Field}$) is.

equation and Grad-Shafranov (transfield) equation, later being quasi-linear second order partial differential equation which is the projection perpendicular to the magnetic field of the poloidal part of the equation of motion. While the field aligned dynamics of the rotating MHD wind is dictated by the Bernoulli equation, Grad-Shafranov equations determine its geometry. Eventually Bernoulli-transfield systems have been developed to incorporate the special relativistic (Ardavan, 1997, Li, 1993) as well as the general relativistic MHD flows in Kerr space-time (Beskin, et al, 1993, Nitta, et al, 1991, Camenzind, 1986, Beskin, 1997).

It is to be noted at this point that unlike the hydrodynamic accretion powered flows with single acoustic velocity, there are three types of wave mode in MHD plasma flow; they are fast waves, intermediate or Alfvén wave and slow wave. Three critical points would be found along a transonic flow line where the flow becomes sonic, they are fast magnetosonic point, slow magnetosonic point and Alfvén point † with respect to the three above mentioned category of wave modes. A physically acceptable solution probably has to pass through all these three critical points smoothly.

3.2 Analytical/Semi-analytical Works:

The work due to Blandford and Payne (1982, BP82 from now onwards) laid a cornerstone in the field of analytical/semi-analytical study of MHD winds from a rotating accretion disk. Even till date, a major part of the investigations in this area are basically outgrowth of BP82. Assuming infinite conductivity and ignoring the effect of thermal pressure (except within the disk corona), BP82 found self-similar steady state solutions of the ideal MHD equations for a cold, axially symmetric magnetospheric flow from a thin Keplerian disk in which the magnetic field strength B was assumed to be scaled with radius r as $B \propto r^{-5/4}$. Assuming that the disk is threaded by an open poloidal magnetic field lines corotating with the disk at the Keplerian velocity, it was proposed that magnetic stresses can extract the angular momentum from a thin accretion disk facilitating accretion of matter independently of the presence of viscosity. Close to the disk, matter is centrifugally driven outward by gas pressure in a hot magnetically dominated corona

† Toroidal components of the velocity and magnetic field can be expressed in terms of poloidal variable. The quantity $r_A = \left(\frac{L(a)}{\Omega(a)}\right)^{1/2}$ is called the Alfvén radius whose value depends on the magnetic surface. The point $r = r_A$ on a given field line is its Alfvén point, named that way because at this position the poloidal fluid velocity equals the Alfvén speed associated with the poloidal field. The locus of all Alfvén points is the Alfvén surface.

and is frozen along the field lines. A toroidal magnetic field is generated which becomes dynamically dominant at larger radii close to rotation axis and eventually collimates the outflowing winds into a pair of anti-parallel jets moving perpendicular to the Keplerian accretion disk. The self similar solutions are obtained with scaling all physical quantities with spherical radius measured from the centre along a given direction which is equivalent to ignore the boundary conditions at large and small radii. Two classes of collimated wind solutions, depending on final flow velocity, was found. They are

- a) fast magnetosonic winds with paraboloidal asymptotic streamlines.
- b) trans-fast magnetosonic winds that focus onto the rotation axis.

Despite having a number of significant contributions, BP82 suffers from some serious limitations. Firstly, self-similar models are quite unsatisfactory in this aspect that they must have a cut off at a cylindrical inner radius r_{in} which is not too small, whereas present observations suggests that jet originates from the inner region of the disk very close to the central accretor. Secondly, current theoretical as well as observational studies confirm that accretion disk, as well as outflows, being a complex physical system, do follow some particular length scales and can never be self-similar. Thirdly, the formulation of BP82 is for the thin Keplerian flow only, but it is now widely accepted that jet originates from hot and puffed up sub-Keplerian part of the disk. Fourth, BP82 solutions are not imposed to cross the fast magnetosonic points which causes a collapse of the solutions on the symmetry axis at large distances. Lastly, estimation of the matter contained in the jet (amount of matter flowing out per unit time \dot{M}_{out}) was never attempted in their work (or any work related to BP82, so to say). However, still BP82 demands a special attention and it stands as a seminal paper mainly because of the fact that more or less it was a pioneering work in this field which initiated further studies.

Other radial self-similar solutions have been studied by a number of authors (Contopoulos & Lovelace, 1994, Rosso & Pelletier, 1994, Pudritz & Norman, 1986, Königl, 1989). Assuming that the kinetic energy flux comparable to the Poynting flux can be obtained, BP82 model has been extended to the special relativistic case (Li, et al, 1992). A different type of scaling has been proposed very recently (Sauty, et al, 1994, Trussoni, et al, 1996) where latitudinal self-similarity is used with all physical quantities expressed in separable form which permits a better representation of the regions around the rotation axis of the system that are singular in BP82. Without requiring a polytropic equation of state, the heating/cooling conditions to maintain the outflow can be derived in these solutions

a posteriori from the solution, in order to determine whether they are physically reproducible.

Chakrabarti & Bhaskaran (1992) showed that it is possible to obtain a well-collimated bipolar outflow from magnetized accretion disks by analytically solving the complete set of Euler-Maxwell equations with a power law angular momentum distribution in self-similar framework. Their solutions were obtained from the mid-plane of the disk until the outflow reaches the Alfvén point.

Among the other class of MHD winds, one approach (Lovelace, et al, 1991) is based on simplifying the Grad-Shafranov equations, but the solutions suffer from the limitations that they are valid in some restricted region only.

Contribution due to Pelletier & Pudritz (1992) deserves some special attention in this context for identifying a non-self-similar solution (for $\alpha = 3$) and for arguing that BP82 is a special case of their two-dimensional generalised model capable of explaining origin and collimation of centrifugally driven, MHD winds from the surface of a Keplerian disk surrounding both black holes as well as YSOs. Assuming that the magnetic flux in the disk scales as a power law in disk radius r_{disk} as $\Psi \propto r_{disk}^{3/2\alpha}$, they found solutions for a number of quantities in outflows.

Meanwhile, attempts to couple the process in the disk to the outflows have been initiated. However, it has been understood that simultaneously tackling both the disk and the wind region are very difficult due to a number of constraints, the difference of time scales associated with accretion and jets for example. Contopoulos (1996) initiated the study of general solution for axisymmetric flows without imposing the condition that poloidal velocity is parallel to the poloidal magnetic field which allows the magnetic field to be advected by the accreting flows and accumulated onto the axis of symmetry. It has been postulated quite recently that the jet and disk around a BH are symbiotic features which may describe the broad-band emission from a sample of both radio loud and radio quiet quasars and that of our galactic centre, along with a successful modelling of the UV bump of the AGNs (Falcke, 1994 and references therein). Blandford and Königl model had been applied to initiate the link between disk and the jet in some of their work. The total energy of the jet possess an upper bound which is determined from the gravitational potential energy release by the accreting matter in between the marginally stable orbit and the base radius of the jet.

In this context, it is important to mention the necessity of considering the role of general

relativity in studying MHD winds. It has been argued that while dealing with a rotating accretor (a Kerr black hole for example) and a strong gravitational field, use of the full machinery of the general relativistic MHD theory has to be incorporated. Fully relativistic treatment of MHD wind has been investigated (Camenzind, 1986) which shows that it has same number of critical points (slow and fast magnetosonic and Alfvén) as that of the non-relativistic flow. The wind equations can be obtained along the flux tube and the wind carries a current which determines the total angular momentum lost through the outflow.

3.2.1 *Tapping the Hole*

Rotation of thin accretion disk around a spinning black hole may cause the magnetic lines to sweep the ambient plasma which consequently feels a strong induced poloidal electric field thus generates electromagnetic winds from force-free magnetospheres above the disk and both energy and angular momentum are carried away by an electromagnetic Poynting flux: energy is focussed on the rotation axis and carried away along it as an electromagnetic wind (Blandford, 1976, Lovelace, 1976, Blandford & Znajek, 1977, MacDonald & Thorne, 1982, Phinney, 1982). At large distance, an ambient plasma can absorb the Poynting flux and give rise to particle jets. Possibility of rotational energy extraction from Kerr black holes have been extensively investigated. A spinning BH threaded by magnetic field lines supported by external currents flowing in an equatorial disk, a large electric potential difference is established between the poles and the equator. § This large amount of potential difference may produce a cascade of electron-positron pairs by vacuum breakdown and a surrounding force-free magnetosphere would be established. After deriving a set of equations describing a stationary axisymmetric magnetosphere, details of the energy and angular momentum balance are discussed and electromagnetic extraction of energy and angular momentum are demonstrated. Idea of the Poynting flux driven jets are incorporated to discuss models of AGN containing a SMBH surrounded by a magnetized accretion disk to produce two oppositely oriented channelling of energy to outer medium.

§ For a $10^8 M_{\odot}$ hole with 10^4 G magnetic field, $\sim 10^{20}$ V potential drop may develop capable of maintaining $\sim 10^{18}$ Amp current from horizon to infinity!

3.3 Numerical Simulation Work:

Because of the formidable difficulties in providing exact solutions of intrinsically complicated set of multidimensional nonlinearly coupled partial differential equations describing fully the jets launching from rotating magnetized accretion disks and magnetospheres around the central accretor, analytical solution for MHD jets are limited in their applications which motivated efforts to study jet formation using numerical simulation. Fully time dependent 3-D analysis is required to explore the onset and evolution of the physical effects beyond the linear level. Usually, perfect MHD conditions are imposed and the jet producing objects enters only in the form of a set of boundary conditions. Relaxation to a stationary state is not granted, especially so when the back reaction of angular momentum extraction by the MHD flow on the source is considered. Broadly speaking, two specific regions addressed by numerical simulation of MHD winds are:

- The region from which MHD winds are launched. Accreting matter enters in this region (usually) with sub slow-magnetosonic speed and leaves this region (usually) with super fast-magnetosonic speed.
- The accretion disk along with its various kind of dynamical instabilities like Velikhov-Chandrasekhar-Balbus-Hawley instability which demands a good 3-D simulation to tackle MHD turbulence.

As already mentioned, the set of equations governing a thermodynamic system of compressible fluid are non-linearly coupled multidimensional partial differential equations. They are transformed into a linear system of equations by a finite difference scheme and are solved by adopting implicit or explicit algorithm with adaptive choice of grids. Dissipative processes through shocks are treated by different methods like classical Lax-Wedroff (artificial viscosity introduced by adopting dissipation terms in linear approximation), hybrid flux-correlated transport FCT (dissipation is non-linear and different for two different zones), Godunov method adopted in the Parabolic Piecewise Method PPM (solves a standard Riemann problem for the non-linear waves by considering cells to be uniform states and by an upwind differentiation in the direction of characteristics), Smoothed Particle Hydrodynamics SPH (treats cells as particles interacting via collisional terms) and Total Variation Diminishing TVD method.

3.3.1 Non-stationary Winds:

By solving an initial value problem in axisymmetric geometry using a Lax-Wendroff numerical scheme, Uchida and Shibata (1985, 1986,) first initiated the study of time dependent non-linear impulsive MHD disk-winds from systems that were initially violently out of equilibrium. These results have been extended to the complete 3-D geometry (Shibata & Uchida, 1990), to the accretion/ejection system which starts from close to the equilibrium situation (Matsumoto et al, 1996) and to general relativistic conditions(Koide et al, 1998). In the later case a pressure-driven wind appeared to emanate from the region devoid stable orbit around a Schwarzschild hole. Usually in these kind of models, ideal MHD equations are solved in cylindrical geometry by assuming the existence of a cold geometrically thin disk rotating at Keplerian or sub-Keplerian azimuthal velocity. Uniform magnetic field penetrates the disk vertically and presence of a non-rotating corona outside the disk is assumed. A toroidal structure is developed by bending of poloidal lines by disk rotation and the magnetic tension of the disk is released as large-amplitude torsional Alfvén waves along the poloidal lines. This process extracts angular momentum from the disk and mass is ejected along the poloidal lines giving rise to a hollow cylindrical jet. The jet propagates with a local speed greater than the Keplerian velocity. Investigations of launching of MHD winds from axisymmetric thick disks instead of thin Keplerian disks has also been performed. The back reaction of jet formation has been studied there. Results are similar to that obtained from thin disk case except that the accretion avalanche can actually be seen. Magnetic reconnection was shown to take place and it was suggested that it might be used to produce nonthermal particles.

Ouyed and Pudritz (Ouyed & Pudritz, 1997) applied their model to analyze the influence of the magnetic topology on the solution and proposed a robust method of solving the case of bursting outflows. Their model of episodic outburst did not reach a stationary state because the strong toroidal field in a well-defined region of the inner jet tends to re-collimate the flow towards the axis, producing a series of MHD shocks. A compact confined structures periodically launched from the disk and knotty structures would automatically be produced. Back-reaction from the jets are, however, had been neglected in their work. Countopoulous (1995) proposed another time-dependent analysis of self-collimated explosive outbursts launched from the disk due to strong pressure gradient

between the disk and the corona over it. A knotty structure is also reported in fully general relativistic calculations (Van-Putten, 1996).

3.3.2 Stationary Winds:

However, outflows in all models described above are not stationary; matter flux in the jet grows to a peak and then decreases to relatively small values. This kind of simulations thus produce a temporary outburst of matter rather than a continuous outflow. A condition for stationary outflow is the continuous supply of matter and magnetic field to the disk corresponding to the steady output of power along the jet by the Poynting flux of the torsional Alfvén waves. Below we describe some important works which deal with stationary outflows.

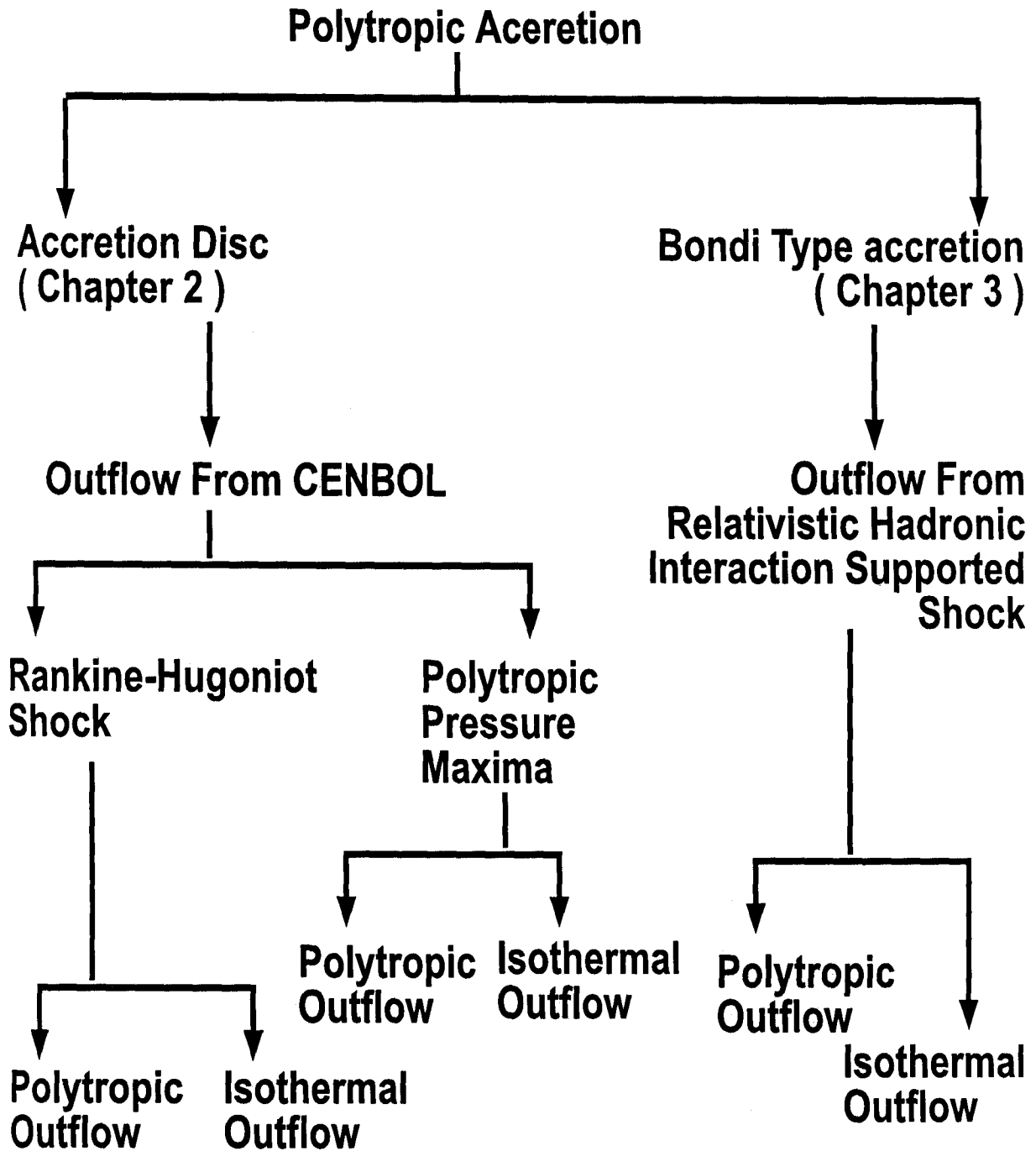
Romanova et al (1997) initiated the study of stationary MHD winds by assuming an outflow originating from a disk that is considered as a fixed boundary: the initial magnetic field was taken to be a tapered monopole field. Subsonic matter pushed out of the disk was accelerated through three MHD sonic points and becomes super-fast magnetosonic. Their work could not provide collimation at large distances. Ustyugova et al (1995) took the initial magnetic field to be a split-monopole poloidal field configuration frozen into the disk. The disk was treated as a perfectly conducting time-dependent density boundary in Keplerian rotation which is different from earlier work of small velocity outflows. Close to the disk, the outflow was driven by the centrifugal force while at all larger distances the flow is driven by the magnetic force assumed to be proportional to $-\vec{\nabla}(rB_\phi)^2$, B_ϕ being the toroidal field. Ouyed and Pudritz (1997a) presented 2.5 - D time-dependent simulations of the evolution of nonrelativistic outflows from Keplerian disks steadily orbiting a central point mass accreting at sub-Eddington rate. A cold corona was assumed to prevail the disk and matter was injected from the disk at very low speed into the corona. Collimation is obtained due to the pinching force on the toroidal field that is self-consistently generated by the outflow dynamics. In another approach which is basically consistent with the analytical work of BP82, Meier et al (1997) performed an extended analysis of the parameter space of time dependent numerical simulation of the outflow induced by the corona of magnetized accretion disks. The advantages of their work is that the strength of the field used in their work could be much higher than in most other simulations. A thin cold dense gas along with a tenuous hot corona was assumed, initial

magnetic fieldlines were purely poloidal and are anchored in the disk and protrude into the corona at an angle $\theta \lesssim 60^\circ$ with respect to the disk. The resulting outflow is collimated into a jet in all cases and its dynamical characteristics depend on the ratio of the Alfvén velocity (of the corona) to escape velocity. The correlation of weakly magnetized outflow with FR I jets and of highly magnetized ones with FR II jets was also suggested in their work. Their simulations can easily be extended to the special relativistic case showing the break down of current MHD wind theories for low magnetic fields, as they pointed out, in this regime, gravitational effects that are generally neglected, become important. Their solution provides a high Lorentz factor of jet as large as $\Gamma_j \approx 10$.

Though magnetocentrifugal mechanism possess two important advantages over other mechanisms; firstly, magnetically accelerated flows can attain much higher Lorentz factors than flows accelerated by radiation and/ or gas pressure and secondly, the development of a predominantly toroidal field will lead to the self-collimation of a magnetized flow which need not require introduction of any ad hoc mechanism to explain the collimation of jets, a number of shortcomings are also there associated with this mechanism. Firstly, there are indications (Begelman, 1993) that the rate of collimation produced by magnetic stress alone is rather low. Secondly, high Lorentz factor MHD outflows tend to recollimate towards the jet axis and their evolution beyond that point is uncertain (Contopoulos & Kazanas, 1995 and references therein). An important ingredient of these models is that the disk and the associated magnetic field exists to values of the cylindrical radius $R = 0$, otherwise the pressure balance in the plane perpendicular to the jet direction is not maintained which might be a severe problem for AGN jets because region along the jet axis is devoid of magnetic field mainly because of the presence of the black hole and/ or the power instabilities which tend to disrupt the smooth disk and ordered magnetic field needed for the mechanism to work in the black hole vicinity (Contopoulos & Kazanas, 1995 and references therein). In the absence of an additional pressure to maintain the equilibrium, such a configuration would suffer a z-pinch instability (Eichler, 1993) and the geometry required for the MHD acceleration and the formation of a jet might be destroyed. Another important problem with self-similar MHD wind is that a self-similar model requires that the poloidal magnetic field scale with radius as $B_p \propto R^{-5/4}$. A field which varies so steeply with decreasing radius R , whether exists in reality at all, is genuinely a debatable issue. Situation get worse if slipping of field lines are allowed (Begelman, 1993).

4 'JET LAGG': THE MISSING PHYSICS

The various categories of mechanisms for extraction of winds from accretion disk discussed so far in this chapter, though works excellently in investigating a number of important issues in the context of formation, dynamics and collimation of galactic and extragalactic jets, suffers from limitations when used to investigate some crucial features. As argued in Chapter 1.1 and Chapter 1.3, formation of jets/ outflows emanating from sources powered by compact objects must be explained only from the knowledge of associated accretion processes. Also the major quantities associated with outflows and its dependence on various parameters should be calculated using the accretion parameters only. Another extremely important point to be emphasized is that self-similar models (mostly used to explain jet formation), however mathematically correct they are, must not be considered to represent the actual physical situation because outflows *do* choose a *specific* location on the disk to be launched from and the location of this base of the jet *must be as close as possible* to the central object with the ratio of the radius at which launching takes place to the radius of the central compact object $\lesssim 10^2$ (that this *genuinly* happens in reality, is firmly supported by latest observations of extra-galactic jets, see Chapter 4.) rather than what happens in self-similar flows where most of the mass is lost at larger radii. Thus along with a general prescription capable of explaining the jet formation mechanism as well as rightly locating the *exact* region of the disk from where the jets launch, self-consistent computation of the fraction of accreting matter being expelled as jet should make the solid building blocks of a viable outflow model as we believe. At the best of our knowledge, none of the models present in the literature (though Pelletier & Pudritz (1992) proposed a scheme for calculating the mass loss rate and could identify a non-self-similar solution for $\alpha = 3$, their results are highly restrictive and are not general enough because of the fact that in their work investigation of complete parameter space spanned by energy, angular momentum and accretion rate, the three most important ingredients for accretion flows, have not been achieved satisfactorily) could satisfactorily address these two extremely important issues. In next chapters we will describe our model which successfully attempts to address these issues as we believe. A schematic 'flow-chart' diagram illustrating the organization of our whole work is presented in next page.



Global Transonic Advective Accretion: The Complete Prescription for Diving into the Hole

Chapter 2.1

SUMMARY

Basic properties of advective accretion, which is used in order to describe inflow in our disk-outflow model, is thoroughly described. Fundamentals of shock formation in transonic astrophysical flows are rigorously discussed.

1 PRESENTING THE MODEL: BASIC PHILOSOPHY AND GOVERNING EQUATIONS

As discussed in chapter 1.2, the spherical Bondi accretion and the Keplarian disk (standard thin SS73 disk.) are both extreme cases of the general accretion phenomena. While the former (Bondi accretion) only advects with no rotation (dynamical velocity of accretion is considered to be primarily radial), the latter (thin disk) does not include advection in a self-consistent manner. This made the Bondi accretion a conserved energy flow (extremely high radial velocity does not allow energy radiation), whereas standard thin disk model is highly dissipative (for low viscosity and high accretion rate). Realistic flow can never be mapped with either of these two models individually since accretion will have at least some amount of intrinsic angular momentum (whether it comes from the binary companion or from the orbiting stars around the compact object ^{*} which will resist the flow to have radial velocity only. Similarly, the inner boundary condition at black hole horizon and the intense gravitational attraction close to the hole resists matter from rotating eternally without a finite radial velocity (one must remember that matter *has to* fall through the event horizon anyway). Again, unlike a standard thin disk where the

^{*} However, for the later case, Bondi flow, sometime, may be a very good approximation when vector sum of the angular momentum of accreting matter coming from different stars approaches zero by cancelling the individual angular momentum vector; see Chapter.

Keplarian distribution of angular momentum is dogmatically granted to be satisfied independent of viscosity prescription, in reality, the angular momentum distribution, in principle, *can* deviate from Keplarian value due to the presence of various dissipative mechanisms present in large scale real astrophysical flows.

Thus a realistic astrophysical flow *must* follow an intermediate description lying between purely advective (Bondi type) or purely rotating (thin disk) flow and it (the flow) *should* possess angular momentum distribution which *does deviate* from Keplarian value. Depending on various realistic initial boundary conditions, the distribution may be super/sub Keplarian and flow may join with Keplarian part at some viable distance, but it *must not* be Keplarian *everywhere* in space. On the other side, nature of the emitted radiation from the vicinity of black hole candidates (binary black hole as well as the holes residing at galactic centre) are very complex and simple solutions like Bondi flow or standard thin disk model can not take care of it completely. For Bondi type accretion, as already mentioned, high free fall velocity of matter does not allow a considerable amount of mass to energy conversion efficiency thus is unable to explain the energy sources and spectrum of highly luminous astrophysical objects like Quasars and AGNs (see Chapter 1.2). Also the standard disk model, though had been very useful in interpreting some observational results in binary systems and active galaxies (Pringle, 1981, Sapiro and Teukolsky, 1983, Frank et al, 1992) and worked well in explaining some interesting features like Big Blue Bump (BBB) seen in UV regions of active galaxies (Malkan, 1982, Sun and Malkan, 1989 and references therein), is not quite sufficient to explain more detail and recent observational results in a satisfactory manner. As for example, with the advent of space-based observations, the X-ray and γ -rays spectra of AGNs show that there could be even bigger bumps (compared to BBB) in the X-ray regions of their spectra which could not be properly explained using standard disk model. Another important issue has been the 'two-faced' spectra of some galactic black hole candidates (like GS1124-68) which shows two distinct spectral components (soft and hard) which apparently vary quite independently (Tanaka 1989, Ebisawa et al, 1993, Inoue, 1992). This phenomenon was also remained unexplained when only standard disk model had been in use. It was gradually understood that the standard thin disk solution, being a cooler one in general, cannot explain the production of energetic X-rays and γ -rays. Also the zero time lag correlated variabilities observed in some active galaxies (NGC 4151, NGC 5548 for example, see Clivel et al 1990, Peterson et al, 1991, and Perola et al, 1986) could not be explained by

invoking SS73 model only. Explanation of the hard components seen in the spectra of neutron stars and the black holes (galactic as well as extra-galactic) could not be explained in the framework of standard disk model only. Also, theoretically speaking, standard thin disk model was unable to provide what happens to accreting matter after crossing the marginally bound orbit ($3r_g$ for a nonrotating hole where the disk terminates) and the prescription to satisfy the inner boundary conditions on black hole horizon was not provided. Also it was pointed out (Lightmann and Eardly 1974) that the inner regions of the disk was viscously unstable.

Meanwhile, it was realized that neither the Bondi flow nor the standard thin disk model could individually fit the bill completely and theoreticians were convinced about the necessity of having an intermediate model which could bridge the gap between purely spherical flow (Bondi type) and purely rotating flow (standard thin disk) by making attempts to successfully incorporate a self-consistent advection term which could take care of finite velocity of accreting material (for the black hole candidates which may gradually approaches the velocity of light to satisfy the inner boundary condition on event horizon) along with its rotational velocity and generalised heating and cooling terms (Hoshi and Shibasaki, 1977, Liang and Thompson, 1980, Paczyński and Wiita, 1980, Ichimaru, 1977, Paczyński and Bisnobhatyi-Kogan, 1981, Abramowicz and Zurek, 1981, Muchotrzeb and Paczyński, 1982, Fukue, 1987, Abramowicz et al, 1988, Narayan and Yi, 1994). Several conclusions drawn in various works were not satisfactorily self-consistent and, though were able to explain some features in a case-by-case basis, those models were not globally valid. Paczyński and his collaborators (Paczyński and Bisnobhatyi-Kogan, 1981, Paczyński and Wiita, 1980) had attempted to include advection and pressure effects in the so-called transonic accretion disks although no systematic study of global solutions was performed. Global solutions of thick accretion disks could be performed (Paczynski and Wiita, 1980) only when advection term was dropped (see §4.2 of Chapter 1.2 for details). The global solution of Abramowich et al (1988) was not completely satisfactory because the angular momentum distribution in their work, instead of joining to Keplerian, deviates away from it close to the outer edge of the disk. The existence of a special α parameter in Muchortzeb (1983) was contested by Abrmowicz and Kato (1989) as an artifact of finite distance of boundary. Solutions due to Narayan and Yi (1994), though mathematically correct, studied self-similar solution only. A black hole accretion, as is evident from current theoretical as well as observational knowledge, can *never* be self-

similar: thus *only* the solution which are *not* self-similar, should be of proper interest.

The first satisfactory global solutions in the optically thin or thick limit with advection, viscosity and general heating and cooling properly included, have been presented in a series of work by Chakrabarti and others (Chakrabarti, 1989 (C98 from now onwards), 1989a, 1989b, Chakrabarti, 1990, Chakrabarti, 1996 (C96 from now onwards), Chakrabarti, 1996a, 1996b, Chakrabarti, 1997 (C97 from now onwards), Chakrabarti & Titarchuk, 1995 (CT95 from now onwards), Chakrabarti and Molteni 1993, 1995, Molteni, Lanzafame & Chakrabarti, 1994). Global solution was predicted for inviscid flow (C89) as well as viscous flow (C96), isothermal flow (Chakrabarti, 1989b) as well as polytropic flow and flows on Schwarzschild as well on Kerr black hole (C96b). It was specifically mentioned in their work that disks are *not* Keplarian everywhere, especially at the inner boundary. A Keplarian flow at the outer boundary can become sub-Keplarian at the inner edge (or, contrarily, an initially sub-Keplarian flow can become almost Keplarian when viscosity in the flow is very high (CT95). A unified description of what the flow might do suggests that the flow will have multiple sonic points (C89). For a given entropy of the flow, when the accretion rate is small enough, the flow passes through the outer sonic point and remain supersonic before falling into the hole, while it passes through the inner sonic point when the rate is high. In the intermediate case, flow may be disrupted by a Rankine-Huoniot kind of shock. The combined effects of the shock and the viscosity generates the right amount of entropy to allow the flow to pass through the inner sonic point. The energy of the flow is either constant or nearly so, because the energy and entropy are advected with the flow towards the hole. So it means that advective accretion flows are those which self-consistently include advection velocity as in Bondi flow as well as include rotation at the same time along with properly taking care of general heating and cooling processes and viscosity at the flow.

Based on analytical solutions of generalised advective accretion disk model (C89, C96, CT95, Chakrabarti and Molteni, 1995, C97) it has been shown that an accretion disk should naturally segregate into two regions, one a Keplarian disk on equatorial plane and the other a sub-Keplarian halo flanking the Keplarian disk, although eventually the Keplarian component should also become sub-Keplarian close to the hole, in order to satisfy boundary conditions on the horizon. The sub-Keplarian halo is hot, optically thin and faces a centrifugal barrier close to the hole: as a result, its density increases much faster than that of a spherical Bondi flow and produce a puffed up optically thin gas lo-

cated just outside the horizon, which may intercept soft photons coming from the cooler Keplerian disk and re-emit them as photons of higher energy (hard X-rays and γ -rays in case of galactic black holes and UV and soft X-rays in case of SMBHs).

1.1 Governing Equations

The set of stationary steady state equations governing the general advective accretion disk models are (C96):

(i) The radial momentum equation

$$u \frac{du}{dx} + \frac{1}{\rho} \frac{dp}{dx} + \frac{l_{kep}^2 - l^2}{x^3} = 0 \quad (1a)$$

(ii) The continuity equation

$$\frac{d}{dx} (\Sigma x u) = 0 \quad (1b)$$

(iii) The azimuthal momentum equation

$$u \frac{dl(x)}{dx} - \frac{1}{\Sigma x} \frac{d}{dx} (x^2 W_{x\phi}) = 0 \quad (1c)$$

(iv) The entropy equation

$$\begin{aligned} \Sigma u T \frac{ds}{dx} &= \frac{h(x)u}{\Gamma^3 - 1} \left(\frac{dp}{dx} - \Gamma_1 \frac{P}{\rho} \frac{d\rho}{dx} \right) = Q^+ - Q^- \\ &= \alpha q^+ - g(x, \dot{M}) q^+ \\ &= f(\alpha, x, \dot{M}) Q^+ \end{aligned} \quad (1d)$$

Where, $l_{kep} = \sqrt{\frac{x^3}{2(x-1)^2}}$ is the Keplerian angular momentum, $l(x)$ is distance dependent specific angular momentum, u is the radial velocity, s is the entropy of the flow, α is the Shakura Sunyaev (1973) viscosity parameter, $W_{x\phi}$ is the so called ' π stress' (C96), Σ is the vertically averaged density, \dot{m} is the mass accretion rate, Q^+ and Q^- are the general heating and cooling terms and

$$\Gamma_1 = \beta + \frac{(4 - 3\beta)^2(\gamma - 1)}{\beta + 12(\gamma - 1)(1 - \beta)}, \quad \Gamma_3 = 1 + \frac{\Gamma_1 - \beta}{4 - 3\beta}$$

Where $\beta(x)$ is the ratio of gas pressure to total pressure

$$\beta = \left[\frac{\left(\frac{\rho k T}{\mu m_p} \right)}{\left(\frac{\sigma T^4}{3} \right) + \left(\frac{\rho k T}{\mu m_p} \right)} \right]$$

σ being Stephan's constant, k Boltzmann's constant, m_p mass of the proton, and μ is the mean molecular weight.

It follows from eqn. (1a) that advective accretion flow can never be Keplerian everywhere. Had it been the case that the disk would be strictly Keplerian everywhere, l would be equal to l_{kep} everywhere and eqn. (1a) would be satisfied only if

$$u \frac{du}{dx} + \frac{1}{\rho} \frac{dp}{dx} = 0 \quad (2a)$$

at all the points. For a polytropic flow, $p = p(\rho)$ and the integral of eqn.(2a) gives

$$\frac{u^2}{2} - \Phi(p) = \Phi_0 \quad (2b)$$

Where Φ_0 is the value of the potential $\Phi = -\int \frac{dp}{\rho}$ at $u = 0$ surface. Since the potential must be negative for a bound flow, we see that above equation cannot be satisfied unless $\Phi = 0 = u$ everywhere, i.e., when the flow is strictly non advecting.

2 NON-DISSIPATIVE, INVISCID, TRANSONIC, POLYTROPIC THIN ADVECTIVE ACCRETION: OUR INFLOW MODEL

A realistic system found in nature is full of complex details and is extremely difficult to completely study analytically (or even, by means of numerical simulation also). Usual procedure to model a system is to treat it in such a manner which retains the salient features of the original system, yet the analysis remains simple enough so that the detailed study of the principle aspects may be possible. In the context of the disk-outflow system, we consider an idealistic inflow to keep the problem tractable. The equations of motion are written on the equatorial plane of the central compact object but the flow is in hydrostatic equilibrium in the transverse direction; that is, the radial momentum equation and equation of continuity are formulated on the equatorial plane while the shock conserved momentum balance equation is vertically integrated. Axially symmetric, dissipation free, thin, rotating adiabatic accretion onto the central accretor is considered. The vertical equilibrium in the transverse direction is assumed, while any dynamical velocity along it is neglected. Flow has been assumed to be inviscid near the hole thus specific angular momentum of accreting matter is taken to be practically constant. Matter is assumed to accrete only due to pressure gradient force. Accretion is taken to be radiatively inefficient in the sense that the entropy generated at the shock (if forms) as well the entire energy is assumed to completely advected towards the hole. So in some sense, we concentrate only on dissipation-free flows (absence of any explicit heating and cooling everywhere

except at post-shock location), dissipation is only allowed at the shock † (if forms) where temperature rises and entropy is generated (see §3.2). Self-gravity of the flow is ignored and the potential term is derived from a pseudo-Newtonian description of space time around the Schwarzschild black hole (Paczynski-Wiita potential(PW80), see also §4.2 of Chapter 1.2) which enables one to use the Newtonian equation of motion while keeping the salient features of the black hole space-time intact. Integrating equations (1a) and (1b) by employing a polytropic equation of state $p = K\rho^\gamma$, two stationary conservation equations expressed in geometric units are (C89, Das 1998, Das and Chakrabarti, 1999)

(i) Conservation of specific energy:

$$\mathcal{E} = \frac{u_e^2}{2} + na_e^2 + \frac{\lambda^2}{2r^2} - \frac{1}{2(r-1)}. \quad (3a)$$

where, u_e and a_e are the radial and polytropic sound velocities respectively. $a_e = (\gamma p_e / \rho_e)^{1/2}$, p_e and ρ_e are the pressure and density of the flow. For a polytropic flow, $p_e = K\rho_e^\gamma$, where K is a constant and is a measure of entropy of the flow. Here, λ is the specific angular momentum and n is the polytropic constant of the inflow, $n = (\gamma - 1)^{-1}$; γ is the polytropic index. The subscript e refers that the quantities are measured on the equatorial plane.

(ii) Conservation of inflow Barion number:

$$\dot{M}_{in} = u_e \rho_e r h_e(r), \quad (3b)$$

where $h_e(r)$ is the half-thickness of the flow at radial co-ordinate r having the following expression

$$h_e(r) = a_e r^{\frac{1}{2}} (r-1) \sqrt{\frac{2}{\gamma}}. \quad (3c)$$

Another useful way of writing the mass inflow is to introduce an entropy dependent quantity $\dot{\mathcal{M}} \propto \gamma^n K^n \dot{M}$ which can be expressed as

$$\dot{\mathcal{M}} = u_e a_e^\alpha r^{\frac{3}{2}} (r-1) \sqrt{\frac{2}{\gamma}} \quad (3d)$$

Where, $\dot{\mathcal{M}}$ is really the entropy accretion rate (C89, Das & Chakrabarti, 1999). When the shock is not present (see §2.2.2.1), $\dot{\mathcal{M}}$ remains constant in a polytropic flow. When the shock is present, $\dot{\mathcal{M}}$ will increase at the shock due to increase of entropy. $\alpha = (\gamma + 1)/(\gamma - 1) = 2n + 1$.

† A realistic flow, however, should have dissipations in various form everywhere, not only at the shock. The structure of the weak shocks would be more affected by various dissipation mechanisms compared to the strong shocks. (Chakrabarti, 1989a).

At this point, it is worth discussing the validity of the basic equations discussed and upto what extent they capture the physical process in accretion. The energy conservation equation, as stated earlier, is obtained by integrating the radial momentum equation written in one dimension. If one wants to study the general flow characteristics analytically (which is done here in this work), nothing better could be done till date. It is argued that (Chakrabarti, 1989a) minor changes in the form of energy equation would not drastically change the topology of the solutions. The vertical component of velocity has been neglected throughout which can be shown to be valid where the flow is thin and the shocks are angular momentum supported (which is true for model described here) which is the case in reality close to the hole. Mass conservation equation (eqs. (3b)) would have been derived in two different ways as follows:

(i) The continuity equation is written on the equatorial plane, but the flow thickness is calculated with assumption of vertical equilibrium.

(ii) The continuity equations are first vertically averaged (Matsumoto et al, 1984) and then is integrated. Also the pressure balance equations at shock, as has been urged (Chakrabarti, 1989a) can not be obtained in closed analytic form unless the flow is simplified to be strictly one dimensional.

So it is clear that the assumptions made to simplify the equations of flow dynamics are not unjustified and the model used here does represent the real physical scinario to a close approximation.

3 GETTING SHOCKED WHILE FLOWING IN: PHYSICS OF SHOCK FORMATION IN TRANSONIC ASTROPHYSICAL ADVECTIVE ACCRETION

As already mentioned several times, for accretion onto central black hole in binary systems and in active galaxies, the angular momentum distribution need not always be Keplarian everywhere. A sub-Keplarian flow originated by any of the various possible reasons discussed in §1 will have a significant radial velocity since in these kind of flows the centrifugal force would not be sufficient enough to locally overcome the gravity. It (the flow) would first accretes quasi-spherically with an infall time scale similar to that of free fall time scale ($\tau_{quasi-spherical} \sim \tau_{free-fall}$) until the specific angular momentum of the flow becomes comparable to the local Keplarian angular momentum at a distance of around $\sim \lambda^2(r)$ where the flow may be virtually stopped by the centrifugal barrier re-

sulting disruption of flow followed by angular momentum supported shock formation. Location of shock depends on various accretion parameters and on different heating and cooling mechanisms. The shock heated zone with shock generated higher entropy density may occupy a considerably large area of the disk thereby greatly influences the disk spectra. In our work also, the formation of shock along with its location and strength significantly contribute to the outflow mechanism and potentially controls the mass outflow rate. So it is obvious that the question of the shock formation and its existence around the central accretor is important and does deserve a somewhat detail discussion. We do it in subsequent parts of this section. In §3.1 (largely adopted from Landau & Lifshitz, 1998) we illustrate the primary notions of shock formation in general fluid flow while in §3.2 we describe shock formation in polytropic thin advective accretion flows around a Schwarzschild black hole.

3.1 Fundamentals of Shock Formation in General Fluid Flow

One of the most important distinctive features of the supersonic flow (flow characterized by the condition $M > 1$; M being the Mach number of the flow which is the ratio of the dynamical velocity of the flow to its sound velocity) is that shock may occur in it due to various kind of perturbations in propagation. By perturbation we mean a slight change in any of the quantities characterizing the state of the flow. Perturbations in entropy and viscosity are of special importance in this regard that they do not propagate with the velocity of sound and for perturbations of entropy and vorticity, the characteristics are streamlines. Some of the perturbations of specific nature may produce discontinuities in the flow. A discontinuity in a flow is said to take place over one or more surfaces when quantities characterizing the flow (dynamical as well as thermodynamic), some or all, may change discontinuously as such a surface(s) are crossed; the surface(s) is (are) called *surface (surfaces) of discontinuity*. In non-steady flow the surfaces of discontinuity, in general, do not remain fixed. Certain boundary conditions must be satisfied on surfaces of discontinuities; the usuals are density ρ , mass flux density ρu , energy flux density $\rho u \left(\frac{1}{2} u^2 + w \right)$ and the momentum flux density $(p + \rho u^2)$ must be continuous across the surfaces of discontinuities. Mathematically the continuity equations (in one dimension, say, along the x direction) may be summarized as (Landau and Lifshitz, 1998):

$$[\rho u_x] = 0 \quad (4a)$$

$$\left[\rho u_x \left(\frac{u}{2} + w \right) \right] = 0 \quad (4b)$$

$$\left[p + \rho u_x^2 \right] = 0 \quad (4c)$$

$$[\rho u_x u_y] = 0 = [\rho u_x u_z] \quad (4d)$$

Where $[A + B] = \{(A + B)_+ - (A + B)_-\}$, (+) and (-) refers the quantities measured just after and just before the flow encounters the surface of discontinuity. The above equations are the complete set of boundary conditions which are to be satisfied at the surface(s) of discontinuities. Two types of discontinuities are possible in general:

(i) *Type1*: Mass flux through the surface of discontinuity is zero. The normal component of viscosity and gas pressure are continuous while the tangential velocity and all other thermodynamic quantities (except pressure) concerned may be discontinuous by any amount. This is called *tangential discontinuity*. A particular class of this kind of discontinuity is referred as a *contact discontinuity* where the velocity is continuous, but not the density (and the other thermodynamic quantities except pressure). For this type of discontinuities, it can be shown (Landau and Lifshitz, 1998) that for both compressible as well as incompressible fluids, the discontinuity in tangential velocity component are unstable and must spread to form turbulence.

(ii) *Type2*: Non-zero mass flux through the surface(s) of discontinuity. Tangential velocity component is continuous while normal component of velocity along with all thermodynamic quantities including pressure are discontinuous. The modified set of boundary conditions (as both u_y and u_z are continuous, u^2 may be replaced by u_x^2 in eqn. (4d)) are:

$$[\rho u_x] = 0 \quad (5a)$$

$$\left[p + \rho u_x^2 \right] = 0 \quad (5b)$$

$$\left[\frac{1}{2} u_x^2 + w \right] = 0 \quad (5c)$$

Discontinuity of this kind is called a *shock wave* or simply a *shock*. Thus shocks are the more general kind of discontinuities compared to the tangential discontinuity. If the shock is perpendicular to the direction of propagation, it is called a *normal shock*, otherwise is called an *oblique shock*.

3.2 Standing shock in Transonic Astrophysical Accretion

Shock waves (steady or non-steady) in transonic astrophysical accretion are nowadays thought to be an indispensable part of low angular momentum region of an advective accretion disk (Chakrabarti, 1996a, C96, Fukue, 1987, Lu, et al, 1997, 1997a, 1998, Bisnovatyi-Kogan, 1998). In the context of study of solar and stellar winds, where the variation of geometrical shape of the wind and deposition of radiation momentum led to the formation of more than one sonic point and some stationary solutions including shocks, have been constructed by introducing sudden changes in the flow cross section or by momentum deposition (Holzer, 1977, Ferrari, et al, 1985 and references therein). In the context of accretion onto compact objects, the presence of significant amount of intrinsic angular momentum in accreting matter increases the number of saddle type sonic points from one to two (Liang & Thompson, 1980). Early numerical simulation works revealed the presence of travelling waves in low angular momentum accretion flows (Hawley, Smarr & Wilson, 1984,1985). Subsequently, using a simple model of conical adiabatic flows, it was pointed out that similar to the solar wind case, multiple sonic points may lead to a solution with shock waves in the disk as well (Fukue, 1987). Along with the examples of axisymmetric shocks, either analytical or semi-analytical non-axisymmetric shock solutions are also present in the literature (Swada et al, 1986, Spruit, 1987). In above mentioned works, shock solutions were produced on a case by case basis and no general dependence on global accretion parameters were provided. † Abramowich & Chakrabarti (1990) were the first who pointed out, in general terms, the possibilities of three types of discontinuities in accretion flows depending upon the three extreme physical conditions in shocks and the full set of shock solutions for inviscid, rotating, thin 1.5 dimensional accretion flows onto Schwarzschild black holes was presented in related works for adiabatic accretion (C89) and for isothermal accretion (Chakrabarti, 1989b). In their classification, apart from preserving the baryon number flux densities and momentum flux densities, the flow was shown to preserve the energy (Rankine-Hugoniot shock, will be referred as RSHK from now onwards), the entropy (Isoentropic compression waves, will be referred as ICW from now onwards) or the temperature (Isothermal shocks, will be referred as ISH from now onwards) through the surface(s) of discontinuities. Though we mainly concentrate on RSHK and related details in our disk-outflow model, it is of no harm

† We do not refer works dealing with shocks in spherical accretion here. Those will be discussed in Chapter 3. in detail.

to spend a few paragraphs to provide a sketchy outline of shocks of these three types, namely RSHK, ICW and ISH, and features differentiating them. We do it in following paragraphs. In passing, it is to be mentioned that the treatment for obtaining full set of shocks for an inviscid flow have been modified to incorporate viscosity and general heating and cooling mechanism as well (CT95, C96). Like flows on Schwarzschild geometry, complete set of shock solutions have been investigated for accretion onto Kerr black hole as well using full general relativistic framework (Chakrabarti, 1996b, Lu, et al, 1997, 1997a, 1998).

Let \mathcal{E} , T , S and $\dot{\mathcal{M}}$ are the specific energy, temperature, specific entropy and entropy accretion rate respectively at the shock. Subscript plus (+) and minus (−) denote quantities before and after the shock respectively. Following are then the fundamentals of three types of shocks already mentioned (see Chakrabarti, 1990 for a detail discussion):

(i) *RSHK*: Radiative cooling mechanism in this type of discontinuity is extremely inefficient. No energy is radiated away through the surface of the flow and specific energy \mathcal{E} of accreting matter is a shock conserved quantity. Higher post-shock temperature (because of the excess shock-generated entropy) puffs up the postshock flow and post shock sound velocity is also increased. The following relations hold for RSHK:

$$\mathcal{E}_+ = \mathcal{E}_-$$

$$T_+ > T_-$$

$$s_+ > s_-$$

$$\dot{\mathcal{M}}_+ > \dot{\mathcal{M}}_-$$

Accretion flow with lower entropy passes through the outer sonic point and the post-shock flow with shock generated higher entropy passes through the inner critical point. Jump in entropy joins the post-shock subsonic branch to the pre-shock supersonic branch.

(ii) *ICW*: Corresponds to the opposite of RSHK. Entropy of the flow is a shock conserved quantity. Some energy is lost at the discontinuity. The amount of entropy generated at the shock front exactly compensates the amount of entropy radiated away. ICW is radiatively more efficient compared to RSHK. Pre-shock accretion with higher energy passes through the outer critical point while post-shock flow with lower energy passes through the inner critical point. Jump in energy joins the pre-shock supersonic flow to its

post-shock subsonic branch. Relations hold in shock surface are in order:

$$\mathcal{E}_+ < \mathcal{E}_-$$

$$T_+ > T_-$$

$$s_+ = s_-$$

$$\dot{\mathcal{M}}_+ = \dot{\mathcal{M}}_-$$

(iii) *ISH*: For more efficient radiative cooling compared to RHSHK and ICW. A Part of energy and entropy are lost from the shock surface to keep the post-shock temperature equal to its pre-shock value which maintains the thickness of the flow exactly same just before and after the shock. Simultaneous jumps in energy and entropy join the pre-shock supersonic flow to its post-shock subsonic counterpart. Relations hold in the shock surface are:

$$\mathcal{E}_+ < \mathcal{E}_-$$

$$T_+ = T_-$$

$$s_+ < s_-$$

$$\dot{\mathcal{M}}_+ < \dot{\mathcal{M}}_-$$

It is obvious that ISH is of less general kind compared to RHSHK or ICW.

We are now in a position to describe RHSHK and related shock quantities in detail for shocks forming at thin advective accretion disk. We concentrate only on polytropic accretion because disk-outflow system in our work is modelled based on polytropic inflow only §.

The first question which may be asked in this regard is, “Do *all* solutions encounter a RHSHK?” Answering this question invites another more fundamental question, that is “When does a flow contain shock?” Below we try to provide the answer for this.

Complete solution of conservation equations for energy and baryon number in vertically averaged thin advective accretion disks in Paczyński-Wiita potential shows the possibility of formation of three sonic points (at the most) encountered by the flow (Chakrabarti,

§ However, isothermal inflow may also have importance in dealing with another kind of model where outflows from isothermal accretion flows would be studied which we won't discuss here.

1989). Among these three critical points, two are of saddle type (outer and inner Bondi type sonic point) and one centre type (sometimes referred as “O” type sonic-point) sonic point is flanked between them. Whether or not these three points would actually exist simultaneously would depend on \mathcal{E} , λ , \dot{M}_{Edd} and γ of inflow. Loosely speaking, for $\frac{4}{3} < \gamma < \frac{5}{3}$, significant angular momentum may produce all three points. In the absence of considerable angular momentum (spherical/ quasi-spherical flows) these three points would merge into a single one as in the case of Bondi type flow. ¶ Even for same values of \mathcal{E} and λ , \dot{M} is *not* equal for solutions passing through two different saddle type critical points (the outer and the inner sonic point, which will be denoted by X_{out} and X_{in} respectively throughout this work unless mentioned otherwise) in general. However, for a given λ , there is *only one* value of energy \mathcal{E}' and vice-versa such that the corresponding entropy accretion rate \dot{M}' follows the relation:

$$\dot{M}'(\mathcal{E}', \lambda, X_{out}) = \dot{M}'(\mathcal{E}', \lambda, X_{in}) \quad (6a)$$

Solutions containing the O type critical points are not of much interest and are treated as ‘unphysical’ since real transonic flow can not pass through that point (solutions can only encircle that point in a closed loop quasi-elliptical in shape, (see Fig. 5.2 Page.328 of Chakrabarti, 1996a). For a particular value of λ and \mathcal{E} , the difference

$$\Delta\dot{M} = [\dot{M}(X_{in}) - \dot{M}(X_{out})] \quad (6b)$$

distinguishes the solutions (with *exactly* same other characteristic parameters) passing through the inner (X_{in}) and the outer (X_{out}) sonic points and measures the difference in entropy content of flow for these two solutions. If the flow obeys some specific conditions (discussed in next paragraph), these two solutions may be joined by attributing a shock transition which allows a jump from lower entropy solution (solution passing through X_{out} and having entropy accretion rate $\dot{M}(X_{out})$) to higher entropy solution (solution passing through X_{in} and having entropy accretion rate $\dot{M}(X_{in})$) by gaining entropy of $\Delta\dot{M}$ amount (see eqs. 6b) which is used to heat the flow in post-shock region. It is to be noted here that as the basic equations governing the flow (energy and baryon number conservation equation, namely eqs. (3a) and eqs. (3b)) contain no dissipative term and the

¶ Although the above results are derived by solving the problem in pseudo-Newtonian geometry, a fully general relativistic treatment would also produce the same number of sonic points and display the same flow behaviour. For more general transonic flows which include viscosity, the central O type sonic point is changed into a spiral type and in the case of magnetized flows, the number of sonic points could be as much as five (Chakrabarti, 1996a, and references therein).

flow is assumed to be inviscid, shocks which may be produced in this way can only be of Rankine-Hugoniot type which conserves energy. The shock thickness must be very small in this case otherwise non-dissipative flows may radiate energy through the upper and the lower boundaries because of the presence of strong temperature gradient in between the inner and outer boundaries of the shock thickness. The shock transition for present case, thus, must also be a very fast process. So tracking a flow element in presence of shock may give the following flow profile:

Subsonic flow starting from infinity first becomes supersonic after crossing X_{out} and somewhere in between X_{out} and X_{in} (an to the right side of the middle sonic point X_{med} , i.e., the O type sonic point) the shock transition takes place which forces the solution (the flow in reality) to jump onto the corresponding subsonic branch. The hot and dense post-shock subsonic flow produces in this way again becomes supersonic after crossing X_{in} and ultimately dives onto the hole supersonically to satisfy the inner boundary condition on the black hole horizon. Flow heading towards a neutron star may encounter another shock after it crosses the inner sonic point because the hard surface boundary condition of a neutron star dictates the flow to hit the star surface subsonically.

3.2.1 Shock Conditions

A RSHK produced in the way described above may be characterised by the following four a priori unknown quantities in general (see Chakrabarti, 1996a):

$$x = X_{shock} \quad (7a)$$

$$\Delta a = a_+(X_{shock}) - a_-(X_{shock}) \quad (7b)$$

$$\Delta u = u_+(X_{shock}) - u_-(X_{shock}) \quad (7c)$$

$$\Delta \dot{M} = \dot{M}_+(X_{shock}) - \dot{M}_-(X_{shock}) \quad (7d)$$

Δa , Δu and $\Delta \dot{M}$ are the possible jumps in sound velocity, dynamical velocity and entropy accretion rates respectively where (+) / (−) signs indicate post- and pre-shock quantities respectively. Independent of the nature of shock transition, two more constraints are the conservation of baryon number flux density and momentum flux density, i.e.,

$$\dot{M}_+ = \dot{M}_- \quad (8a)$$

$$W_+ + \Sigma_+ u_+^2 = W_- + \Sigma_- u_-^2 \quad (8b)$$

W and Σ being vertically averaged pressure p and density ρ respectively and could be computed as (Matsumoto et al, 1984):

$$\Sigma_{\pm} = \int_{-h}^h \rho_{\pm} dz = 2\rho_0 I_n h(r)$$

$$W_{\pm} = \int_{-h}^h P_{\pm} dz = 2P_0 I_{n+1} h(r)$$

$h(r)$ being the local vertical half-thickness of the disk and I_n is defined as:

$$I_n = \left[\frac{(2^n n!)^2}{(2n+1)!} \right]$$

So the standard RHSHK condition for non-dissipative inviscid flow ultimately boils down to the following set of equations:

$$[\mathcal{E}] = 0 \quad (9a)$$

$$[\dot{M}] = 0 \quad (9b)$$

$$[W + \Sigma u^2] = 0 \quad (9c)$$

Where $[A + B]$ means $\{(A_+ + B_+) - (A_- + B_-)\}$. For flow with various heating and cooling mechanisms, another extra parameter:

$$\mathbf{f}(X_{shock}) = \frac{(Q_+ - Q_-)_+}{(Q_+ - Q_-)_-}$$

is introduced which determines the energy dissipation and generation of entropy at shock surface (Abramowicz & Chakrabarti, 1990). Q_{\pm} are the heat gained/lost by the flow. Introduction of this term may deviate the nature of the shock from that of standard RHSHK type. One of the possible reasons for this departure is that a part of shock generated entropy may be radiated away instead of being advected with the flow.

However, the generalised shock condition may formally be written as (Chakrabarti, 1990):

$$\mathcal{A}(\mathcal{E}_+ - \mathcal{E}_-) - \mathcal{B}(\dot{M}_+ - \dot{M}_-) = 0 \quad (10)$$

For a given set of $\{\mathcal{E}, \lambda, \dot{M}_{Edd}, \gamma\}$, variation of the ratio $\left(\frac{\mathcal{B}}{\mathcal{A}}\right)$ reproduces all the standard discontinuities. For example, while $\left(\frac{\mathcal{B}}{\mathcal{A}}\right) = 0$ gives RHSHK, $\left(\frac{\mathcal{B}}{\mathcal{A}}\right) = \infty$ produces ICW. ISH may form for an intermediate value of $\left(\frac{\mathcal{B}}{\mathcal{A}}\right)$.

A useful way to determine whether shock forms for a given set of $\{\mathcal{E}, \lambda, \dot{M}_{Edd}, \gamma\}$ and to compute its location is to find a suitable Mach number relation and then to investigate its invariance. By relating the Mach number of the flow just after and before the shock (M_{\pm}) and by rewriting shock conditions in terms of M_{\pm} one obtains (C89):

$$\frac{1}{2} \left(\frac{1}{M_+} + \gamma M_+ \right) = \frac{1}{2} \left(\frac{1}{M_-} + \gamma M_- \right) = C \quad (a \text{ constant.}) \quad (11a)$$

$$C = \frac{\left\{M_+(3\gamma - 1) + \frac{2}{M_+}\right\}^2}{2 + (\gamma - 1)M_+^2} = \frac{\left\{M_-(3\gamma - 1) + \frac{2}{M_-}\right\}^2}{2 + (\gamma - 1)M_-^2} \quad (11b)$$

or using [] notation,

$$\left[\frac{\left\{M(3\gamma - 1) + \frac{2}{M}\right\}^2}{2 + (\gamma - 1)M^2} \right] = 0 \quad (12)$$

The constant C as defined above is another shock-invariant quantity. Mach number just before and after the shock can be computed as:

$$M_{\mp} = \left\{ \frac{2(3\gamma - 1) - C_{\mp}\sqrt{C^2 - 8\gamma C}}{(\gamma - 1)C - (3\gamma - 1)^2} \right\}^{0.5} \quad (13a)$$

and the product of them is,

$$M_+M_- = 2\{(3\gamma - 1)^2 - (\gamma - 1)C\}^{-0.5} \quad (13b)$$

However, it must be mentioned that for transonic astrophysical advective accretion, it is *not* the *only* choice to encounter a shock *always*. It can be shown that in a large region of parameter space spanned by $\{\mathcal{E}, \lambda, \dot{M}_{Edd}, \gamma\}$, shock *does not* form. The flow passes either through X_{out} *only*, or passes through X_{in} *only*. Highly viscous flow may simultaneously have both of the choices sometimes, though, in such cases, it ‘chooses’ to cross the inner sonic point only because solutions passing through the inner sonic point will have higher entropy density. Shocks, once formed, may not be steady or standing, in some cases they may propagate backwards to infinity making the whole disk subsonic and possibly Keplerian. This case is of particular interest when matter supply is time-dependent (see Chakrabarti, 1996a and references therein). Flow passing only through X_{out} may form ion supported advective flows (Rees et al, 1982).

In §2.2.1 (largely adopted from Chakrabarti, 1997) we would like to present the classification scheme for the entire parameter space spanned by \mathcal{E} and λ to classify various solutions with and without shocks. This parameter space will be the basis of our range of choice of inflow for generation of outflow by simultaneously solving the inflow-outflow equations.

3.2.2 Classification of Parameter Space

In Fig. 2.1.1, the *entire* parameter space is classified according to the type of solutions of thin inviscid flow that are prevalent around a Schwarzschild black hole. Two conserved parameters are used, namely, specific energy \mathcal{E} and specific angular momentum l (analogous to λ) for classification. The adiabatic index $\gamma = 4/3$ has been chosen. The whole

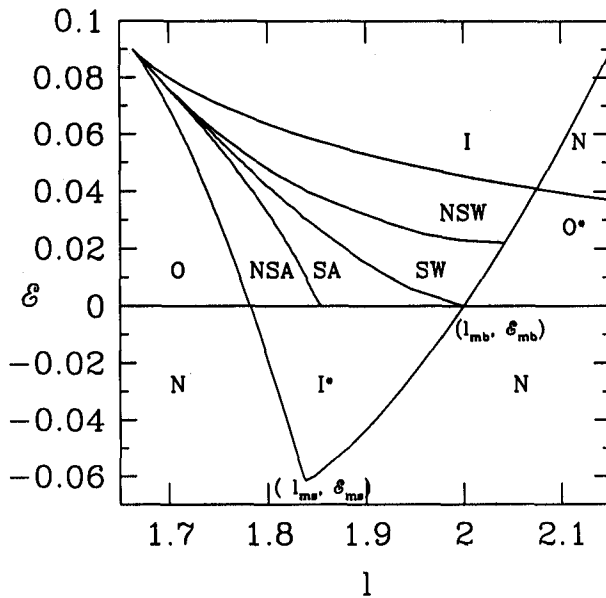


Fig. 2.1.1:

Classification of entire parameter space spanned by specific energy \mathcal{E} and specific angular momentum λ (or, alternatively, l) of non-dissipative, inviscid, rotating thin polytropic advective accretion. Figure reproduced from Ckkrabarti, 1997 with kind permission.

space is divided into nine regions marked by N , O , NSA , SA , SW , NSW , I , O^* , I^* . The horizontal line at $\mathcal{E} = 0$ corresponds to the rest mass of the flow.

The parameters from region N do not produce any transonic solution. The solutions from the region 'O', which have very low angular momentum and energy are similar to a Bondi flow and have only the outer sonic point. The solutions from the regions NSA and SA have two 'X' type sonic points with the entropy density S_o at the outer sonic point less than the entropy density S_i at the inner sonic point. However, flows from SA pass through a standing shock since the Rankine-Hugoniot condition is satisfied. The entropy generated at the shock, $S_i - S_o$, is advected towards the black hole to enable the flow to

pass through the inner sonic point. Rankine-Hugoniot condition is not satisfied for flows around a black hole from the region NSA . However, for flows around a neutron star the shock condition is satisfied right outside the star surface (C89). Numerical simulations show (Ryu, Chakrabarti & Molteni, 1997) that the flow from this region could be very unstable and could exhibit periodic changes in emission properties as the flow constantly tries to form the shock wave, but fails to do so. These solutions explain quasiperiodic oscillations very satisfactorily.

The solutions from the regions SW and NSW are very similar to those from SA and NSA . However, $S_o \geq S_i$ in these cases. Shocks can form only in winds from the region SW . The shock condition is not satisfied in winds from the region NSW even though two sonic points are present. This may make the NSW flow unstable as well. A flow from region I only has the inner sonic point and thus can form shocks (which require the presence of two saddle type sonic points) only if the inflow is already supersonic due to some other physical processes (such as flaring of the inflow, or capturing of companion winds; see, C96). Each solution from regions I^* and O^* has two sonic points (one 'X' and one 'O') only but none produces any complete and global solution. The region I^* has an inner sonic point but the solution does not extend subsonically to a large distance. The region O^* has an outer sonic point, but the solution does not extend supersonically to the horizon. When a significant viscosity is added, the closed topologies of I^* and O^* open up as described in C96, and the flow may join with a cool Keplerian disk with $\mathcal{E} < 0$. These special solutions of viscous transonic flows need not have centrifugally supported shock waves as they have only one inner sonic point. However, hot flows deviating from a Keplerian disk, or sub-Keplerian winds from companions, or cool flows subsequently energized by magnetic flares (for instance) will have $\mathcal{E} > 0$, and thus could have standing or periodically varying shock waves as discussed above. The post-shock region or the enhanced density region radiates most of the observed hard radiation. The present classification is done using thin flows in the Paczyński–Wiita (1980) potential. A similar division of parameter space in the Kerr geometry has also been performed (Chakrabarti, 1996b).

4 ACCRETION POWERED OUTFLOWS: ATTEMPT TO MAKE

SELF-CONSISTENT CONNECTION BETWEEN ACCRETION AND WINDS

It is obvious from above discussion that a transonic astrophysical advective flow need not encounter a standing shock always, rather only a restricted region of parameter space spanned by $\{\mathcal{E}, \lambda, \dot{M}_{Edd}, \gamma\}$ produces shock transition of steady RSHK type. Our fundamental aim is to self-consistently connect the solutions of ‘accretion-zone’ in parameter space (SA or I to be specific, region O never produces outflow in our model, see discussions in §1 of Chapter. 4.) to its corresponding ‘wind-zone’ so that the outflow is capable of emerging from accretion flows. This is done (Das, 1998, Das & Chakrabarti, 1999) by varying the γ of the flow (change in γ is achieved either due to the shock generated entropy or due to turbulence generated at the location of maximum polytropic pressure, see Das 1998 and Das & Chakrabarti, 1999 for detail) at a suitable distance from the central accretor where the centrifugal pressure dominated hot and dense region acts as the virtual ‘physical’ envelop around the hole which could be considered to mimic the ordinary stellar surface regarding mass loss. In this way it has been possible to extract outflows and to investigate the dependence of its rate on various physical quantities ($\mathcal{E}, \lambda, \dot{M}_{Edd}, \gamma$ etc.) from the knowledge of accretion parameter only, which has *never* been achieved in any existing disk-wind model in literature till date. We describe this formalism in detail in next chapter, i.e., in Chapter 2.2.

Lifting the Face from the Disk: The Outflow Model

Chapter 2.2

SUMMARY

After explaining the fundamentals of the physical process by which the outflow may generate from advective accretion disks around a compact object, details of a mathematical scheme capable of simultaneously solving the equations governing accretion and wind are provided. Connection between inflow-outflow topologies has been established along with self-consistent computation of the mass outflow rate $R_{\dot{M}}$. Also the dependence of this rate on all possible accretion as well as shock parameters are thoroughly investigated.

1 GETTING 'KICKED UP' BY THE CENBOL: THE BASIC PHYSICS

Being equipped with the state-of-the-art advective accretion disk model in hand, our aim is now to investigate how outflows could be generated from such accretion flows and to compute the mass outflow rate $R_{\dot{M}}$ (the fraction of accreting matter being kicked out as wind, i.e., the ratio of the time rate at which matter flows out to the time rate at which matter falling in; $\left(\frac{M_{out}}{M_{in}}\right)$) from first principle and to study its dependence on various parameters governing the accretion. For the sake of simplicity, our model will be characterized by a set of stationary equations describing non-dissipative, inviscid, thin (our assumption for thinness is for the sake of computation of the thermodynamic quantities only, the real flow itself need not be physically thin (see Das & Chakrabarti, 1999)) polytropic accretion.

Before we proceed, we describe some basic properties of the rotating matter around a black hole which will be of our interest. Rotating matter behaves in a spatial manner at two radial distances (Shapiro & Teukolski, 1983) — (a) marginally stable orbit (r_{ms}) and (b) marginally bound orbit (r_{mb}). For $r < r_{ms}$, no time-like orbit is stable. The corresponding Keplerian angular momentum is $\lambda_{ms} = 3.67GM/c$ for a Schwarzschild black hole of

mass M , G and c being the universal gravitational constant and velocity of light respectively. For $r < r_{mb}$, any closed orbit is impossible and matter must dive into a black hole. The corresponding Keplerian angular momentum is $\lambda_{mb} = 4GM/c$. Matter with a larger angular momentum ($\lambda > \lambda_{mb}$) must require a positive energy at infinity in order to enter into a black hole since the centrifugal barrier becomes otherwise unsurmountable (see, Fig. 12.3 of Shapiro & Teukolski, 1983). Thus, normally, for a black hole accretion, one is interested in flows with $\lambda < \lambda_{mb}$. The centrifugal force

$$F_c \sim \lambda^2/r^3 \quad (1a)$$

fighters against the gravitational force

$$F_g \sim -GM/r^2 \quad (1b)$$

and in a Keplerian disk (consists of a collection of closed timelike geodesics) these two forces balance. In exact form, the Keplerian distribution of specific angular momentum in Schwarzschild geometry is given by (Shapiro & Teukolski, 1983):

$$\lambda_{Kep} = \frac{\sqrt{GM r}}{1 - \frac{2GM}{c^2 r}} \quad (2)$$

With this distribution, there is no centrifugal barrier left, since the two forces exactly cancel each other.

On the other hand, a rotating inflow with a specific angular momentum $\lambda(r)$ entering into a black hole will have angular momentum $\lambda \sim \text{constant}$ close to the black hole for any moderate viscous stress. Physically, this is due to fact that viscosity transports momentum, and therefore angular momentum to outer parts of the disk and it takes much longer time (than the infall time of matter) to do so. Problem with a constant angular momentum flow with $\lambda_{ms} < \lambda < \lambda_{mb}$ is that it must be sub-Keplerian [eq. (2)] for $r < r_{mb}$. A second, and more important reason why a flow must deviate from a Keplerian disk can be understood in the following way: Consider a perfect fluid with the stress-energy tensor (using $G = c = M = 1$),

$$T_{\mu\nu} = \rho u_\mu u_\nu + p(g_{\mu\nu} + u_\mu u_\nu) \quad (3)$$

where, p is the pressure and $\rho = \rho_0(1 + \pi)$ is the mass density, π being the internal energy. We assume the vacuum metric around a Kerr black hole to be of the form (Shapiro & Teukolski, 1983):

$$ds^2 = g_{\mu\nu} dx^\mu dx^\nu = -\frac{r^2 \Delta}{A} dt^2 + \frac{A}{r^2} (d\phi - \omega dt)^2 + \frac{r^2}{\Delta} dr^2 + dz^2 \quad (4)$$

Where,

$$A = r^4 + r^2 a^2 + 2ra^2; \quad \Delta = r^2 - 2r + a^2; \quad \omega = \frac{2ar}{A}$$

Here, $g_{\mu\nu}$ is the metric coefficient and u^μ is the four velocity component.

$$u_t = \left[\frac{\Delta}{(1 - V^2)(1 - \Omega\lambda)(g_{\phi\phi} + \lambda g_{t\phi})} \right]^{1/2}. \quad (5)$$

Here, $\lambda = -u_\phi/u_t$ is the specific angular momentum and $\Omega = u^\phi/u^t$. On the horizon, for all a , $\Delta = 0$. Since all the other terms behave smoothly, V must be unity, i.e., velocity of light. Since in the extreme equation of state of $p = \rho/3$, the sound speed is $1/\sqrt{3}$. Thus the Mach number is larger than unity, and the flow must be supersonic on the horizon. A supersonic flow is always sub-Keplerian (see §1.1 of Chapter 2.1). It is to be noted that the investigations made so far are from Keplerian disks only. In the present work, we investigate outflow formation from more realistic flows which are necessarily sub-Keplerian.

Going back to equations (1a) and (1b), one notes that the F_c increases much faster compared to the F_g and becomes comparable at around $r_{cb} \sim \lambda^2/GM$. (In the rest of this chapter) we use $R_g = 2GM/c^2$ as the length unit, c is the unit of velocity, and the mass of the black hole M to the unit of mass.) Here, (actually, a little farther out, due to thermal pressure) matter starts piling up and produces the CENtrifugal pressure supported BOundary Layer (CENBOL for short). Further close to the black hole, the gravity always wins and matter enters the horizon supersonically after passing through a sonic point. This centrifugal pressure supported region, may or may not have a sharp boundary, depending on whether standing shocks form or not (see §3.2.2 of Chapter 2.1 for a detail classification of parameter space). Generally speaking, in a polytropic flow, if the polytropic index $\gamma > 1.5$, then shocks do not form and if $\gamma < 1.5$, only a region of the parameter space forms the shock. In this layer (CENBOL) the flow becomes hotter and denser (with opacity $\tau \sim \dot{M}_{Edd}$, where \dot{M}_{Edd} is the accretion rate scaled in the unit of Eddington rate) and for all practical purposes behaves as the stellar atmosphere so far as the formation of outflows are concerned. Inflows on neutron stars behave similarly, except that the 'hard-surface' inner boundary condition dictates that the flow remains subsonic between the CENBOL and the surface rather than becoming supersonic as in the case of a black hole. On or very near to (just outside) the CENBOL, accreting matter slows down and its thermal energy increases. In some region of parameter space this slowing down takes place rather abruptly through a Rankine-Hugoniot type standing shock. Most of the

thermal energy of the flow could be extracted from this region through inverse compton effect if soft photons are injected here from the Keplarian disk component. Whereas the boundary layer of a white dwarf is of thickness less than a percentage of its radius, the thickness of CENBOL of a black hole is several times larger than its radius. If the Neutron star is not compact enough (radius not less than inner sonic point of the flow), its boundary layer would be of similar size. For compact neutron stars, the boundary layer could be very thin because unlike the black hole accretion, the shock transition just outside its (neutron star's) hard surface is allowed unless the entire flow is subsonic. In case where the shock does not form, regions around pressure maximum achieved just outside the inner sonic point would also drive the flow outwards. In the back of our mind, we have the picture of the outflow which is thermally and centrifugally accelerated but confined by external pressure of the ambient medium.

CENBOL happens to have just the right set of properties: the efficiency of its emission is neither almost zero as in a spherical Bondi flow, nor fixed and maximum as in a Keplarian disk. Its size and optical depth are determined by viscosity and accretion rates and therefore may give rise to varieties of spectral properties as are observed.

At a first glance, it may be astonishing that a black hole, which has no hard surface, should allow a 'boundary layer' or CENBOL. Observationally, in the context of spectral properties of black hole candidates, the presence of this boundary layer has been established long ago (see, Chakrabarti, 1996a). It turns out that most of the hard X-rays from black hole accretion disk comes out of this region (Crary et al, 1996). Most interestingly, the CENBOL can also oscillate similar to the boundary layer of a white dwarf (Molteni, et al, 1996), thus proving beyond doubt the existence of a CENBOL. This oscillation has also been observed recently (Crary et al, 1996, Strohmayer, et al, 1996). By numerical simulation work (which do not invoke any self-consistent analytical prescription), formation of outflow from this region is clearly seen both for inviscid flow (Molteni et al, 1996) and for viscous flow (Lanzafame et al, 1998).

Concept of CENBOL formation might also be useful in explaining hard and soft states of galactic black hole candidates and triggering of their transitions, constancy of slopes in hard and soft states, variation of inner edge of the Keplarian component etc. The oscillation of CENBOL may successfully explain the general properties of quasi-periodic oscillation of black holes and neutron stars as well (see Chakrabarti, 1998 and references therein).

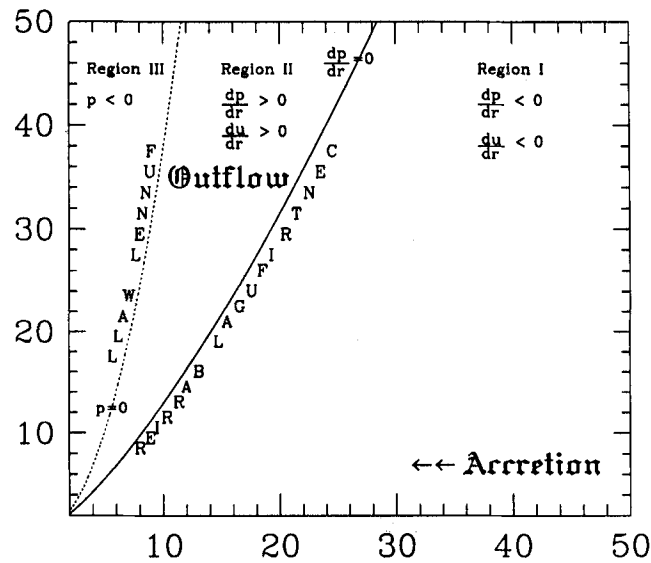


Fig. 2.2.1:

Wind formation from an accretion flow is schematically shown. The especial properties of centrifugal barrier and funnel wall make them ideal candidates to collimate outflows from regions close to the black hole, see text for detail.

There are two surfaces of utmost importance in flows with angular momentum. One is the 'funnel wall' where the effective potential (sum of gravitational potential and the specific rotational energy) vanishes. In the case of a purely rotating flow, this is the 'zero pressure' surface. Flows *cannot* enter inside the funnel wall because the pressure would be negative. (Fig. 2.2.1) The other surface is called the 'centrifugal barrier'. This is the surface where the radial pressure gradient of a purely rotating flow vanishes and is located *outside* the funnel wall simply because the flow pressure is higher than zero on this surface. Flow with inertial pressure easily crosses this 'barrier' and either enters into a black hole or flows out as winds depending on its initial parameters (detail classification of the parameter space is in §3.2.2 of Chapter 2.1). We assume that the outflow generally hugs the 'funnel wall' and goes out in between these two surfaces.

It is interesting to 'visualize' how the combined accretion-outflow system along with the central accretor would 'look like' in reality. In Fig. 2.2.2 we attempt to illustrate the combined multicomponent flow geometry in 3-Dimension.

Outflow rates from accretion disks around black hole and neutron stars must be related to the properties of CENBOL which in turn, depend on the inflow parameters. Subsonic outflows originating from CENBOL would pass through sonic points and reach far distances as in wind solutions. Assuming free-falling conical polytropic inflow and isother-

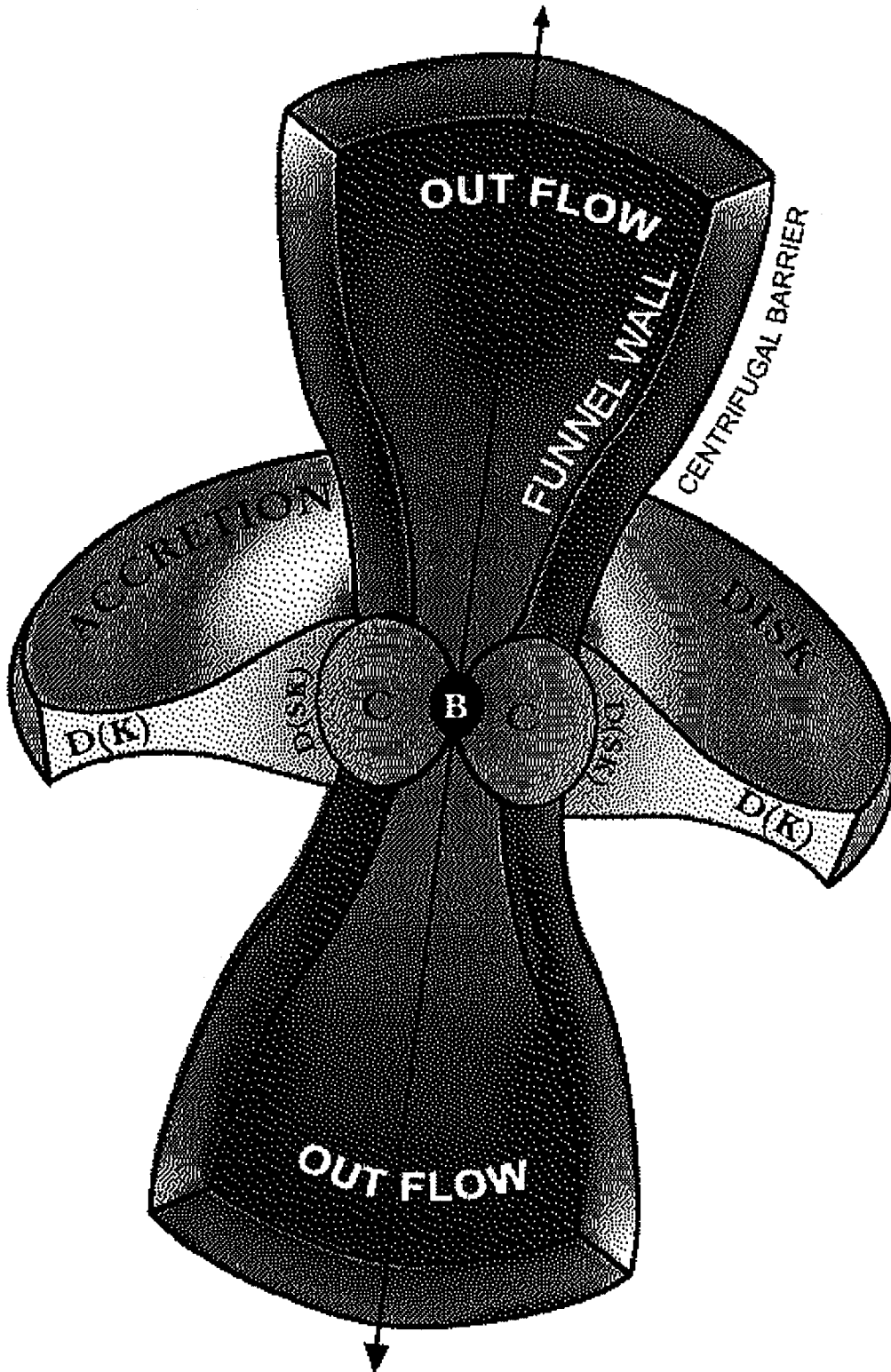


Fig. 3.2.2:

Schematic diagram illustrating the 3-D geometry of coupled disk-outflow system according to our model. **B** is the accreting Schwarzschild black hole while **C**'s represent the hot and dense CENBOL region. **D(K)** and **D(SK)** represent the thin Keplarian part and puffed-up sub-Keplarian part of the advective accretion disk respectively (measurements not in scale). Due to the axisymmetry assumption in accretion, two oppositely directed jet are expelled from the close vicinity of **B**. The inner and the outer surfaces of the outflow are the funnel wall and centrifugal barrier respectively as explained in text.

mal outflows (as in stellar winds), it is easy to provide a qualitative estimation of the ratio of outflowing and inflowing rates in a simplified manner (Chakrabarti, 1999):

$$\frac{\dot{M}_{out}}{\dot{M}_{in}} = \frac{\Theta_{out}}{\Theta_{in}} \frac{R}{4} e^{-(f_0 - \frac{3}{2})} f_0^{3/2} \quad (6)$$

where, Θ_{out} and Θ_{in} are the solid angles of the outflow and inflow respectively, and

$$f_0 = \frac{(2n + 1)R}{2n}. \quad (7)$$

Here, R is the compression ratio of inflowing matter at the CENBOL and $n = 1/(\gamma - 1)$ is the polytropic constant.

The aim of this chapter is to provide a formulation which could compute the mass loss rate more realistically than what has been attempted so far. We calculate (Das, 1998, Das & Chakrabarti, 1999, Das, 1999c) this rate as a function of the inflow parameters, such as specific energy and angular momentum, accretion rate, polytropic index etc. We explore both the polytropic and the isothermal outflows. Our conclusions show that the outflow rate is sensitive to the specific energy and accretion rate of the inflow. Specifically, when the outflow is not isothermal, outflow rate generally increases with the specific energy and the polytropic index γ_o of the outflow, generally decreases with the polytropic index γ of the inflow, but somewhat insensitive to the specific angular momentum λ . In the case of isothermal outflow, however, mass loss rate is sensitive to the inflow rate, since the inflow rate decides the proton temperature of the advective region of the disk which in turn fixes the outflow temperature. In this case the outflow is at least partially temperature driven. The outflow rate is also found to be anti-correlated with specific angular momentum λ of the flow.

This chapter is organized as follows: In the next section, we describe our model and present the governing equations describing the flow. In §3, we present the solution procedure of the equations. In §4, we present results of

our computations. Finally, in §5, we illustrate the applicability of our model to various related fields.

2 GOVERNING EQUATIONS, FLOW GEOMETRY AND SOLUTION PROCEDURE

2.1 Outflow Models

Inflow model for disk-outflow system has already been discussed in §2 of Chapter 2.1. Three equations, viz eqs. 3a, 3b and 3d of Chapter 2.1 will serve as main conservation equations for our purpose. Below we describe our outflow model in detail.

We consider two types of outflows. In ordinary stellar mass loss computations (Tarafdar, 1988 and references therein), the outflow is assumed to be isothermal till the sonic point. This assumption is probably justified, since copious photons from the stellar atmosphere deposit momenta on the slowly outgoing and expanding outflow and possibly make the flow close to isothermal. This need not be the case for outflows from compact sources. Centrifugal pressure supported boundary layers close to the black hole are very hot (close to the virial temperature) and most of the photons emitted may be swallowed by the black holes themselves instead of coming out of the region and depositing momentum onto the outflow. Thus, the outflows could be cooler than isothermal flows. In our first model, we choose polytropic outflows with same energy as the inflow (i.e., no energy dissipation between the inflow and outflow) but with a different polytropic index $\gamma_0 < \gamma$. Nevertheless, it may be advisable to study the isothermal outflow to find out the behaviour of the extreme case. Thus an isothermal outflow is chosen in our second model. In each case, of course, we include the possibility that the *inflow* may or may not have standing shocks.

On the one hand, our assumption of thin inflow is for the sake of computation of the thermodynamic quantities only, but the flow itself need not be physically thin. Secondly, the funnel wall and the centrifugal barrier are purely geometric surfaces, and they exist anyway and the outflow could be supported even by ambient medium which may not necessarily be a part of the disk itself.

2.1.1 Polytropic Outflow

In this case, the energy conservation equation takes the form:

$$\mathcal{E} = \frac{v^2}{2} + n' a_e^2 + \frac{\lambda^2}{2r_m^2(r)} - \frac{1}{2(r-1)} \quad (8)$$

and the mass conservation in the outflow takes the form:

$$\dot{M}_{out} = \rho v \mathcal{A}(r). \quad (9)$$

Here, $n' = (\gamma_o - 1)^{-1}$ is the polytropic constant of the outflow. It is important to note that unlike the conservation equations for *inflow*, here for *outflow*, the rotational energy term contains

$$r_m(r) = \frac{\mathfrak{R}(r) + R(r)}{2}, \quad (10a)$$

as the mean *axial* distance of the flow. The expression of $\mathfrak{R}(r)$, the local radius of the centrifugal barrier comes from balancing the centrifugal force with the gravity, i.e.,

$$\frac{\lambda^2}{\mathfrak{R}^3(r)} = \frac{\mathfrak{R}(r)}{2r(r-1)^2}. \quad (10b)$$

We thus obtain,

$$\mathfrak{R}(r) = [2\lambda^2 r(r-1)^2]^{\frac{1}{4}} \quad (11a)$$

And the expression for $R(r)$, the local radius of the funnel wall, comes from vanishing of total effective potential, i.e.,

$$\begin{aligned} \Omega_{tot\,eff}(r) &= -\frac{1}{2(r-1)} + \frac{\lambda^2}{2R^2(r)} = 0 \\ R(r) &= \lambda [(r-1)]^{1/2} \end{aligned} \quad (11b)$$

Here, $\mathcal{A}(r)$ is the area between the centrifugal barrier and the funnel wall. This is computed with the assumption that the outflow is external pressure supported, i.e., the centrifugal barrier is in pressure balanced with the ambient medium. Matter, if pushed hard enough, can cross centrifugal barrier in black hole accretion (the reason why rapidly rotating matter can enter into a black hole in the first place). An outward thermal force (such as provided by the CENBOL) in between the funnel wall and the centrifugal barrier causes the flow to come out. Thus the cross section of the outflow is,

$$\mathcal{A}(r) = \pi[\mathfrak{R}^2(r) - R^2(r)]. \quad (12)$$

The outflow angular momentum λ is chosen to be the same as in the inflow, i.e., no viscous dissipation is assumed to be present in the inner region of the flow close to a black hole. Considering that viscous time scales are longer compared to the inflow time scale, it may be a good assumption in the disk, but it may not be a very good assumption for the outflows which are slow prior to the acceleration and are therefore, prone to viscous transport of angular momentum. Such detailed study has not been attempted here particularly because we know very little about the viscous processes taking place in the pre-jet

flow. Therefore, we concentrate only those cases where the specific angular momentum is roughly constant when inflowing matter becomes part of the outflow, although some estimates of the change in R_m is provided when the average angular momentum of the outflow is lower. Detailed study of the outflow rates in presence of viscosity and magnetic field is in progress and would be presented elsewhere.

2.1.2 Isothermal Outflow

The integration of the radial momentum equation yields an equation similar to the energy equation (eq. 8):

$$\frac{\vartheta_{iso}^2}{2} + C_s^2 \ln \rho + \frac{\lambda^2}{2r_m(r)^2} - \frac{1}{2(r-1)} = \text{Constant} \quad (13)$$

In this case the thermal energy term is different, behaving logarithmically. The constant sound speed of the outflow is C_s . The mass conservation equation remains the same:

$$\dot{M}_{out} = \rho \vartheta_{iso} A(r). \quad (14)$$

Here, the area function remains the same above. A subscript *iso* of velocity ϑ is kept to distinguish from the velocity in polytropic case. This is to indicate the velocities are measured here using completely different assumptions.

In both the models of the outflow, we assume that the flow is primarily radial. Thus the θ -component of the velocity is ignored ($\vartheta_\theta \ll \vartheta$).

2.2 Simultaneous Solution of Inflow-Outflow Equations

Before we go into the details, a general understanding of the transonic flows around a black hole is essential. In §3.2.2 of Chapter 2.1 all the solution topologies of the polytropic flow in pseudo-Newtonian geometry have been provided. In regions **I** and **O** of the parameter space the flow has only one sonic point X_{in} or X_{out} . Matter with positive energy at a large distance must pass through that point before entering into the black hole supersonically. In regions **SA** and **SW** shocks may form in accretion and winds respectively, but no shocks are expected in winds and accretions if parameters are chosen from these branches. In **NSW** and **NSA**, two saddle type sonic points exist, but no steady shock solutions are possible.

Suppose that matter first enters through the outer sonic point and passes through a shock. At the shock, part of the incoming matter, having higher entropy density is likely to return back as winds through a sonic point, other than the one it just entered. Thus

a combination of topologies, one from the region **SA** and the other from the region **O** is required to obtain a full solution. In the absence of the shocks, the flow is likely to bounce back at the pressure maximum of the inflow and since the outflow would be heated by photons, and thus have a smaller polytropic constant, the flow would leave the system through an outer sonic point different from that of the incoming solution. Thus finding a complete self-consistent solution boils down to finding the outer sonic point of the outflow and the mass flux through it. Below we present the list of parameters used in both of our models and briefly describe the procedure to obtain a satisfactory solution.

2.2.1 Polytropic Outflow

We assume that

- (a) In this case, a very little amount of total energy is assumed to be lost in each bundle of matter as it leaves the disk and joins the jet. The specific energy \mathcal{E} remains fixed throughout the flow trajectory as it moves from the disk to the jet.
- (b) Very little viscosity is present in the flow except at the place where the shock forms, so that the specific angular momentum λ is constant in both inflows and outflows close to the black hole. At the shock, entropy is generated and hence the outflow is of higher entropy for the same specific energy.
- (c) The polytropic index of the inflow (γ) and outflow (γ_o) are free parameters and in general, $\gamma_o < \gamma$, because of heating effect of the outflow (e.g., due to the momentum deposition coming out of the disk surface). In reality γ_o is directly related to the heating and cooling processes of the outflow. When \dot{M}_{in} is high, heating of outflow by photon momentum deposition is higher, and therefore $\gamma_o \rightarrow 1$.

Thus a supply of parameters \mathcal{E} , λ , γ and γ_o make a self-consistent computation of R_m possible when the shock is present. When the shock is absent, the compression ratio of the gas at the pressure maximum between the inflow and outflow R_{comp} is supplied as a free parameter, since it may be otherwise very difficult to compute satisfactorily. In the presence of shocks, such problems do not arise as the compression ratio is obtained self-consistently.

The following procedure is adopted to obtain a complete solution:

From two conservation equations for *accretion*, viz, eqs. (3a) and (3b) of Chapter 2.1, we

derive an expression for the derivative,

$$\frac{du}{dr} = \left(\frac{\frac{\lambda^2}{r^3} + \frac{na^2}{\alpha} + \frac{5r-3}{r(r-1)} - \frac{1}{2(r-1)^2}}{u - \frac{2na^2}{\alpha u}} \right). \quad (15)$$

At the sonic point, the numerator and denominator separately vanish, and give rise to the so-called sonic point conditions:

$$a_c = \left(\frac{\frac{1}{2(r_c-1)^2} - \frac{\lambda^2}{r_c^3}}{\frac{\alpha(r_c-1)r_c}{n(5r_c-3)}} \right) \quad (16a)$$

$$u_c = \sqrt{\frac{2n}{\alpha} a_c} \quad (16b)$$

where, the subscript c represents the quantities at the sonic point. The derivative of the flow at the sonic point is computed using the L'Hospital's rule. Using fourth order Runge-Kutta method $\vartheta(r)$ and $a(r)$ are computed along the flow till the position where the Rankine-Hugoniot condition is satisfied (if shocks form) and from there on the sub-sonic branch is integrated for the accretion as usual. With the known γ_o , \mathcal{E} and λ , one can compute the location of the outflow sonic point from eqs. (8) and (9),

$$\frac{d\vartheta}{dr} = \left(\frac{\frac{a^2}{\mathcal{A}^2(r)} \frac{d\mathcal{A}(r)}{dr} + \frac{\lambda^2}{r_m^3(r)} \frac{dr_m(r)}{dr} - \frac{1}{2(r-1)^2}}{\vartheta - \frac{a^2}{\vartheta}} \right) \quad (17)$$

from where the sonic point conditions at the outflow sonic point r_{co} obtained are given by,

$$\frac{a_{co}^2}{\mathcal{A}_{co}^2(r)} \frac{d\mathcal{A}(r)}{dr} \Big|_{co} + \frac{\lambda^2}{r_{mco}^3(r)} \frac{dr_m(r)}{dr} \Big|_{co} - \frac{1}{2(r_{co}-1)^2} = 0 \quad (18a)$$

and

$$\vartheta_{co} = a_{co}. \quad (18b)$$

At the outer sonic point, the derivative of ϑ is computed using the L'Hospital's rule and the Runge-Kutta method is used to integrate towards the black hole to compute the velocity of the outflow at the shock location. The density of the outflow at the shock is computed by distributing the post-shock dense matter of the disk into spherical shell of 4π solid angle. The outflow rate is then computed using eq. (9).

It is to be noted that when the outflows are produced, one cannot use the usual Rankine-Hugoniot relations at the shock location, since mass flux is no longer conserved

in accretion, but part of it is lost in the outflow. Accordingly, we use,

$$\dot{M}_+ = (1 - R_m)\dot{M}_- \quad (19)$$

where, the subscripts + and – denote the pre- and post-shock values respectively. Since due to the loss of matter in the post-shock region, the post-shock pressure goes down, the shock recedes backward for the same value of incoming energy, angular momentum & polytropic index. The combination of three changes, namely, the increase in the cross-sectional area of the outflow and the launching velocity of the outflow and the decrease in the post-shock density decides whether the net outflow rate would increased or decreased than from the case when the exact Rankine-Hugoniot relation was used.

In the case where the shocks do not form, the procedure is a bit different. It is assumed that the maximum amount of matter comes out from the place of the disk where the thermal pressure of the inflow attains its maximum. We calculate the expression for the polytropic pressure for the inflow in vertical equilibrium to be,

$$\mathcal{P}_e(r) = \frac{a_e^{2(n+1)}\dot{M}_{in}}{\gamma^{(1+n)}\mathcal{M}} \quad (20)$$

This is maximized and the outflow is assumed to have the same quasi-conical shape with annular cross-section $\mathcal{A}(r)$ between the funnel wall and the centrifugal barrier as already defined. In the absence of shocks the compression ratio of the flow between the incoming flow and outgoing flow at the pressure maximum cannot be computed self-consistently unlike the case when the shock was present. Thus this ratio is chosen freely. We take the guidance for this number from what was obtained in the case when shocks are formed. However, in this case even when the mass loss takes place, *the location* of the pressure maximum remains unchanged. Since the compression ratio R_{comp} is a free parameter, R_m remains unchanged for a given R_{comp} . Let us assume that $\dot{\mu}_-$ is the *actual* mass inflow rate and it is same before and after the pressure maximum had the mass loss rate been negligible. Let $\dot{\mu}_+$ be the mass inflow rate *after* the pressure maximum, when the loss due to outflow is taken into account. Then, by definition, $\dot{\mu}_- = \dot{M}_{out} + \dot{\mu}_+$ and $R_m = \dot{M}_{out}/\dot{\mu}_-$. Thus the *actual* ratio of the mass outflow rate and the mass inflow rate, when the mass loss is taken into consideration is given by,

$$\frac{\dot{M}_{out}}{\dot{\mu}_+} = \frac{R_m}{1 - R_m} \quad (21a)$$

However, this static consideration is valid only when $R_m < 1$. Otherwise, we must have,

$$-\frac{dM_{disk}}{dt} + \dot{\mu}_- = \dot{\mu}_+ + \dot{M}_{out}$$

i.e.,

$$-\frac{dM_{disk}}{dt} = \dot{\mu}_-(R_{\dot{m}} - 1) + \dot{\mu}_+ \quad (21b)$$

Here, M_{disk} is the instantaneous mass of the disk. Since $R_{\dot{m}} > 1$, the disk has to evacuate. These cases hint that the assumptions of the steady solution break down completely and the solutions may become highly time dependent.

2.2.2 Isothermal Outflow

We assume that

(a) The outflow has exactly the *same* temperature as that of the post-shock flow, but the energy is not conserved as matter goes from disk to the jet. In other words the outflow is kept in a thermal bath of temperature as that of the post-shock flow.

(b) Same as (b) of §2.2.1.

(c) The post-shock proton temperature is determined from the inflow accretion rate \dot{M}_{in} using the consideration of Comptonization of the advective region. The procedure to compute typical proton temperature as a function of the incoming accretion rate has been adopted from Chakrabarti, 1997.

(d) The polytropic index of the inflow can be varied but that of the outflow is always unity.

Thus a supply of parameters \mathcal{E} , λ and γ makes a self-consistent computation of $R_{\dot{m}}$ possible when the shock is present. When the shock is absent, the compression ratio of the gas at the pressure maximum between the inflow and the outflow R_{comp} is supplied as a free parameter exactly as in the polytropic case.

The following procedure is adopted to obtain a complete solution:

(a) From eqs. (13) and (14) we derive an expression for the derivative,

$$\frac{d\vartheta}{dr}\Big|_{iso} = \left(\frac{\frac{C_s^2}{\mathcal{A}(r)} \frac{d\mathcal{A}(r)}{dr} + \frac{\lambda^2}{r_m^3(r)} \frac{dr_m(r)}{dr} - \frac{1}{2(r_c - 1)^2}}{\vartheta_{iso} - \frac{C_s^2}{\vartheta_{iso}}} \right). \quad (22)$$

At the sonic point, the numerator and denominator separately vanish, and give rise to the so-called sonic point conditions:

$$\frac{C_s^2}{\mathcal{A}_{co}(r)} \frac{d\mathcal{A}(r)}{dr}\Big|_{co} + \frac{\lambda^2}{r_{mco}^3(r)} \frac{dr_m(r)}{dr}\Big|_{co} - \frac{1}{2(r_{co} - 1)^2} = 0, \quad (23a)$$

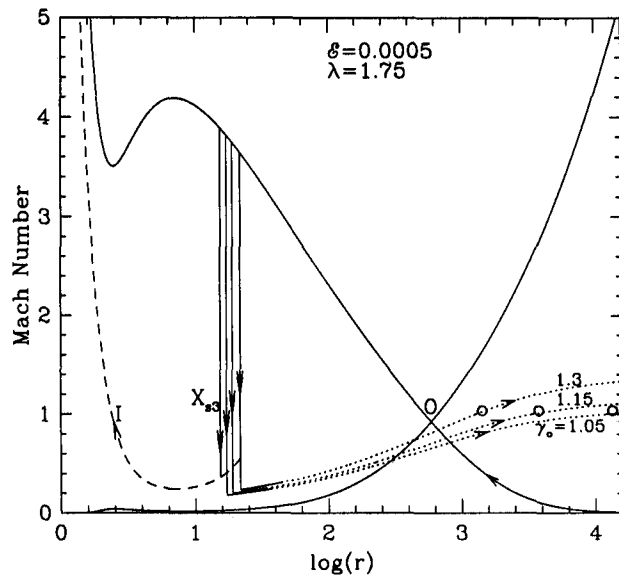


Fig. 2.2.2:

Few typical solutions which combine accretion and outflow. Input parameters are $\mathcal{E} = 0.0005$, $\lambda = 1.75$ and $\gamma = 4/3$. Solid curve with an incoming arrow represents the pre-shock region of the inflow and the dashed curve with an incoming arrow represents post-shock inflow which enters the black hole after passing through the inner sonic point (I). Dotted curves are the outflows for various γ_0 (marked). Open circles are sonic points of the outflowing winds and the crossing point 'O' is the outer sonic point of the inflow. The leftmost shock transition (X_{s3}) is obtained from unmodified Rankine-Hugoniot condition, while the other transitions are obtained when the mass-outflow is taken into account.

and

$$v_{co} = C_s, \tag{23b}$$

where, the subscript co represents the quantities at the sonic point of the outflow. The derivative of the flow at the sonic point is computed using the L'Hospital's rule. The procedure is otherwise similar to those mentioned in the polytropic case and we do not repeat them here.

3 COMPUTATION OF R_M AND ITS DEPENDENCE ON VARIOUS ACCRETION AND SHOCK PARAMETERS

3.1 Polytropic outflow coming from the post-shock accretion disk

3.1.1 Combined Flow Topology

By simultaneously solving the proper set equations in appropriate geometry (as described in §2.2), we get the *combined* flow topologies which is presented in Fig. 2.2.3. It shows a typical solution combining the accretion and the outflow. Mach number (the ratio of me-

chanical to thermal velocity of the fluid) is plotted along the ordinate while the distance measured from the central accretor (scaled in the unit of r_g) is plotted in logarithmic scale along abscissa. The input parameters are $\mathcal{E} = 0.0005$, $\lambda = 1.75$ and $\gamma = 4/3$ corresponding to relativistic inflow. The solid curve with an arrow represents the pre-shock region of the inflow and the long-dashed curve represents the post-shock inflow which enters the black hole after passing through the inner sonic point (I). The solid vertical line at X_{s3} (the leftmost vertical transition) with double arrow represents the shock transition obtained with exact Rankine-Hugoniot condition (i.e., with no mass loss). The actual shock location obtained with modified Rankine-Hugoniot condition (eq. 19) is farther out from the original location X_{s3} . Three vertical lines connected with the corresponding dotted curves represent three outflow solutions for the parameters $\gamma_o = 1.3$ (top), 1.15 (middle) and 1.05 (bottom). The outflow branches shown pass through the corresponding sonic points. It is evident from the figure that the outflow moves along solution curves completely different from that of the 'wind solution' of the inflow which passes through the outer sonic point 'O'. The mass loss ratio $R_{\dot{m}}$ in these cases are 0.256, 0.159 and 0.085 respectively.

3.1.2 Dependence of $R_{\dot{M}}$ on Various Flow Parameters

Figure 2.2.4 shows the ratio $R_{\dot{m}}$ as γ_o is varied. Only the range of γ_o and energy for which the shock-solution is present is shown here. The general conclusion is that as γ_o is increased the ratio is also increased non-linearly. When the inflow rate is very low, due to paucity of the photons, the outflow is not heated very much and γ_o remains higher. The reverse is true when the accretion rate is higher. Thus, effectively, the ratio $R_{\dot{m}}$ is going up with the decrease in \dot{M}_{in} . In passing we remark that with the variation in the inflow angular momentum, λ , the result does not change significantly, and $R_{\dot{m}}$ changes only by a couple of percentage at the most.

In Fig. 2.2.5a, we show the variation of the ratio $R_{\dot{m}}$ of the mass outflow rate and inflow rate as a function of the shock-strength (dotted) M_-/M_+ (Here, M_- and M_+ are the Mach numbers of the pre- and post-shock flows respectively.), the compression ratio (solid) Σ_+/Σ_- (Here, Σ_- and Σ_+ are the vertically integrated matter densities in the pre- and post- shock flows respectively), and the stable shock location (dashed) X_{s3} . Other parameters are $\lambda = 1.75$ and $\gamma_o = 1.05$. Note that the ratio $R_{\dot{m}}$ does not peak near the strongest shocks! Shocks are stronger when they are located closer to the black hole, i.e.,

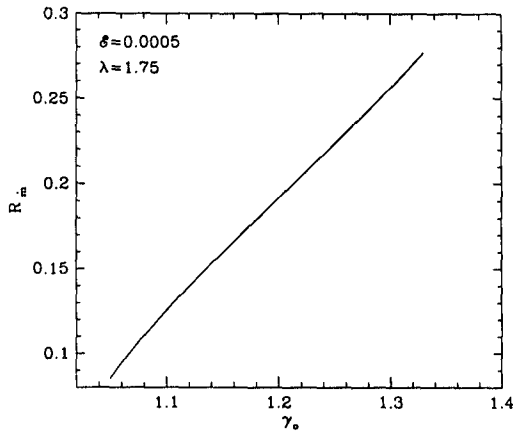


Fig. 2.2.4

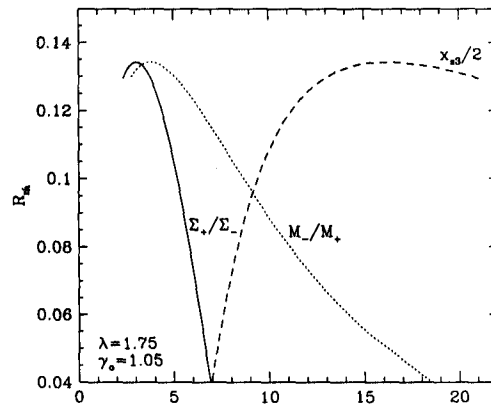


Fig. 2.2.5a

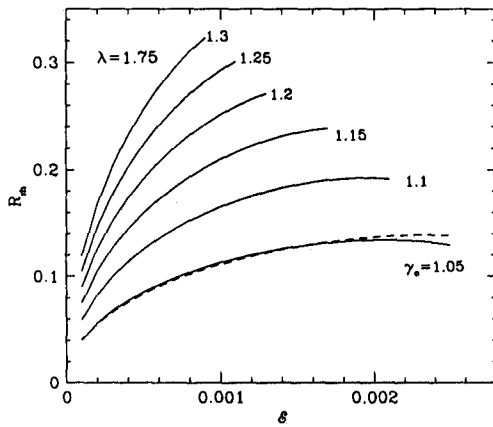


Fig. 2.2.5b

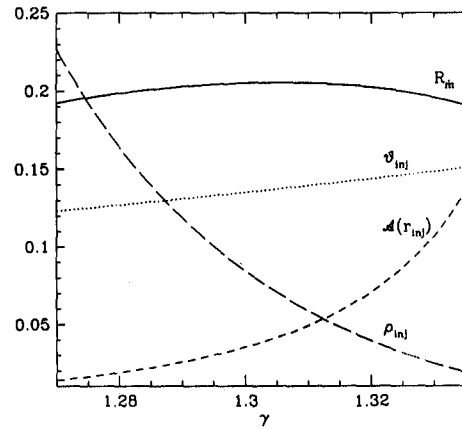


Fig. 2.2.6

Fig. 2.2.4 - 2.2.6:

- Fig. 2.2.4: Ratio R_m as outflowing polytropic index γ_o is varied. Only the range of γ_o for which the shock-solution is present is shown here. As γ_o is increased, the ratio is also increased. Since γ_o is generally anti-correlated with \dot{m}_{in} , this implies that R_m is correlated with \dot{m}_{in} .
- Fig. 2.2.5(a-b): Variation of R_m as a function of
 - (a) Shock Strength M_-/M_+ (dotted) compression ratio Σ_+/Σ_- (solid) and the shock location X_{s3} (dashed) for $\gamma_o = 1.05$.
 - (b) Variation of R_m as a function of specific energy \mathcal{E} for various γ_o (marked). $\lambda = 1.75$ throughout.
- Fig. 2.2.6: R_m as a function of the polytropic index γ of the inflow. The range of γ shown is the range for which shock forms in the flow. Suitably scaled density, velocity and area of the flow (at the base of the outflow) on the disk surface are also shown. See text for details. Non-monotonicity in R_m can be understood by the fact that the shock location, i.e., the area $\mathcal{A}(r_{inj})$ and velocity ϑ_{inj} of the outflow at the outflow origin go up with γ , but the density ρ_{inj} goes down.

for smaller energies. The non-monotonic behaviour is more clearly seen in lowest curve of Fig. 2.2.5b where $R_{\dot{m}}$ is plotted as a function of the specific energy \mathcal{E} (along x-axis) and γ_o (marked on each curve). Specific angular momentum is chosen to be $\lambda = 1.75$ as before. The tendency of the peak in $R_{\dot{m}}$ is primarily because as \mathcal{E} is increased, the shock location is increased which generally increases the outflowing area $\mathcal{A}(r)$ at the shock location. However, the density of the outflow ρ at the shock, as well as the velocity of the outflow at the shock increases. The outflow rate, which is a product of these quantities, thus shows a peak. For the sake of comparison, we present the results for $\gamma_o = 1.05$ (dashed curve) when the Rankine-Hugoniot relation was not corrected by eq. (19). The result generally remains the same because of two competing effects: decrease in post-shock density and increase in the area from the the outflow is launched (i.e., area between the black hole and the shock) as well as the launching velocity of the jet at the shock. The peak observed in the solid curve (variation of $R_{\dot{M}}$ with compression ratio Σ_+/Σ_-) is expected to be responsible for burst/quiescence features of transient sources and has been used to explain some important features of quasi-periodic oscillations in the black hole candidate GRS 1915+105 (Chakrabarti & Manickam, 2000). To have a better insight of the behaviour of the outflow we plot in Fig. 2.2.6 $R_{\dot{m}}$ as a function of the polytropic index of the *incoming* flow (γ) for $\gamma_o = 1.1$, $\mathcal{E} = 0.002$ and $\lambda = 1.75$. The range of γ shown is the range for which shock forms in the flow. We also plot the variation of injection velocity v_{inj} , injection density ρ_{inj} and area $\mathcal{A}(r)$ of the outflow at the location where the outflow leaves the disk. The incoming accretion rate has been chosen to be 0.3 (in units of the Eddington rate). These quantities are scaled from the corresponding dimensionless quantities as $v_{inj} \rightarrow 0.1v_{inj}$, $\rho_{inj} \rightarrow 10^{22}\rho_{inj}$ and $\mathcal{A} \rightarrow 10^{-4}\mathcal{A}$ respectively in order to bring them in the same scale. With the increase in γ , the shock location is increased, and therefore the cross-sectional area of the outflow goes up. The injection velocity goes up (albeit very slowly) as the shock recedes, since the injection surface (CENBOL) comes closer to the outflow sonic point. However, the density goes down (gas is less denser). This anti-correlation is reflected in the peak of $R_{\dot{m}}$.

So far, we assumed that the specific angular momentum of the outflow is exactly the same as that of the inflow, while in reality it could be different due to presence of viscosity. In the outflow, a major source of viscosity is the radiative viscosity whose coefficient is,

$$\eta = \frac{4aT^4}{15\kappa_T c \rho} \text{ cm}^2 \text{ sec}^{-1} \quad (24)$$

This could be significant, since the temperature of the outflow is high, but the density is low. Assuming that the angular momentum distribution reaches a steady state Inside the jet (Chakrabarti, 1996a and references therein).

$$l_j = C_j R^{n_j} \quad (25)$$

where C_j and n_j are constants, the vanishing condition of the azimuthal Velocity on the axis requires that $n_j > 1$ inside the jet. The matter distribution in the *rotationally dominant* region of the 'pre-jet' is computed by integrating Euler equation. It is easy to show that the 'hollow' jet thus produced carry most of the matter and angular momentum in the outer layers of the jet [1]. In other words, the average angular momentum of the outflow *away from the base* may remain roughly constant even in presence of viscosity. This is to be contrasted with the disk, where matter is more dense towards the centre while more angular momentum is concentrated towards the outer edge. If, however, the average angular momentum *at the base* of the outflow goes down due to losses to ambient medium, by, say, a factor of two, we find that the mass loss rate is also reduced by around the same factor. This shows that the outflow is at least partially centrifugally driven.

An important point to note: the ratio between the 'specific entropy measure' of the outflow to that of the post-shock inflow is obtained from the definitions of entropy accretion rate \dot{M} :

$$\frac{K_o}{K_+} = \frac{\dot{M}_{out}^{\gamma_o-1}}{\dot{M}_+^{\gamma-1}} \left(\frac{1 - R_m}{R_m} \right)^{\gamma_o-1} \dot{M}_+^{(\gamma-\gamma_o)} \frac{\gamma}{\gamma_o} \quad (26)$$

As $R_m \rightarrow 1$, $\frac{K_o}{K_+} \rightarrow 0$. Thus, we expect that for a polytropic flow with shocks, a hundred percent outflow is impossible since the outgoing entropy must be higher. In isothermal outflows such simple consideration do not apply.

If we introduce an extra radiation pressure term (with a term like Γ/r^2 in the radial force equation, where Γ is the contribution due to radiative process), particularly important for neutron stars, the outcome is significant. In the inflow, outward radiation pressure weakens gravity and thus the shock is located farther out. The temperature is cooler and therefore the outflow rate is lower. If the term is introduced only in the outflow, the effect is not significant.

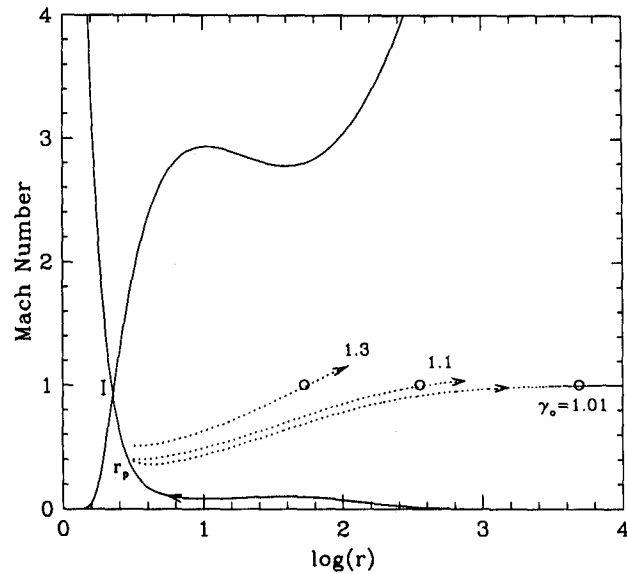


Fig. 2.2.7:

Few typical solutions for outflows forming out of an advective disk which does not include a standing shock wave. Incoming arrowed solid curve shows the inflow and the dashed arrowed curves with outgoing arrows show the outflows for $\gamma_0 = 1.3$ (top), 1.1 (middle) and 1.01 (bottom). At r_p , thermal pressure of the inflow is maximum.

3.2 Polytropic outflow coming from the region of the maximum pressure

3.2.1 Combined Flow Topology

In this case, the inflow parameters are chosen from region I (see §2.1.1 of Chapter 2.1) so that the shocks do not form. Here, the inflow passes through the inner sonic point only. The outflow is assumed to be originated from the regions where the polytropic inflow has a maximum pressure. This assumption is justified, since it is expected that winds would get the maximum kick at this region. Figure 2.2.7 shows a typical solution. The arrowed solid curve shows the inflow and the dotted arrowed curves show the outflows for $\gamma_0 = 1.3$ (top), 1.1 (middle) and 1.01 (bottom). The ratio R_m in these cases is given by 0.66, 0.30 and 0.09 respectively. The specific energy and angular momentum are chosen to be $\mathcal{E} = 0.00584$ and $\lambda = 1.8145$ respectively. The pressure maximum occurs outside the inner sonic point at r_p when the flow is still subsonic.

3.2.2 Dependence of R_M on Various Flow Parameters

Figure 2.2.8a shows the variation of thermal pressure of the flow with radial distance. The peak is clearly visible. Since the pressure maximum occurs very close to the black

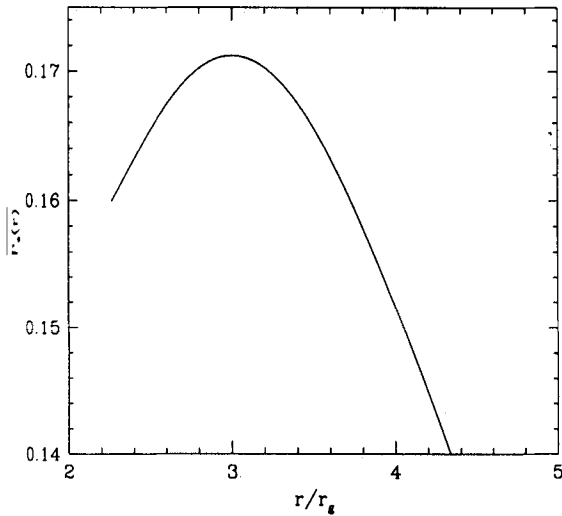


Fig. 2.2.8a

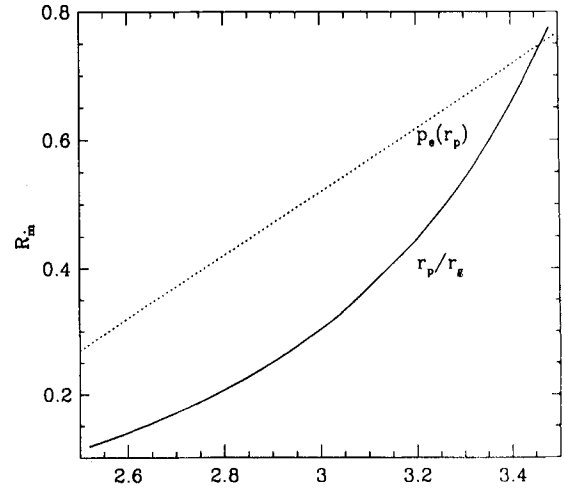


Fig. 2.2.8b

Fig. 2.2.8(a-b):

- (a) Variation of thermal pressure P_e of the incoming flow with radial distance. In a shock-free hydrodynamic flow, winds may form from the region around the pressure maximum.
- (b) Variation of R_m (solid) as a function of the location r_p of the maximum pressure and the non-dimensional pressure (dotted) $P_e(r_p)$ (multiplied by 1.5×10^{24} to bring to scale) are plotted.

hole as compared to the location of the shock, the area of the outflow is smaller, but the radial velocity as well as the density of matter at the base of the outflow are much higher. As a result the outflow rate is exorbitantly higher compared to the shock case.

The location of maximum pressure being close to the black hole, it may be generally very difficult to generate the outflow from this region. Thus, it is expected that the ratio R_m would be larger when the maximum pressure is located farther out. This is exactly what we see in Fig. 2.2.8b, where we plot R_m against the location of the pressure maximum (solid curve). Secondly, if our guess that the outflow rate could be related to the pressure is correct, then the rate should increase as the pressure at the maximum rises. That is also observed in Fig. 2.2.8b we plot here R_m as a function of the actual pressure at the pressure maximum (dotted curve). The mass loss is found to be a strongly correlated with the thermal pressure. Here we have multiplied non-dimensional thermal pressure by 1.5×10^{24} in order to bring it in the same scale.

Figure 2.2.9 shows the ratio R_m as a function of γ_o for various choices of the compression ratio R_{comp} of the outflowing gas at the pressure maximum: $R_{comp} = 2$ for the rightmost curve and 7 for the leftmost curve. We have purposely removed the solutions with $R_m >$

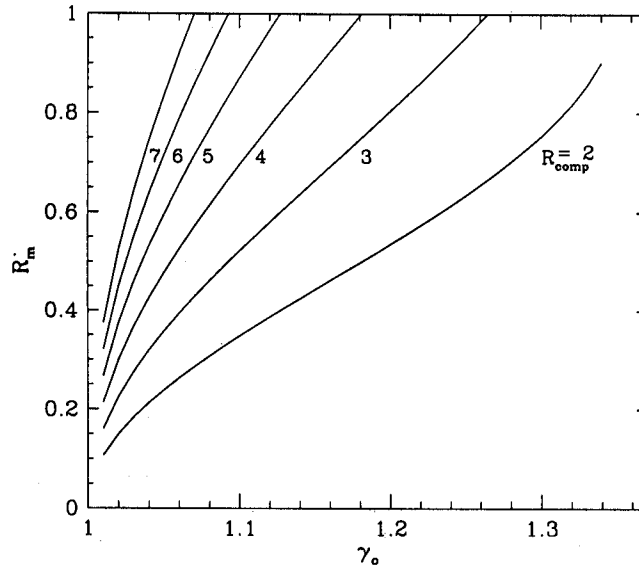


Fig. 2.2.9:

R_m as a function of outflowing polytropic index γ_o for various choices of the compression ratio R_{comp} of the outflowing gas at the pressure maximum. From bottom to top curve, $R_{comp} = 2, 3, 4, 5, 6$ & 7 respectively.

1, because the solution should be inherently time-dependent (see, eq. 21b) in these cases and a steady state approach is not supposed to be trusted completely. This is different from the results of §3.1, where shocks are considered, since R_m is non-monotonic in that case.

3.3 Isothermal outflow coming from the post-shock accretion disk

In this case, the outflow is assumed to be isothermal. The temperature of the outflow is obtained from the proton temperature of the advective region of the disk. The proton temperature is obtained using the Comptonization, bremsstrahlung, inverse bremsstrahlung and Coulomb processes (Chakrabarti, 1997 and references therein). Figure 2.2.10 shows the effective proton temperature and the electron temperature of the post-shock advective region as a function of the accretion rate (in units of Eddington rate, in logarithmic scale) of the Keplerian component of the disk. The soft X-ray luminosity for stellar mass black holes or the UV luminosity of massive black holes is basically dictated by the Keplerian rate of the disk. It is clear that as the accretion rate of the Keplerian disk is increased, the advective region gets cooler as is expected.

In Fig. 2.2.11a, we show the ratio R_m as a function of the accretion rate (in units of Eddington rate) of the incoming flow for a range of the specific angular momentum. In the

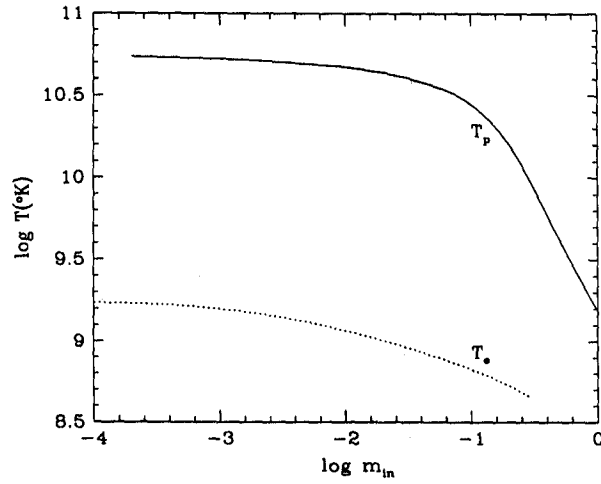


Fig. 2.2.10

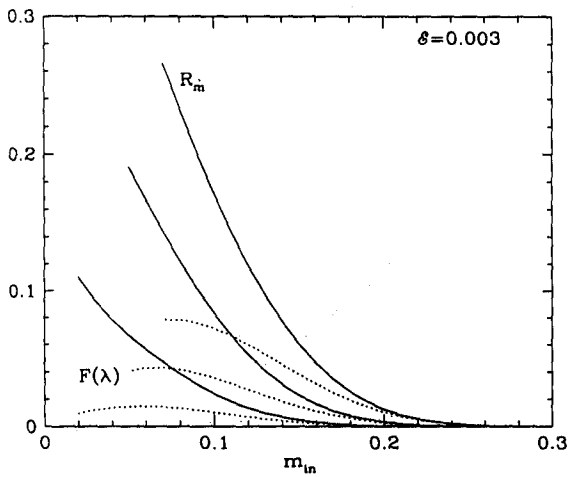


Fig. 2.2.11a

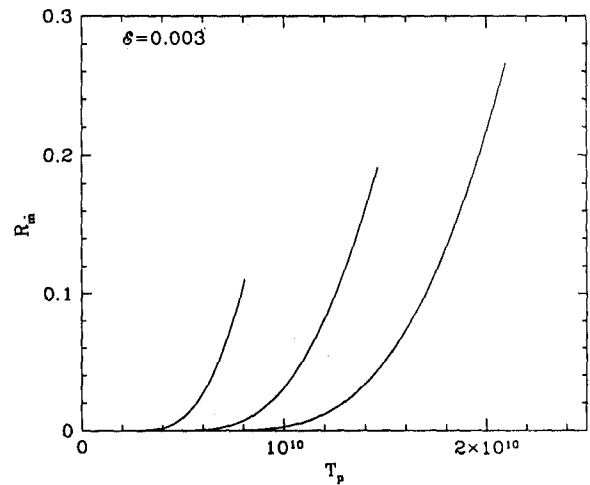


Fig. 2.2.11b

Fig. 2.2.10-2.2.11(a-b):

- Fig. 2.2.10 Variation of effective proton (solid) and electron (dotted) temperatures in the advective regions of the accretion disk around a 10 solar mass black hole as functions of the accretion rates of the Keplerian flow. As Keplerian rate increases, both protons and electrons cool down.
- Fig. 2.2.11(a-b)
 - (a) Variation of R_m as functions of the Eddington rate of the Keplerian component of the incoming flow for a range of the specific angular momentum. In the low luminosity objects the ratio is larger. The angular momentum flux $F(\lambda)$ of the outflow is also shown (dashed curve).
 - (b) R_m as a function of the proton temperature T_p of the post-shock region. In (a), $\lambda = 1.7$ (top curve), $\lambda = 1.725$ (middle) and 1.75 (bottom curve).

low luminosity objects the ratio is larger. Angular momentum is varied from $\lambda = 1.7$ (top curve), 1.725 (middle curve) and 1.75 (bottom curve). The specific energy is $\mathcal{E} = 0.003$. Here we have used the modified Rankine-Hugoniot relation as before (eq. 19). The ratio R_m is clearly very sensitive to the angular momentum since it changes the shock location rapidly and therefore changes the post-shock temperature very much. We also plot the outflux of angular momentum $F(\lambda) = \lambda \dot{m}_{in} R_m$ which has a maximum at intermediate accretion rates. In dimensional units, these quantities represent significant fractions of angular momentum of the entire disk and therefore the rotating outflow can help accretion processes. Curves are drawn for different λ as above. In Fig. 2.2.11b, we plot the variation of the ratio directly with the proton temperature of the advecting region. The outflow is clearly thermally driven. Hotter flow produces more winds as is expected. The angular momentum associated with each curve is same as before.

3.4 Isothermal outflow coming from the region of the maximum pressure

This case produces very similar result as in the above case, except that like Section 3.2 the outflow rate becomes very close to a hundred percent of the inflow rate when the proton temperature is very high. Thus, when the accretion rate of the Keplerian flow is very small, the outflow rate becomes very high, close to evacuating the disk. As noted before, this may also be related to the quiescent state of the X-ray novae.

4 COMPARISON WITH NUMERICAL SIMULATION WORKS

In the literature, not many results are present which deal with exact computations of the mass outflow rate. Molteni, Lanzafame & Chakrabarti 1994, in their SPH simulations, found that the ratio could be as high as 15 – 20 per cent when the flow is steady. In Ryu, Chakrabarti & Molteni, 1990, 10 – 15 per cent of the steady outflow is seen and occasionally, even 150 of the inflow is found to be ejected in non-stationary cases. Our result shows that high outflow rate is also possible, especially for absence of shocks and low luminosities. In Eggum, Coroniti & Katz, 1985, radiation dominated flows showed $R_m \sim 0.004$, which also agrees with our results when we consider high accretion rates (see, e.g., Fig. 9a).

5 CONNECTIONS TO OTHER FIELDS AND SCOPES FOR RELATED WORKS

5.1 Outflow Driven Contamination of Metallicity to the Outer Galaxies

A number of observational evidences suggest that the fluid (in interstellar/ intergalactic plasma form) accreting onto black hole has potential to become as hot as its virial temperature $T_{virial} \sim 10^{13} K$ (Rees, 1984). Through various cooling mechanism, such as Bremsstrahlung and Comptonization, hot and tenuious infalling gas may be cooled down to a temperature which supports significant nucleosynthesis to take place in accretion disks around black holes (Mukhopadhyaya, 1998, Mukhopadhyaya & Chakrabarti, 1999 and references therein). Hot and dense puffed up sub-Keplarian flow, after deviating from a cooler Keplarian disk, remains sufficiently hot producing the favourable temperature to produce heavier elements through significant nuclear reactions. Normally, the basic difference between the neucleosynthesis in sub-Keplarian advective accretion disk and that in the interior of ordinary stellar bodies is that while in stellar nucleosynthesis same set of nuclear reactions take place at different radii (because of the more or less uniform radial temperature distribution in the zone where nuclear burning is significant for stellar cases), radial variation of disk temperature for sub-Keplarian advective accretion simultaneously triggers different reaction/ set of reactions at different radii of the disk. It is easy to understand that presence of a centrifugal pressure supported boundary layer (generated by standing RSHK or otherwise, see §1) enhance the reaction rate and change of composition much more due to sudden rise of temperature in post-shock flows (if shock forms) and density by slowing down of infalling matter in this region thereby raising the residence time of matter considerably. Stepping ahead of the preliminary calculations of neucleosynthesis in cooler accretion disks (Hogan & Aplegate, 1987, Chakrabarti, Jin & Arnett, 1987, Jin, Arnet & Chakrabarti, 1989, Arai & Hasimoto, 1992, Hasimoto et al., 1993), change in composition of matter due to neclear reaction has been worked out for hot sub-Keplarian advective accretion flows around a Schwarzschild black hole (Mukhopadhyaya, 1998, Chakrabarti & Mukhopadhyaya, 1999, Mukhopadhyaya & Chakrabarti, 1999). A number of interesting results were obtained in their calculations contesting results from earlier work in this field. Operating a generalised reaction network containing 255 nuclear specieses, a large region of parameter space ($0.0001 \lesssim \alpha \gtrsim 1.0$, $0.001 \lesssim \dot{m} \gtrsim 100.0$, $0.01 \lesssim \beta \gtrsim 1$, $\frac{4}{3} \lesssim \gamma \gtrsim \frac{5}{3}$, symbols bear usual meaning) was explored for shock induced nucleosynthesis as well as for the cases

without shock formation. Accretion onto stellar mass black hole as well as onto SMBHs were considered.

Among a number of interesting results, our interest is in the production of some specific heavier elements. It is interesting to investigate whether the fate of the shock induced nucleosynthesis generated heavier elements could be predicted by our disk-outflow model. One of the major speculations of our model (Das, 1998, Das, 1999, Das & Chakrabarti, 1999) that outflows from the hot and dense CENBOL (where the composition change is much more significant) would carry away modified compositions and contaminate the atmosphere of the surrounding stars and galaxies in general. Unlike the works presented in this Chapter, where the outflows were assumed to be consists of m_p only (proton jet), attempts could have been made to incorporate the weighted average of the heavier elements produced by the nucleosynthesis in jet formation region as the constituent elements of the outflow. The following procedure could be adopted for this investigation. Let us suppose that sub-Keplarian inflow (with a specific nuclear composition) with some specific accretion parameters (energy, angular momentum etc..) encounters a standing RSHK at a radial distance r_{sh} and the corresponding inner sonic point is obtained as r_{in} along with the post-shock temperature T_{sh} and shock compression ratio R_{comp} . We then investigate the inflow with *exactly same* initial boundary conditions and nuclear composition and try to see whether a particular modified element, say ${}^A X_M$, is produced by nuclear reaction, and if so, we compute the *minimum* radial distance (measured from the event horizon in the unit of r_g) r_{nuc} where it may start forming. It is easy to show that if the following condition:

$$(r_{nuc})_{Shock} \gtrsim 0.5946 r_{sh}^{0.25} \lambda_{sh}^{0.5} (1 + \lambda_{sh}^{0.5}) (r_{sh} - 1)^{0.5} \quad (1)$$

(λ_{sh} being the value of specific angular momentum at the shock) is satisfied, we are assured that the element ${}^A X_M$ could be carried out through outflow. Eqs. (1) comes from the fact that the outflow is assumed to be launched from the shock generated CENBOL with a annular shaped launching surface (see Das, 1998, Das & Chakrabarti, 1999 for detail outflow geometry). If shock does not form and regions of pressure maxima drives the outflow (Das, 1998, Das & Chakrabarti, 1999), the condition:

$$(r_{nuc})_{Pressure} \gtrsim 0.5946 r_p^{0.25} \lambda_p^{0.5} (1 + \lambda_p^{0.5}) (r_p - 1)^{0.5} \quad (2)$$

assures the extraction of ${}^A X_M$ through outflow, r_p and λ_p being the radial location of the pressure maxima and the value of specific angular momentum at pressure maxima. Since

r_p forms closer to the hole compared to r_{sh} , $(r_{nuc})_{Pressure} < (r_{nuc})_{shock}$ in general. Thus elements which are produced relatively close to the hole for certain initial parameters, would preferably choose the pressure maxima generated wind to get dispersed.

Once we can calculate the percentage loss of several elements through winds, it is obvious that part of this wind could be intercepted by the companion star (for black hole binary systems) and one can expect that these new elements may be detected in the stellar atmosphere through spectroscopic analysis of line emissions. For accreting SMBHs, heavy elements produced in the disk may supply metallicity in the galaxies. Strong indications of disk-evacuation by wind for a region of parameter space (see §3.2.2.) suggests that overall such contributions to metallicity must not be neglected. Significant work in this direction is in progress by us and is expected to be reported in near future.

5.2 Explanation and Modification of Spectral Properties Due to the Presence of Outflows

As is clear from Fig. 2.2.9. §3.3.2, an interesting situation arises when the polytropic index of the outflow is large and the compression ratio is also very high. In this case, the flow virtually bounces back as the wind and the outflow rate can be equal to the inflow rate or even higher, thereby evacuating the disk completely. Even for the small compression ratios especially when the sonic point of the outflow is right outside the pressure maximum, very high massflow could take place in some range of parameter space spanned by \mathcal{E} and λ . In this range of parameter space, most of the steady state assumptions used in investigating the flow is likely to breakdown because the situation is supposed to become inherently time-dependent (see eqs. 21a and 21b.). These cases can cause runaway instabilities by rapidly evacuating the disk. It is possible that some of the black hole systems, including that in our own galactic centre, may have undergone such evacuation phase in the past and gone into quiescent phase. Results obtained in §3.2.2, thus, could explain the quiescent states in X-ray novae systems like GS2000+25 or GRS1124-633 etc. (Tanaka, 1995, Udea, et al, 1994) and also in some systems with massive black holes, especially the black hole at our galactic centre.

The radio source *Sgr A** situated right at the dynamical centre of the central star cluster of our galaxy is an unique 1 Jy flat spectrum radio point source (Eckart et al, 1993, Eckart & Genzel, 1997, Menten et al, 1998) and is believed to harbour an accreting SMBH of mass

$\sim 10^6 M_\odot$ bounded within ~ 0.015 pc with mean density $\rho_{mean} > 10^{12} M_\odot pc^{-3}$ (Eckart & Genzel, 1997, Ghez et al, 1998). Sgr A* is supposed to accrete gas from the winds of nearby (~ 0.1 pc) massive stars (Krabbe et al, 1991). The bolometric luminosity of Sgr A* is observed to be $\lesssim 10^{37} erg s^{-1}$ (Genzel et al, 1994, Eckart & Genzel, 1997) while the upper limit on the mass accretion rate of Sgr A* (from limits on the X-ray and IR emission) is of the order of $\sim 8 \times 10^{-5} M_\odot Yr^{-1}$, Bondi accretion rate on it (estimated using the observed spacial distribution of mass loosing stars and assuming non-interacting stellar winds) has been approximated as $\sim 3 \times 10^{-5} M_\odot Yr^{-1}$ (Quartart, Narayan & Reid, 1999 and references therein) which indicates that the radiative efficiency of this object is unusually low. We suggest that a possible explanation for this low luminosity could be due to the presence of profuse mass loss from near vicinity of this source (Sgr A*). We have obtained that for such a low accretion rate as that of has been observed for Sgr A*, the mass outflow rate is exorbitantly high, almost to the point of evacuating the disk, (Das, 1998, Das & Chakrabarti, 1999) which prompted us to strongly speculate that the spectral properties of our galactic centre could be explained by inclusion of wind using our model. Also we suggest that explanation of spectral properties of our galactic centre should include outflow according to our model to modify all the characteristics spectra of our galactic centre obtained without the presence of mass loss and also the issue of existance of a "fossil-disk" at the centre of our galaxy (Falcke, 1998) could further be investigated in the framework of our disk-outflow model.

For an weakly viscous two component accretion flow with CENBOL situated close to the hole, the Keplarian component close to the equatorial plane may have a low accretion rate whereas the sub-Keplarian halo surrounding it has a higher accretion rate (CT95). Without incorporating the wind, both these rates should be constant. Inclusion of winds generated according to our disk-outflow model changes this situation by depleting disk matter through wind at the rate determined by the temperature of the CENBOL when other accretion parameters are kept fixed. As the fraction of the accreting matter expelled as outflows is increased, Keplarian part of the disk surrounding the advective region will have higher efficiencies for Compton cooling, thus the spectra of the power law component for the same multifrequency black-body component will be modified and the energy spectral index α will increase causing overall softening of the spectra. by inclusion of wind according to our model (Chakrabarti, 1998 and references therein). It has been suggested that (CT95) the Fe K_α lines produced close to the black hole might be due to

outflows from advective region. Thus it is not unjustified to propose that combined investigation of Fe K_{α} line intensity with the spectral softening of black hole candidates would provide a definitive scheme to detect the signature of winds from CENBOL.

Outflow From Spherical Accretion

Chapter 3

SUMMARY

Generation of outflows from spherical/quasi-spherical accretion (with negligible intrinsic angular momentum) onto non-rotating black holes are thoroughly investigated. Proposing that a relativistic hadronic pressure supported steady and standing spherical shock may be treated as the virtual hard surface from where the outflow could be generated, mass outflow rate R_M is computed and its dependence on various flow parameters have been studied by simultaneously solving the set of equations governing accretion and wind.

In this chapter we describe * how to extract outflows from a spherical/quasi-spherical accretion (Bondi type accretion (Bondi, 1952)). Absence of considerable intrinsic angular momentum in accreting material may lead to this situation. This may happen when the central SMBH at the galactic centre is surrounded by dense stellar cloud in such a way that the vector sum of the angular momentum of tidally disrupted matter (from a number of stars with trajectories approaching sufficiently close to the hole) almost vanishes. Absence of angular momentum then rules out the possibility of formation of Rankine-Hugoniot shock as well as the polytropic pressure maxima. So, for accretion of this type, CENBOL formation is not possible, thus, unlike disk accretion, freely falling accreting material here may not encounter any 'virtual surface' in the way it has been described in Chapter 2.2. As it is obvious from §1 of Chapter 2.2, the fundamental and necessary ingredient of our outflow model in the presence of a hot and dense surface which mimics the stellar surface in regards of mass outflow, absence of CENBOL led us to seek for some alternative physical mechanism which may produce such kind of 'virtual' boundary around the hole from where outflow may be generated.

* §3,4 and 5 of this chapter are largely based on Das, 1999a, 1999b, 2000.

1 IN SEARCH FOR A SUITABLE SURFACE

While trying to explain the high luminosity of Quasars and AGNs and to model their broad band spectrum, it was realized that matter falling freely onto the black hole (radial accretion) need not radiate all its potential energy (Sapiro, 1973). Normally, in a spherical accretion of adiabatic matter, flow may have exactly one sonic point. The sonic surface is spherically symmetric. Such a flow has been shown to be stable using general form of perturbation in a full general relativistic frame work. Moncrief (Moncrief, 1980) had shown that a suitable energy norm of the perturbation outside the sonic surface remains bounded by its initial value and no perturbation inside the sonic surface extends to regions outside the sonic surface. It has also been argued that no unstable mode corresponds to a standing shock at the sonic surface thus no unstable mode exists inside the sonic surface. The perturbation within the sonic surface are advected within the black hole through the horizon. Therefore a flow, subsonic at a large distance and becoming supersonic at the sonic point, may not have a shock. However, for accretion slightly departed from exact adiabatic equation of state with non-constant, density dependant polytropic index ($\gamma = \gamma(\rho)$) and with local source of heating and cooling, it has been shown that (Chang and Ostriker, 1985) the inflow may pass through more than one sonic point thus may have shocks in between. Investigating standard radial, time-independant fluid hydrodynamic equations with simplified Compton heating and bremstrahlung cooling functions, it was argued that if n (polytropic constant of the flow) would be a decreasing function of a (the inflow sound speed), more than one sonic points could exist. Particularly, if n oscillates around $\frac{3}{2}$, more than one sonic point is obtained and shock formation is possible. Since for a perfect monoatomic gas $n > \frac{3}{2}$ corresponds to cooling and $n < \frac{3}{2}$ corresponds to heating of the flow, a combination of bremstrahlung cooling and Compton heating allows to contrast quite a few self-consistent cases where spherical shocks may form. It has been suggested that somewhere in the part of the flow where Compton heating is dominant, the gas is heated enough to flow subsonically but interior to this it cools and falls in a free fall manner towards the hole occurrence of which was argued to be justified by attaching the subsonic portion via a standing shock to the outer quasi-isothermal free fall zone. For some values of luminosity and efficiency, it was shown that no steady solutions would exist without shocks, but allowing for the possible existance of a standing shock, unique new solutions were found.

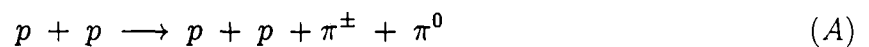
However, at this point it is worth mentioning why we did not consider shock surface found by Chang and Ostriker as our effective surface. Firstly, no stability analysis was provided for shock generated in this process rather it was speculated that they may not be stable to radial perturbations. Secondly, (and *mainly*), shock locations in their work are quite far away from the hole (always of the order of $10^6 r_g$ or more). Typically the outer (isothermal) sonic point, shock location and inner sonic points were of the order of (Chang and Ostriker, 1985) $10^7 r_g$, $10^6 r_g$, and $10^4 r_g$ respectively. We find no reason to take this shock surface located such a large distance away from the central accretor to generate outflows because it is clear that at a distance of the order of $\sim 10^6 r_g$ or even more from the hole, the amount of gravitational potential energy available to be put onto the accreting fluid to pump it out as wind would be extremely small and the mass outflow rate R_M will be negligible; unrealistically low so to say. So we seek for some other form of mechanism which may produce shocks located reasonably closer to the accreting black hole.

It was understood that accretion onto a black hole could be efficient to produce radiative energy if the directed infall motion could be randomized close to the hole by some suitable mechanism best of which would be shock formation by some means. For radial accretion, a novel mechanism has been proposed (Protheros and Kazanas, 1983, Kazanas and Ellison, 1986; PK83 and KE86 from now onwards) in which the kinetic energy of spherically accreting material has been randomized by proposing a steady, collisionless, self-supported relativistic hadronic pressure supported shock around a Schwarzschild black hole which produces a nonthermal spectrum [†] of high energy (relativistic) protons. Radio, X-rays and γ -rays observations show that some quasars appear to emit roughly equal energy per decade from radio to γ -ray energies (over 10 - 12 orders of magnitude in energy, see Ramaty and Lingenfelter, 1982). Since radial infall (freely falling situation) in a gravitational potential is unlikely to release more than $\sim 0.1 mc^2$ per particle which is quite insufficient to produce the observed high luminosity and high energy tail of the spectrum for most of the quasars, it has been suggested in PK83 and KE86 that the relativistic particles required to account for the observed radio, X-ray and γ -ray emission may result from shock acceleration of a part of infalling plasma via first order Fermi ac-

[†] A thermal distribution of particles may also be produced at the shock which radiates by thermal bremsstrahlung (PK83) but only the radiation resulting from the non-thermal (which might actually contain most of the energy; see Axford, 1981) was considered in their model.

celeration (Axrod, Leer and Skardon, 1977, Blandford and Ostriker, 1978, Cowsik & Lee, 1981, 1982, Blandford & Eichler, 1987, Kirk and Duffy, 1999) which transforms directed kinetic energy into relativistic particle energy thus produces relativistic protons with high efficiency. A steady state situation is assumed to be developed where a standing collisionless spherically symmetric shock is proposed to form.

The question of the existence of a steady shock for spherical inflow deserves some elaborate discussion and clarification. As already mentioned; absence of considerable angular momentum in accreting material supports no standard shock of Rankine-Hugoniot type, assumption of a steady and standing spherically symmetric shock for freely falling material, may apparently contradict our previous statement. The situation, however, is different if the relativistic protons of sufficient energy density are present around the black hole. Let's see what happens when freely falling supersonic [†] plasma approaches close (some factor of tens of r_g or may even less) to the black hole. Due to various possible instabilities in supersonic plasma flow, any small disruption mechanism may slow down the flow and may create a 'piston' which produces a shock (KE86). Thus the initial formation of shocks may be attributed either to convection of ambient relativistic particles or to dissipation in magnetic fields as suggested in literature (see PK83 and references therein). Once the shock is produced, it accelerates a part of infalling matter to relativistic energies. Infalling thermal particles with free fall velocity are then assumed to be shock accelerated via first order Fermi acceleration and relativistic protons will be produced. Because the kinetic energy of these relativistic particles are much larger than their gravitational potential energy and because their scattering mean free path could be larger than the black hole radius, [§] these relativistic protons practically suffer no Compton losses and are not instantly swallowed by the black hole, rather scatter several times and undergo multiple inelastic nuclear and collisions produces pion ($\pi^{\pm,0}$) before captured by the hole (PK83, KE86).



Pions generated by this process decay into relativistic electrons, positrons, neutrinos and antineutrinos and produces high energy γ -rays.

[†] Supersonic because, as we will see later, spherical accretion with inflow energy and accretion rate specified to reasonably realistic value, crosses its sonic point far away (\gtrsim hundreds of Schwarzschild radius or even more) from the black hole.

[§] Furthermore, the converging magnetic field, if present, is also expected to mirror the relativistic particles and help prevent them from being absorbed by the black hole (KE86).

$$\pi^0 \longrightarrow 2\gamma \quad (B1)$$

$$\pi^- \longrightarrow e^- + \bar{\nu}_e \quad (B2)$$

$$\pi^+ \longrightarrow e^+ + \nu_e \quad (B3)$$

As the relativistic protons are assumed to lose energy only through the above mentioned nuclear collisions and since the proton-proton collision time scale τ_{pp} would, in general, be much larger compared to the free fall time scale, a sufficiently high density of relativistic protons could be maintained which provides radially outward pressure sufficient enough to support the sustenance of a steady standing shock. The shock is, thus, self-supported.

The relativistic protons were assumed to be trapped within a radius comparable to the radius of the shock surface by some mechanism (possibly by magnetic fields tied to the accreting matter) because had it been the case that those protons would not be confined to the central region of the quasars, spallation of nuclei in the outer gas cloud responsible for the line emission in Quasars would result in an overabundance of boron (Baldwin et al, 1977), contrary to the observation. In addition, the matter density in this region may be assumed to be sufficiently high so that the relativistic protons are depleted mainly by nuclear interactions which, possibly could set a lower limit (though not very restrictive) on the accretion rate for a given black hole mass (PK83).

It was also suggested in PK83 that if the particles accelerated at the shock were nucleons rather than electrons, then, due to their negligible Compton losses, the Compton catastrophe ¶ could be avoided. The spectrum of protons accelerated by the shock is supposed to follow a power-law momentum dependence, i.e., $Q_p(p) = K_p p^{-\Gamma}$ and nuclear interactions throughout the volume within the shock radius would result in a spectrum of pions at productions given by (PK83)

$$Q_\pi(\mathcal{E}) = \frac{\Gamma}{\Gamma - 1} \int_{\mathcal{E}}^{\infty} Q_p(\mathcal{E}^\nu) \Phi_\pi(\mathcal{E}^\nu, \mathcal{E}^\pi) d\mathcal{E}^\nu$$

$\Phi_\pi(\mathcal{E}^\nu, \mathcal{E}^\pi)$ being the probability of a proton of energy \mathcal{E}^ν producing a pion of energy \mathcal{E}^π in a single nuclear interaction. Electrons originated by pion decay (Eqn. (B)) produce

¶ Compton catastrophe is referred to the fact that the lifetime of the relativistically radiating electrons are much shorter than the light crossing time of the source.

the observed non-thermal radiation from Quasars by synchrotron and inverse Compton scattering and γ -ray spectrum of QSOs are supposed to be generated by inverse Compton scattering of the relativistic elements and via decay of nuclear pion ($\pi \rightarrow 2\gamma$). It is to be noted here that through direct production of electron-positron pairs by interaction of protons with protons may become important at very high energies (Blumenthal, 1970), in their model PK83 and KE86 considered only secondary electrons resulting from nuclear collisions of the non-thermal proton distribution (via $\pi^{\pm,0}$ production) as opposed to the those produced by thermal distribution of protons (Marscher, Vestrand, and Scoll, 1980) and their model predicts a higher flux of high energy neutrinos than in models where electrons are directly accelerated.

We take this pair-plasma supported steady standing collisionless spherical shock surface as the alternative of the CENBOL, which can be treated as the effective physical hard surface, that, in principle, mimics the ordinary stellar surface regarding the mass outflow. As the condition necessary for the development and sustenance of such a shock is satisfied when at shock location, the Mach number of the inflow M_{sh} is considerably high (high supersonic flow at the time it encounters the shock, Ellison and Eichler, 1984), we concentrate on polytropic accretion with such a set of values of specific energy \mathcal{E} and accretion rate (scaled in the unit of Eddington rate) \dot{M}_{Edd} which produces high shock Mach number solution. We *explicitly* compute the *exact* shock location r_{sh} (distance from the event horizon of the BH and measured in r_g) in terms of only three accretion parameters (namely, specific energy \mathcal{E} , accretion rate \dot{M}_{Edd} and polytropic index γ_{in} of inflow) which has not been done before. This three parameter input set $\{\mathcal{E}, \dot{M}_{Edd}, \gamma\}$ will be referred as $\{\mathbf{P}_3\}$ from now onward throughout this chapter.

2 AT THE END OF THE SEARCH

At the shock surface, density of the post-shock material shoots up and velocity falls down abruptly. In other words, highly supersonic inflow becomes subsonic and accreting matter becomes shock-compressed at this surface. Matter starts getting hotter and denser and starts piling up on the shock surface. The post shock relativistic hadronic pressure and thermal pressure (pressure generated by high temperature produced at the shock) then gives a kick to the piled up matter the result of which is the ejection of outflow from the shock surface. Thus a hot and dense spherical shock surface serves as the 'effec-

tive' physical atmosphere regarding the generation of mass outflow from matter accreting onto black holes. For this type of inflow, accretion is expected to proceed smoothly after a shock transition, since successful subsonic solutions have been constructed for accretion onto black holes embedded within normal stars with the boundary condition $u = c$; where u is the infall velocity of matter and c is the velocity of light in vacuum. The fraction of energy converted at the shock surface \mathcal{E}_F through the hadronic ($p - p$) collision and mesonic ($\pi^{\pm,0}$) decay, the shock compression ratio R_{comp} , along with the ratio of post shock relativistic hadronic pressure to infalling ram pressure at a given shock location are obtained from the steady state shock solution of Ellison and Eichler (Ellison & Eichler, 1984,1985). The shock location as a function of $\{P_3\}$ is then self-consistently obtained using the above mentioned quantities. We then calculate the amount of mass outflow rate $R_{\dot{m}}$ from the shock surface using simultaneous solution of exact transonic inflow outflow solutions and study the dependence of $R_{\dot{m}}$ on various physical entities governing the inflow-outflow system. We thus quantitatively compute the mass-outflow rate from the inflow parameters and self-consistently connect the accretion and wind type topologies. To the best of our knowledge, there is no such model available in the literature which could rigorously compute the mass-loss rate from zero angular momentum quasispherical Bondi type accretion onto Schwarzschild black holes in term of *only three* accretion parameters (along with only one outflow parameter γ_{out} when outflow also is polytropic, see Das, 1999b for detail). as has been successfully done in our work.

3 MODEL DESCRIPTION, GOVERNING EQUATIONS AND THE SOLUTION PROCEDURE

3.1 Inflow model

We assume that a Schwarzschild type black hole quasi-spherically accretes fluid obeying polytropic equation of state. The density of the fluid is $\rho(r)$, r being the radial distance measured in the unit of Schwarzschild radius. We also assume that the accretion rate (in the unit of Eddington rate) with which the fluid is being accreted, is not a function of r . For simplicity of calculation, we choose geometric unit (unit of length = $\frac{2GM}{c^2}$ & unit of velocity is c . M is the mass of the black hole, c is the velocity of light and G is the universal gravitational constant. All other relevant physical quantities can be expressed like wise) to measure all the relevant quantities. We ignore the self-gravity of the flow and the cal-

ulation is being done using Paczyński-Wiita (Paczyński & Wiita, 1980) potential which mimics surrounding of the Schwarzschild black hole. Magnetic field is not considered in our calculation for the sake of simplicity. The equations (in dimensionless geometric unit) governing the inflow are :

a) Conservation of specific energy is given by:

$$\mathcal{E} = \frac{u(r)^2}{2} + na(r)^2 - \frac{1}{2(r-1)} \quad (1)$$

$u(r)$ and $a(r)$ are the radial and polytropic sound velocities respectively. $a(r) = \left[\frac{\gamma p(r)}{\rho(r)} \right]^{\frac{1}{2}}$; $p(r)$ being the polytropic pressure. For a polytropic inflow, $p(r) = K\rho(r)^\gamma$ where K is a measure of the entropy which remains constant throughout the flow except at the shock location. n is the polytropic constant of the inflow $n = (\gamma - 1)^{-1}$, γ being the polytropic index.

b) Mass conservation equation is given by,

$$\dot{M}_{in} = \Theta_{in}\rho(r)u(r)r^2 \quad (2)$$

Θ_{in} being the solid angle subtained by the inflow. As already mentioned, we assume that a steady, collisionless shock forms at a distance r_{sh} (measured in the unit of Schwarzschild radius) due to the instabilities in the plasma flow. We also assume that for our model, the effective thickness of the shock Δ_{sh} is small enough compared to the shock standoff distance, i, e,

$$\Delta_{sh} \ll r_{sh}$$

Accreting particles with infall velocity $u(r)$ are then assumed to be shock accelerated via first order Fermi acceleration. Due to this process, relativistic protons will be produced. These relativistic protons, suffer essentially no Compton loss and hence are not readily swallowed by the black hole. Rather they usually scatter several times before being captured by the black hole thus provide sufficient outward pressure necessary to support the shock. These protons, in turn, produce pions through post-shock inelastic nuclear collisions. Pions generated by this process, decay into relativistic electrons, neutrinos & antineutrinos and produces high energy γ rays. These electrons produce the observed non-thermal radiation by Synchrotron and inverse Compton scattering. The overall efficiency of this mechanism depends largely on the shock location. It has been shown (Eichler, 1979) that almost half of the energy flux that goes into relativistic particles is lost

owing to neutrinos.

From eqs. (2), the local density of infalling matter $\rho(r)$ comes out to be

$$\rho(r) = \frac{\dot{M}_{in}}{\Theta_{in} u(r) r^2} \quad (3)$$

When the shock is produced, density of matter will shoot up and inflow velocity fall down abruptly. If (ρ_-, u_-) and (ρ_+, u_+) are the pre and post-shock densities and velocities respectively, then

$$\frac{\rho_+}{\rho_-} = R_{comp} = \frac{u_-}{u_+} \quad (4)$$

Where R_{comp} is the shock compression ratio. For high shock Mach number solution (which is compatible with our low energy accretion model), the expression for R_{comp} can be well approximated as

$$R_{comp} = 1.44 M_{sh}^{\frac{3}{4}} \quad (5)$$

Where M_{sh} is the shock Mach number and eqs. (5) holds good for $M_{sh} \gtrsim 4.0$ (Ellison & Eichler, 1985). We also assume that the relativistic hadrons encounters the full shock compression ratio while crossing the shock surface. The hadronic interaction characteristic time scale τ_{pp} may be expressed as ^{||}

$$\tau_{pp} = \frac{1}{\rho_+ \sigma_{pp} c} \quad (6)$$

Where σ_{pp} is the collision cross section for relativistic protons. Using eqs. (4), τ_{pp} can also be expressed as

$$\tau_{pp} = \frac{1}{R_{comp} \rho_- \sigma_{pp} c} \quad (6a)$$

If we now assume that a fraction \mathcal{E}_F of the infalling energy is converted into radiation through the hadronic collision ($p - p$) and mesonic (π^\pm, π^0) decay, this \mathcal{E}_F will allow convergent steady state solutions and in the case of quasi-spherical infall, allows the development and sustenance of a steady, standing, spherical collisionless shock at a fixed distance r_{sh} measured in the unit of Schwarzschild radius.

The luminosity obtained from this energy \mathcal{E}_F at the shock location r_{sh} is assumed to be \mathcal{L}_1 . For a spherical shock surface and taking care of neutrino losses, the expression for \mathcal{L}_1

^{||} As only a fraction of the accreting matter is shock energized, the value of ρ_+ used to calculate τ_{pp} is, in reality, less than that of the actual ρ_+ , giving a higher value of τ_{pp} . The accurate value of τ_{pp} can be calculated using the cosmic ray energy spectrum and coupling the relativistic and non-relativistic part of the accreting plasma which will be presented elsewhere. Nevertheless, our rough estimation assures that even with the accurate value of τ_{pp} (which is higher than that of used here), the conditions of shock formation are highly satisfied.

can be written as (KE86):

$$\mathcal{L}_1 = 2\pi r_{sh}^2 \rho_{sh} m_p u_{sh}^3 \mathcal{E}_F \quad (7a)$$

where m_p is the mass of the proton and subscript sh indicates that the respective quantities are measured at the shock location.

If we assume that the pressure of the relativistic particles \mathcal{P}_{rel} (uniform inside the shock), the average energy density is then $3\mathcal{P}_{rel}$, so alternatively the luminosity can be expressed in terms of the volume integral of the emissivity ϵ due to the hadronic ($p-p$) collision where

$$\epsilon = \frac{3\mathcal{P}_{rel}}{\tau_{pp}}$$

Thus the alternative expression for the luminosity obtained as function of \mathcal{P}_{rel} would be,

$$\mathcal{L}_2 = \frac{4\pi r_{sh}^3 \mathcal{P}_{rel}}{\tau_{pp}} \quad (7b)$$

Defining δ as the ratio of downstream relativistic particle pressure to incoming ram pressure at the shock, we obtain

$$\mathcal{P}_{rel} = \delta \rho_{sh} m_p u_{sh}^2 \quad (8)$$

Equating (7a) and (7b) and substituting the values of ρ , \mathcal{P}_{rel} , and τ_{pp} from eqs. (3), (6a) and (8) respectively, we get the expression for the shock location as a function of various inflow parameters as

$$r_{sh} = \frac{3\sigma_{pp} c \dot{M}_{in}}{u_{sh}^2 \Theta_{in}} \left(\frac{\delta}{\mathcal{E}_F} \right) \quad (9)$$

The ratio $\left(\frac{\delta}{\mathcal{E}_F} \right)$, *only* as a function of shock Mach number M_{sh} for a high shock Mach number solution (low energy inflow) is obtained from the empirical solution deduced by Ellison and Eichler (Ellison & Eichler, 1984), after suitable modification required for our model and the shock location (without a constant term) is obtained in terms of shock parameters as

$$r_{sh} = \frac{3\sigma_{pp} c \dot{M}_{in}}{u_{sh}^2 \Theta_{in}} \left(\frac{1 - 2.4 M_{sh}^{-0.68}}{1 - 3.2 M_{sh}^{-0.62}} \right) \quad (10)$$

As we will see in §3.3, u_{sh} and M_{sh} are obtained from $\{\mathbf{P}_s\}$ only, r_{sh} can be computed using *only three* accretion parameters as claimed earlier.

3.2 Outflow models

Like disk outflow system, we consider two types of outflows. In ordinary stellar mass loss computations (Tarafer, 1988 and references therein) the outflow is assumed to be isothermal till the sonic point. This assumption is probably justified, since copious photons from the stellar atmosphere deposit momenta on the slowly outgoing and expanding outflow and possibly make the flow close to the isothermal. This need not be the case always for outflow from black hole candidates. Our 'effective' hard surface, being pretty close to the black hole, are very hot and most of the photons emitted may be swallowed by the black hole itself instead of coming out of the region and depositing momentum onto the outflow. Thus, the outflow could be cooler than the isothermal flow in our case. We choose polytropic outflow with a different polytropic index $\gamma_o < \gamma$ due to momentum deposition. Nevertheless, it may be advisable to study the isothermal outflow to find out the behaviour of the extreme cases. Moreover, as near the black hole, electron number density n_e falls off as $r^{-\frac{3}{2}}$ while the photon number density n_γ falls off as r^{-2} , the ratio $\left(\frac{n_e}{n_\gamma}\right) \propto r^{\frac{1}{2}}$ and increases with the increase of radial distance. So a compact object may have a lesser number of electrons available per photon and the momentum transfer may be an efficient process with increase of shock location. Hence taking the outflow to be isothermal (at least upto its sonic point) may be a justified assumption due to the fact that continuous momentum deposition on subsonic outflow might help to keep the outflow temperature roughly constant. Thus an isothermal outflow is chosen in our second model of outflow, which, in some sence, may be treated as a 'hybrid model' which successfully connects flows with two different equations of state (polytropic inflow-isothermal outflow). As a fraction of infalling energy density (\mathcal{E}_F) is converted into radiation, specific energy of the polytropic outflow is somewhat less than that of the inflow. Nevertheless, the outflow specific energy in this case is also kept constant throughout the flow.

3.2.1 Polytropic Outflow

The following two conservation laws are valid for the outflow :

$$\mathcal{E}' = \frac{v(r)^2}{2} + n'a(r)^2 - \frac{1}{2(r-1)} \quad (11)$$

$$\dot{M}_{out} = \Theta_{out}\rho(r)v(r)r^2 \quad (12)$$

Where \mathcal{E}' is the specific energy of the outflow and $\mathcal{E}' < \mathcal{E}$ and $n' = (\gamma_o - 1)^{-1}$ is the polytropic constant of the outflow. Θ_{out} is the solid angle subtended by the outflow and $v(r)$ is the velocity of the outflow.

For simplicity of calculation, we assume that the outflow is also quasi-spherical and $\Theta_{out} \approx \Theta_{in}$. Defining $R_{\dot{m}}$ as the mass outflow rate, we obtain

$$R_{\dot{m}} = \frac{\dot{M}_{out}}{\dot{M}_{in}} \quad (13)$$

It is obvious from the above discussion that $R_{\dot{m}}$ should have some complicated functional dependences on the following parameters

$$R_{\dot{m}} = \Psi(\mathcal{E}, \dot{M}_{in}, r_{sh}, R_{comp}, \gamma, \gamma_o) \quad (13a)$$

3.2.2 Isothermal Outflow

As the isothermality of the outflow (at least upto the sonic point) has already been justified as a valid assumption (see Introduction), the equation of state for the outflowing matter can be written as

$$P = \frac{\mathfrak{R}}{\mu} \rho T = C_s^2 \rho \quad (14)$$

where \mathfrak{R} is the universal gas constant, μ is the mean molecular weight, T is the temperature, ρ is the density and C_s is the isothermal sound speed of the outflow. Because of the fact that the subsonic outflow is taken to be originated from the shock surface, T in eq. (14) is basically the post-shock temperature. Our isothermality assumption demands that the outflow will have exactly the same temperature as that of the post-shock accretion flows, but the energy is not conserved as the matter jumps from the inflow to the outflow branch. In other words, the outflow is assumed to be kept in a thermal bath of temperature as that of the post-shock flow.

Using eq. (14) we integrate the radial momentum conservation equation

$$v(r) \frac{dv(r)}{dr} + \frac{1}{\rho(r)} \frac{dP(r)}{dr} + \frac{1}{(r-1)^2} = 0 \quad (15a)$$

and continuity equation

$$\frac{1}{r^2} \frac{d}{dr} (\Theta_{out} \rho(r) v(r)^2) = 0 \quad (15b)$$

to obtain the following two conservation equations for our outflow:

$$\frac{v_{iso}^2}{2} + C_s^2 \ln \rho_{iso}(r) - \frac{1}{2(r-1)^2} = Constant \quad (16)$$

and

$$\dot{M}_{out} = \Theta_{out} \rho_{iso}(r) v_{iso}(r) r^2 \quad (17)$$

The subscript *iso* indicates that all the relevant physical parameters are measured based on the isothermality assumption. \dot{M}_{out} is the quantity of outflowing mass which is constant for a fixed value of our three input parameter set $\{\mathbf{P}_3\}$ whereas $v_{iso}(r)$ is the radial velocity of the outflow and Θ_{out} is the solid angle subtended by the outflow.

The isothermal sound speed C_s (measured at the shock surface) and the post shock temperature T_{sh} can be written as

$$C_s = \sqrt{\frac{p_+(r_{sh})}{\rho_+(r_{sh})}} \quad (18)$$

$$T_{sh} = \frac{C_s^2 \mu m}{\kappa} \quad (19)$$

where $p_+(r_{sh})$ and $\rho_+(r_{sh})$ are the post-shock pressure and density at the shock surface, μ is the mean molecular weight, m is the mass of the each particle and κ is the Boltzmann's constant. The temperature of the outflow in our work will essentially assumed to be characterised by proton temperature. Hence we replace m by m_p (mass of the proton) and take $\mu = 0.5$ for our calculation. Hence the post shock proton temperature would be

$$T_{psh} = \frac{C_s^2 \mu m_p}{\kappa} \quad (20)$$

As the total pressure (thermal pressure plus ram pressure) of the polytropic inflow is a shock-invariant quantity, we can write

$$p_+(r_{sh}) + \rho_+(r_{sh}) u_+^2(r_{sh}) = p_-(r_{sh}) + \rho_-(r_{sh}) u_-^2(r_{sh}) \quad (21)$$

where the + and - denote the post and pre-shock quantities respectively. For low energy cold inflow, the thermal pressure of the pre-shock accreting material is negligible compared to its ram pressure. Hence using eq. (5), eq. (21) can be approximated as

$$p_+(r_{sh}) = u_{sh}^2 r_{sh} \left(\frac{R_{comp} - 1}{R_{comp}} \right) \quad (22)$$

Using the above value of $p_+(r_{sh})$ and eq. (2,5), it is easy to express isothermal sound speed C_s and post-shock proton temperature (which is being treated as the effective characteristic outflow temperature) T_{psh} in terms of accretion rate and various shock parameters

as

$$C_s = 0.694 M_{sh}^{-0.75} \sqrt{\frac{u_{sh}^3 r_{sh}^3}{\dot{M}_{in}} (1.44 M_{sh}^{0.75} - 1)} \quad (23)$$

and

$$T_{psh} = \frac{0.24 M_{sh}^{-1.5} m_p u_{sh}^3 r_{sh}^3}{\kappa \dot{M}_{in}} (1.44 M_{sh}^{0.75} - 1) \quad (24)$$

As the outflow is taken to be isothermal T_{psh} will be constant throughout the flow (at least upto the sonic point upto which isothermality is sufficiently valid assumption). Also it is to be noted that from eq. (20) as κ and m_p are constant, the outflow sound speed will also be constant for a fixed value of $\{\mathbf{P}_3\}$. However, as all the shock parameters (u_{sh} , r_{sh} and M_{sh}) are derivable from $\{\mathbf{P}_3\}$, both C_s and T_{psh} will vary with the variation of $\{\mathbf{P}_3\}$ for polytropic inflow.

For simplicity of calculation, here also we assume that the outflow is also quasi-spherical and $\Theta_{out} \approx \Theta_{in}$. Also $R_{\dot{M}}$ in this case is defined as it has been done according to eqn (13).

3.3 Simultaneous Solution of Inflow-Outflow Equations

However, in this work, as we are interested to find out the *ratio* of \dot{M}_{out} to \dot{M}_{in} (eq. (13)), and *not* the explicit value of \dot{M}_{out} , individual calculation of Θ_{out} and Θ_{in} is *not* required since the fraction $\left(\frac{\Theta_{out}}{\Theta_{in}}\right)$ (appearing in the expression for $R_{\dot{M}}$ via \dot{M}_{out} and \dot{M}_{in}) becomes unity owing to our simplified assumption of flow geometry (i.e., $\Theta_{out} \approx \Theta_{in}$). Also to be noted that the primary goal of our present work was to compute the outflow rate and to investigate its dependence on various inflow parameters but *not* to study the collimation procedure of the outflow.

Before we proceed into detail, a general understanding of the transonic inflow outflow system in present case is essential to understand the basic scheme of the solution procedure. Let us consider the transonic accretion first. Infalling matter becomes supersonic after crossing a saddle type sonic point, location of which is determined by $\{\mathbf{P}_3\}$. This supersonic flow then encounters a shock (if present) location of which (r_{sh}) is determined from eqs. (9-10). At the shock surface, part of the incoming matter, having higher entropy density (because shock in a fluid flow generates entropy), is likely to return back as wind through a sonic point *other than* the point through which it just entered. Thus a combination of transonic topologies, one for the polytropic inflow and other for the polytropic/isothermal outflow (passing through a *different* sonic point and following the

topology *completely different* than that of the “self-wind” of the accretion), is required to obtain a full solution. So it turns out that finding a complete set of self-consistent inflow outflow solution ultimately boils down to locating the sonic point of the polytropic/isothermal outflow and the mass flux through it. Thus a supply of parameters \mathcal{E} , \dot{M}_{in} (in the unit of \dot{M}_{Edd}), γ and γ_o make a self-consistent computation of R_{in} possible. Here γ_o is supplied as free parameter because the self-consistent computation of γ_o directly using \mathcal{E} , \dot{M}_{in} and γ has not been attempted in this work, instead we put a constrain that $\gamma_o < \gamma$ always and for any value of γ . In reality, γ_o is directly related to the heating and cooling procedure of the outflow.

The following procedure is adopted to obtain a complete simultaneous solution of inflow-outflow equations:

As $a = \sqrt{\frac{\gamma p}{\rho}}$ and $p = K\rho^\gamma$, we get $\rho = \left(\frac{a^2}{\gamma K}\right)^n$. Using this value of ρ , we rewrite equation (2) as

$$\dot{\mathcal{M}} = a^{2n} u r^2 \quad (25)$$

The quantity $\dot{\mathcal{M}} = \dot{M}\gamma^n K^n$ is also conserved in the flow everywhere except at the shock and is a measure of the specific entropy accretion rate of the flow (see Chapter 2.1). By differentiating equation (1) with respect to r we get

$$u \frac{du}{dr} + 2na \frac{da}{dr} + \frac{1}{2(r-1)^2} = 0 \quad (26a)$$

Logarithmic differentiation of equation (25) gives

$$\frac{da}{dr} = -\frac{a}{2n} \left(\frac{1}{u} \frac{du}{dr} + \frac{2}{r} \right) \quad (26b)$$

Substitution this value of $\left(\frac{da}{dr}\right)$ in equation (26a) gives

$$\frac{du(r)}{dr} = \left(\frac{\frac{2a(r)^2}{r} - \frac{1}{2(r-1)^2}}{u(r) - \frac{a(r)^2}{u(r)}} \right) \quad (27)$$

where as already mentioned, $a(r)$ is the polytropic sound speed which is a function of the radial distance measured from the black hole in the unit of Schwarzschild radius.

Since the flow is assumed to be smooth everywhere, if at any point of the flow the denominator vanishes, the numerator *must* also vanish there. This point is called, in mathematical sense, the critical point of the flow. For accretion with spherical symmetry, Mach number is unity at this point hence it is called the sonic point of the flow and is denoted by r_c . The critical surface, on which every point is a critical point, is also spherical in shape for this kind of accretion. This surface can also be described as sonic horizon (or acoustic

horizon) because for every $r < r_c$, $u > a$ and any acoustic disturbance created inside this surface is advected towards the centre and no disturbances created within this radius can cross the sound horizon and escape to infinity unless a shock is produced.

At the sonic point, the numerator and denominator separately vanish and give rise to the so called sonic point condition;

$$u_c = a_c = \frac{\sqrt{r_c}}{2(r_c - 1)} \quad (28)$$

Where the subscript c represents the quantities at the sonic point. The derivative at the sonic point $\left(\frac{du}{dr}\right)_c$ are computed applying the L' Hospital rule on eqn. (27). The expression for $\left(\frac{du}{dr}\right)_c$ is obtained by solving the following polynomial,

$$\left(\frac{2n+1}{n}\right) \left(\frac{du}{dr}\right)_c^2 + \frac{3u_c}{nr_c} \left(\frac{du}{dr}\right)_c - \left\{ \frac{1}{(r_c-1)^3} - \frac{2a_c^2}{r_c} \left(\frac{n+1}{n}\right) \right\} = 0 \quad (29)$$

We obtain the inflow sonic point r_c by solving eq. (1) and eq. (28) as $r_c = \frac{2\mathcal{E}-1}{2\mathcal{E}-(n+\frac{1}{2})}$. Using fourth order Runge Kutta method, $u(r)$, $a(r)$ and the inflow Mach number $\left[\frac{u(r)}{a(r)}\right]$ are computed along the inflow from the *inflow* sonic point r_c till the position where the shock forms. The shock location is calculated by simultaneously solving the eqs. (1), (2), (9) and (10). Various shock parameters (i.e., density, pressure etc at the shock surface) are then computed self-consistently.

For *polytropic* outflow, with the known value of \mathcal{E}' and γ_o , it is easy to compute the location of the sonic point of the *polytropic outflow* from eqs. (11) and (12). At the outflow sonic point, the outflow velocity v_c and polytropic sound velocity a_c is computed in the same manner performed for the inflow. Using eqs. (11) and (12), $\left(\frac{dv}{dr}\right)$ and $\left(\frac{dv}{dr}\right)_c$ is computed as was done for the inflow. Runge -Kutta method is then employed to integrate from the *outflow* sonic point towards the black hole to find out the outflow velocity v and density ρ at the shock location . The mass outflow rate R_M is then computed using eqs.(13).

For *isothermal* outflow, the shock compression ratio R_{comp} , *isothermal* sound speed C_s , and the effective characteristic outflow temperature T_{psh} are then computed using eqs. (5,23,24) respectively.

Using eqs. (16-17), we now express the derivative of the *isothermal outflow* velocity with respect to the radial distance as

$$\frac{dv_{iso}(r)}{dr} = \left(\frac{\frac{2C_s^2}{r} - \frac{1}{2(r-1)^2}}{v_{iso}(r) - \frac{C_s^2}{v_{iso}(r)}} \right) \quad (30)$$

As has been done for the case of polytropic inflow, here also we obtain the sonic point conditions for the outflow from the requirement that the numerator and denominator of

eq. (30) would separately vanish. The two sonic point conditions are thus expressed as follows

$$r_{iso|c}^2 - r_{iso|c} \left(2 + \frac{1}{4C_s^2} \right) + 1 = 0 \quad (31a)$$

and

$$v_{iso|c} = C_s \quad (31b)$$

Eq. (31a) also gives the location of the outflow sonic point $r_{iso|c}$ as the value of C_s is known (by solving eq. (23)) for a fixed set of $\{\mathbf{P}_s\}$. The derivative of the flow velocity at $r_{iso|c}$ (we call it 'critical derivative' and denote by $\left(\frac{dv_{iso}}{dr}\right)_c$) is computed using L' Hospital rule on equation (30) and can be obtain by solving the following equation

$$\left(\frac{dv_{iso}}{dr}\right)_c^2 + \left(\frac{dv_{iso}}{dr}\right)_c + \left\{ \frac{2C_s^2}{r_c^2} - \frac{1}{(r_c - 1)^3} \right\} = 0 \quad (32)$$

Fourth order Runge - Kutta method is then employed to integrate eq. (30) to find out the outflow velocity and density at the shock location. The mass outflow rate $R_{\dot{M}}$ is then computed using eq. (13).

4 COMPUTATION OF $R_{\dot{M}}$ AND ITS DEPENDENCE ON VARIOUS ACCRETION AND SHOCK PARAMETERS

4.1 Combined Accretion-Wind Topologies

4.1.1 Polytropic Outflow

Fig. 3.1a shows a typical solution which combines the accretion and the outflow. While Mach number is plotted along Y axis, the distance (in geometric unit) from the event horizon of the accreting black hole is plotted along X axis in logarithmic scale. The input parameters are $\mathcal{E} = 0.001$, $\dot{M}_{in} = 1.0$ Eddington rate (\mathcal{E}_d stands for the Eddington rate in the figure) and $\gamma = \frac{4}{3}$ corresponding to relativistic inflow. The solid curve with an arrow represents the pre-shock region of the inflow and the solid vertical line with double arrow at X_{pps} (the subscript *pps* stands for *pair plasma supported shock*) represents the shock transition. Location of shock is obtained using the eqs.(4) for a particular set of inflow parameters mentioned above. Three dotted curves show the three different outflow branches corresponding to different polytropic index of the outflow as $\gamma_o = 1.3$ (left most curve), 1.275 (middle curve) and 1.25(rightmost curve). It is evident from the fig-

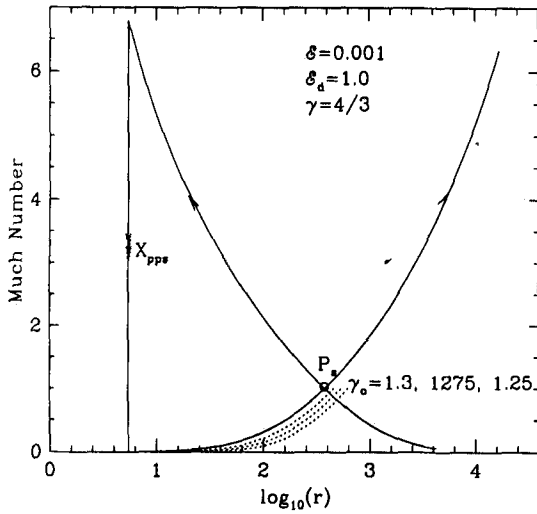


Fig. 3.1a

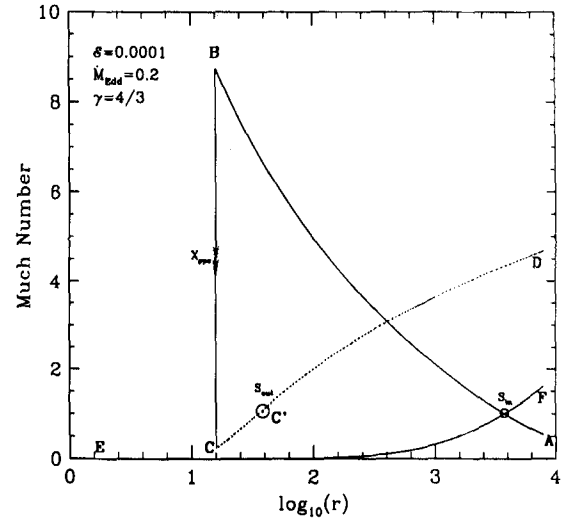


Fig. 3.1b

Fig. 3.1(a-b):

(a) Solution topology for three different γ_o (1.3, 1.275, 1.25) for $\mathcal{E} = 0.001$, $\dot{M}_{in} = 1.0$, $\mathcal{E}_d = 1.0$, $\gamma = \frac{4}{3}$. P_s indicates the sonic point of the inflow where X_{pps} stands for the shock location. See text for details.

(b) Combined solution topology for hybrid transonic inflow-outflow system. solid line AB represents polytropic accretion (upto shock location which is at $15.92 r_g$) while dotted line CC'D is for isothermal outflow. Solid vertical line BC with double arrow X_{pps} represents the shock transition. S_{out} ($35.21 r_g$) and S_{in} ($3753.33c r_g$) are the sonic points for the outflow and the inflow respectively and solid curve EF represents the "self-wind" of the polytropic accretion. Inflow parameters used for this case are $\mathcal{E} = 0.0001$, $\dot{M}_{in} = 0.2$ \dot{M}_{Edd} and $\gamma = \frac{4}{3}$. Mass outflow rate $R_{\dot{m}}$ here comes out to be 0.05. See text for details.

ure that the outflow moves along the solution curves completely different from that of the "self-wind solution" (solid line marked with an outward directed arrow) of the inflow which passes through the sonic point P_s . The mass loss ratio $R_{\dot{m}}$ for these cases are 0.0023, 0.00065 and 0.00014 respectively.

4.1.2 Isothermal Outflow

Fig. 3.1b shows a typical solution which combines the accretion and the outflow. While Mach number is plotted along Y axis, the distance (in geometric unit) from the event horizon of the accreting black hole is plotted along X axis in logarithmic scale. The input parameters are $\mathcal{E} = 0.0001$, $\dot{M}_{in} = 0.2$ Eddington rate (\dot{M}_{Edd} stands for the Eddington rate in the figure) and $\gamma = \frac{4}{3}$ corresponding to relativistic inflow. The solid curve AB represents the pre-shock region of the inflow and the solid vertical line BC with double arrow at X_{pps} (the subscript *pps* stands for *pair plasma supported shock*) represents the shock transition. Location of shock ($15.92 r_g$) is obtained using the eqs.(5) for a particular set of inflow parameters mentioned above. The dotted curve CC'D represents the isothermal outflow

branch which generates, according to our model, from the shock surface. The outflow sonic point S_{out} (marked by \odot at C' on $CC'D$) comes out to be $35.21 r_g$. After crossing the sonic point, outflow becomes supersonic and this supersonic wind $C'D$ extends away to the vastness of intergalactic space. Notice that the outflow sonic point S_{out} ($35.21 r_g$) and solution topology $CC'D$ is *completely different* from that of the 'self-wind' of accretion flow S_{in} ($3753.33 r_g$) and EF . This is due to the fact that outflow comes with shock generated higher entropy density and the outflowing matter is assumed to obey the isothermal equation of state. It is also observed that the outflow sonic point is, in general, located *closer* to the event horizon compared to the inflow sonic point. The mass outflow rate R_m in the case shown in fig is 0.05.

4.2 Dependence of R_m With Various Accretion and Shock Parameters

4.2.1 Polytropic Outflow

In Fig. 3.2., we have plotted the variation of R_m with incoming specific energy \mathcal{E} for a set of values of \dot{M}_{in} (measured in the unit of Eddington rate shown as \mathcal{E}_d in the figure.) shown in the figure. It is observed that R_m monotonically increases with energy. This is because as \mathcal{E} increases keeping the Eddington rate of the inflow fixed, the shock Mach number M_{sh} decreases result of which is the decrement of shock location r_{sh} and post shock density but the increment of the post shock fluid velocity (v_{sh}) with which the matter leaves the shock surface. The outflow rate R_m , which is the product of these three quantities, in general increases monotonically with \mathcal{E} due to the combined tug of war of these three quantities. Moreover, closer the shock forms to the black hole, the greater will be the amount of gravitational potential available to be put onto the relativistic hadrons to provide more outward pressure at the shock boundary which gives a stronger "kick" to the accreting matter, the result of which is the increment in R_m . All these points are manifested in Fig. 3.3 where we have shown the variation of R_m as a function of compression ratio R_{comp} (solid curve), the shock location r_{sh} (dotted curve) and the injection velocity of the outflow v_{sh} (dashed curve). The figure is drawn for a fixed $\gamma = \frac{4}{3}$ and $\gamma_o = 1.3$. R_{comp} and v_{rsh} are scaled as $R_{comp} \rightarrow (R_{comp} - 5.890) \times 10^3$ and $v_{rsh} \rightarrow 4 \times 10^{-6} v_{rsh}$. The unequal gaps between the curves with different \mathcal{E}_d in Fig. 3.2. implies that when inflow energy \mathcal{E} is kept fixed, R_m nonlinearly increases with Eddington rate. This is because, as \mathcal{E} is kept fixed while \dot{M}_{in} is varied, the amount of infalling energy converted to produce

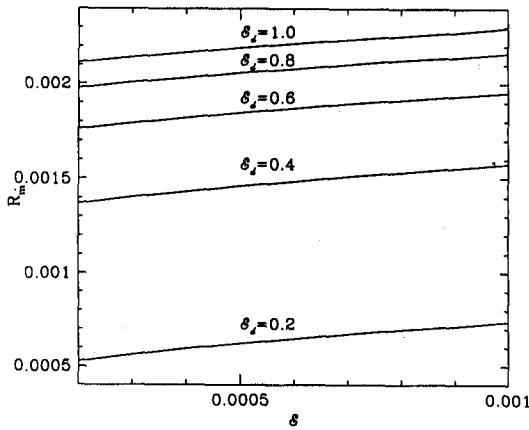


Fig. 3.2

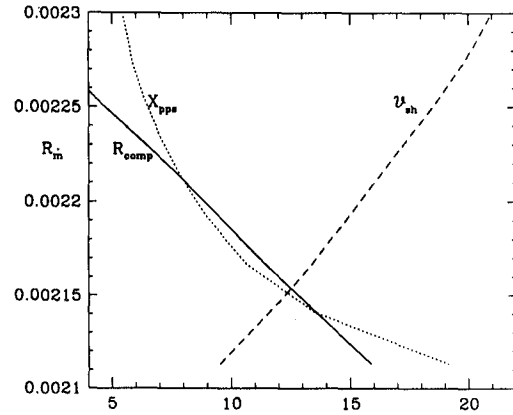


Fig. 3.3

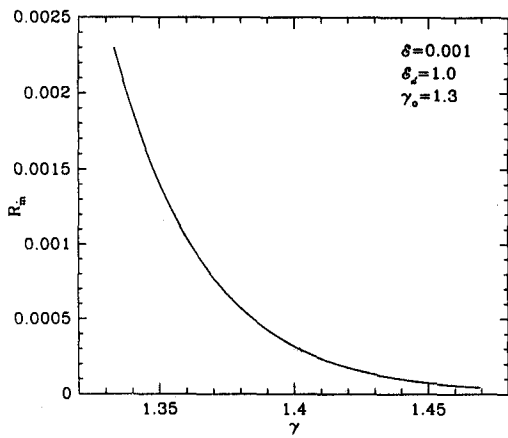


Fig. 3.4a

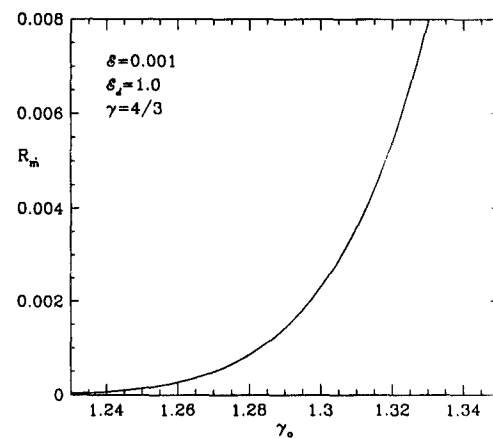


Fig. 3.4b

Fig. 3.2-3.4(a-b):

Fig. 3.2: Variation of R_m with inflow specific energy \mathcal{E} for different Eddington rate (marked as \mathcal{E}_d in the figure). Other parameters are $\gamma = \frac{4}{3}$ and $\gamma_o=1.3$. R_m monotonically increases with \mathcal{E} , see text for detail.

Fig. 3.3: Variation of R_m with the compression ratio R_{comp} (solid curve), shock location X_{pps} (dotted curve) and outflow velocity at shock v_{sh} (dashed curve). Other parameters are $\mathcal{E}=0.001$, $\dot{M}_{in} = 1.0$ (In the unit of Eddington rate), $\gamma = \frac{4}{3}$ and $\gamma_o=1.3$.

Fig. 3.4a: Variation of R_m with polytropic index of inflow γ . Other parameters are $\mathcal{E}=0.001$, $\dot{M}_{in}=1.0$ (in the unit of Eddington rate) and $\gamma_o=1.3$.

Fig. 3.4b Variation of R_m with polytropic index of outflow γ_o . Other parameters are $\mathcal{E}=0.001$, $\dot{M}_{in}=1.0$ (in the unit of Eddington rate) and $\gamma = \frac{4}{3}$.

high energy protons is also fixed, so higher is the value of \dot{M}_{in} (in the unit of Eddington rate), the larger is the distance of the shock surface (measured from the black hole) and the outflowing matter feels low inward gravitational pull, the result of which is the non-linear correlation of $R_{\dot{m}}$ with \dot{M}_{in} .

To have better insight of the behaviour of the outflow, in Fig. 3.4a. and 3.4b, we plot $R_{\dot{m}}$ as a function of the polytropic index of the inflow γ (Fig. 3.4a) and that of the outflow γ_o (Fig. 3.4b) for fixed $\mathcal{E} = 0.001$ and $\dot{M}_{in} = 1.0\mathcal{E}_d$. The range of γ shown here are the range for which shock forms for the specified \mathcal{E} and \dot{M}_{in} . In Fig. 3.4b, it is observed that shock forms for the values of γ_o lower than that shown in the figure, but mass loss rate is then so small that we did not plot for $\gamma_o < 1.23$. The general conclusion is that $R_{\dot{m}}$ correlates with γ_o . This is because as γ_o increases, shock location and post shock density of matter does not change (as γ_o does not have any role in shock formation or in determining the R_{comp}) but the sonic point of the *outflow* is pushed inward, hence the velocity with which outflow leaves the shock surface goes up resulting the increment in $R_{\dot{m}}$. However, $R_{\dot{m}}$ anticorrelates with γ which is observed from Fig. 3.4a.

4.2.2 Isothermal Outflow

4.2.2.1 Dependence of $R_{\dot{m}}$ on $\{\mathbf{P}_3\}$

4.2.2.1a Variation of $R_{\dot{m}}$ with \mathcal{E}

In fig 3.5(a), we have plotted the variation of $R_{\dot{m}}$ with inflow specific energy \mathcal{E} for a set of equispaced values of \dot{M}_{in} (measured in the unit of Eddington rate \dot{M}_{Edd} as marked in the figure). The unequal gaps between the curves implies that when \mathcal{E} is kept fixed, $R_{\dot{m}}$ *non-linearly anticorrelates* with \dot{M}_{in} (which is explicitly manifested in the fig. (3.6a)). It is interesting to note that different curve terminates at different points which indicates that the maximum energy \mathcal{E}_{max} of the *inflow* for which the shock forms, nonlinearly increases with the decrease of Eddington rate. This implies that pair-plasma pressure supported shock does *not* form for all values of $\{\mathbf{P}_3\}$, rather a specific region of parameter space spanned by \mathcal{E} , \dot{M}_{in} and γ allows shock formation. This fact will be further supported from the next set of figures where the dependence of $R_{\dot{m}}$ with \dot{M}_{in} is shown explicitly.

From fig 3.5(a) it is clear that for a fixed value of \dot{M}_{in} , $R_{\dot{m}}$ increases with \mathcal{E} monotonically.

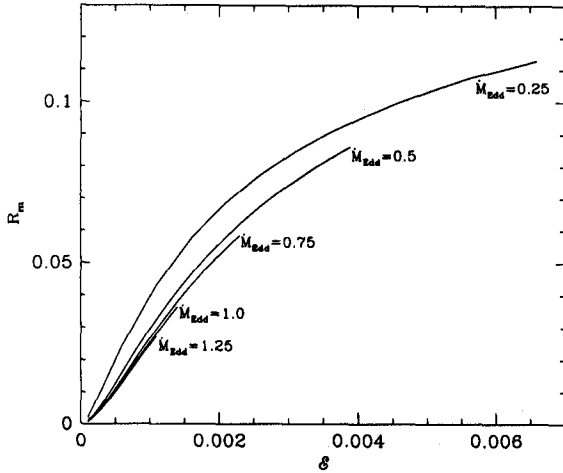


Fig. 3.5a

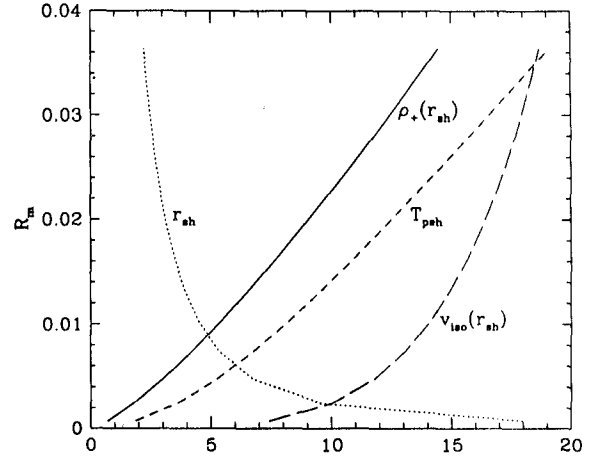


Fig. 3.5b

Fig. 3.5(a-b):

(a) Variation of $R_{\dot{m}}$ as a function of the specific energy \mathcal{E} of the polytropic accretion for different Eddington rate (Marked as \dot{M}_{Edd} in the figure). The maximum energy \mathcal{E}_{max} for which the shock forms, non-linearly increases with decrease of accretion rate. (See text for detail). γ of the inflow is taken to be $\frac{4}{3}$.

(b) Variation of $R_{\dot{m}}$ with different shock parameters for a fixed accretion rate ($1.0 \dot{M}_{Edd}$) but with variable energy. Solid curve marked with $\rho_+(r_{sh})$ represents the variation of post-shock density; dotted curve marked with r_{sh} , short-dashed marked with T_{psh} and long-dashed curve marked with $V_{iso}(r_{sh})$ represents the variation of shock-location, post-shock proton temperature and the launching velocity of outflow at shock surface respectively. γ of the inflow is taken to be $\frac{4}{3}$. while plotting, different shock parameters are scaled as follows $r_{sh} \rightarrow 0.5r_{sh}$, $\rho_+(r_{sh}) \rightarrow \rho_+(r_{sh}) \times 10^{22}$, $T_{psh} \rightarrow T_{psh} \times 0^{10}$ and $V_{iso}(r_{sh}) \rightarrow V_{iso}(r_{sh}) \times 363.64$.

cally and non-linearly. This is because as \mathcal{E} increases keeping the accretion rate constant, the shock Mach number M_{sh} decreases result of which is the decrement of shock location r_{sh} but increment of post-shock density $\rho_+(r_{sh})$, pressure $p_+(r_{sh})$ and temperature T_{psh} . Higher is the post-shock proton temperature, the higher is the isothermal sound speed C_s of the outflow as well as the isothermal bulk velocity $v_{iso}(r_{sh})$ with which outflow leaves the shock surface. The outflow rate, which is the product of three quantities r_{sh} , $\rho_+(r_{sh})$ and $v_{iso}(r_{sh})$ (see eq. (17)), increases in general due to the combined tug of war of these three quantities. Moreover, closer is the shock to the black hole, greater will be the amount of gravitational potential available to be put onto the relativistic protons to provide stronger outward pressure and the closer the shock forms to the black hole, the higher is the post-shock proton temperature (the effective characteristic outflow temperature) and the higher is the amount of outflow (as isothermal wind is highly thermally driven, the fact which will be more strongly established in next set of results). The dependence of mass outflow rate in this case (variable energy with constant accretion

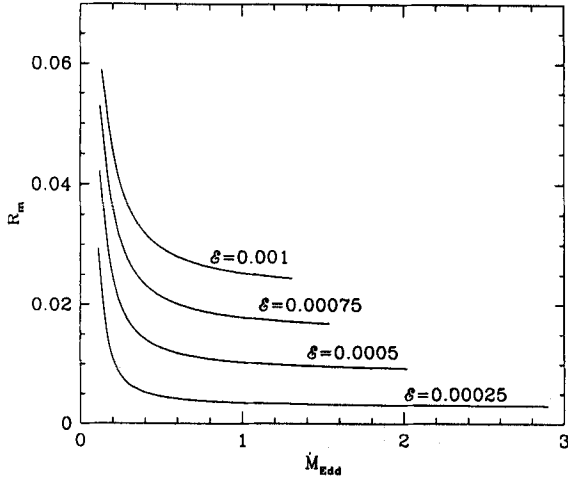


Fig. 3.6a

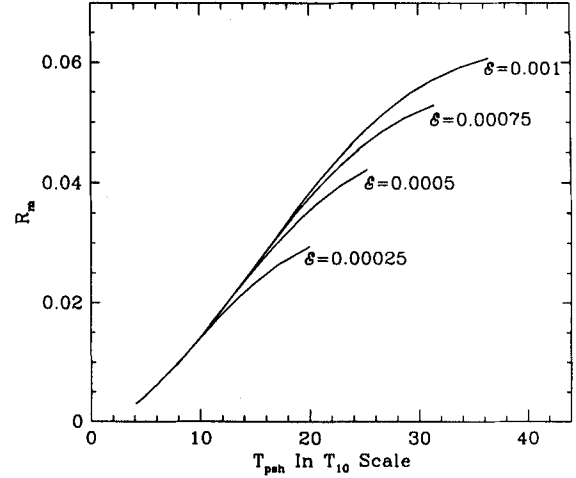


Fig. 3.6b

Fig. 3.6(a-b):

(a) Variation of $R_{\dot{m}}$ as a function of accretion rate (in the unit of eddington rate \dot{M}_{Edd}) for a set of values of specific energy \mathcal{E} of the inflow (marked on the figure). It is observed that $R_{\dot{m}}$ non-linearly anticorrelates with accretion rate which tells that low luminosity objects produce more outflows. The value of γ is taken to be $\frac{4}{3}$. See text for detail.

(b) Variation of $R_{\dot{m}}$ with post-shock proton temperature T_{psh} (scaled in the unit of T_{psh}^{10} and marked as T_{10} in the figure) corresponding to the data set of Fig. 3(a). See text for detail.

rate) on various parameters mentioned above are manifested in fig 3.5(b) where we have shown the variation of $R_{\dot{m}}$ with different shock parameters for a fixed accretion rate ($1.0 \dot{M}_{Edd}$) but with variable energy. Solid curve marked with $\rho_+(r_{sh})$ represents the variation of post-shock density; dotted curve marked with r_{sh} , short-dashed marked with T_{psh} and long-dashed curve marked with $V_{iso}(r_{sh})$ represents the variation of shock-location, post-shock proton temperature and the launching velocity of outflow at shock surface respectively. γ of the inflow is taken to be $\frac{4}{3}$. while plotting, different shock parameters are scaled as follows $r_{sh} \rightarrow 0.5r_{sh}$, $\rho_+(r_{sh}) \rightarrow \rho_+(r_{sh}) \times 10^{22}$, $T_{psh} \rightarrow T_{psh} \times 10^{10}$ and $V_{iso}(r_{sh}) \rightarrow V_{iso}(r_{sh}) \times 363.64$.

As low energy solution corresponds to high shock Mach number and as $R_{\dot{m}}$ increases with \mathcal{E} (for constant \dot{M}_{in}), inflow with *low* shock Mach number (and hence with low shock compression ratio R_{comp} via eq. (4)) produces more outflow.

4.2.2.1b Variation of $R_{\dot{m}}$ with \dot{M}_{in}

In fig 3.6(a), we show the outflow rate $R_{\dot{m}}$ as a function of the accretion rate (measured in

terms of Eddington rate \dot{M}_{Edd}) of the incoming flow for a range of fixed specific energy \mathcal{E} of the inflow. \mathcal{E} corresponding each curve is marked in the figure. It is interesting to note that the outflow occurs for both super and sub-Eddington accretion and low luminosity objects produce more outflow as is observed. It is also to be noted in this context that the maximum value of accretion rate $\dot{M}_{Edd}|_{max}$ for which the shock forms, increases with decrease of the inflow specific energy \mathcal{E} . This figure is drawn for $\gamma = \frac{4}{3}$.

In fig 3.6(b), we plot the variation of $R_{\dot{m}}$ directly with the post-shock proton temperature T_{psh} corresponding to the accretion rate shown in fig 3.6(a). Post-shock proton temperature T_{psh} (in the unit of T_{psh}^{10} ; which we mark as T_{10} in the figure) is plotted along X axis. As is observed from the figure, the outflow is clearly thermally driven. Hotter flow produces more winds as is expected. From fig 3.6(a) and 3.6(b), it is clear that a 'high energy - low luminosity' combination for polytropic accretion maximizes the post-shock proton temperature thus gives rise to the highest amount of outflows.

It is observed that while the shock location decreases with decrease in accretion rate (for a fixed energy), the launching velocity of out flow at shock surface $v_{iso}(r_{sh})$, post shock density $\rho_+(r_{sh})$ and the temperature of the flow increases. It is also observed that the shock Mach number M_{sh} as well as the shock compression ratio R_{comp} increases with decrease in accretion rate. So for varying accretion rate for a fixed energy, high shock Mach number solutions produces higher outflow and the value of R_{comp} is also necessarily high to obtain high $R_{\dot{m}}$. This is in contrast to the results obtained in §4.2.2.1a (dependence of $R_{\dot{m}}$ on \mathcal{E} keeping \dot{M}_{in} constant) where low shock Mach number solutions produced higher outflow rates and the value of R_{comp} was also low for that case. So in some sense, while varying accretion rate for a fixed \mathcal{E} gives high outflow rates for 'strong shock' cases (i.e., high shock Mach number with strong shock compression of matter), variation of inflow specific energy \mathcal{E} (keeping accretion rate \dot{M}_{in} fixed) prefers 'weak shock' solutions (low M_{sh} and low shock compression of matter) to produce high outflow.

4.2.2.1c Variation of $R_{\dot{m}}$ with γ

In previous cases, the polytropic index γ of the accreting matter was always kept fixed at the value $\frac{4}{3}$. To have a better insight of the behaviour of the outflow, we plot $R_{\dot{m}}$ as a function of γ (fig 3.7) for a fixed value of $\mathcal{E} = 0.0001$ and $\dot{M}_{in} = 0.2 \dot{M}_{Edd}$.

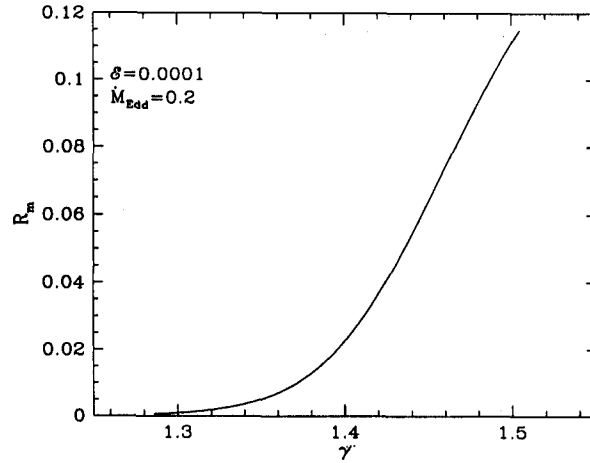


Fig. 3.7

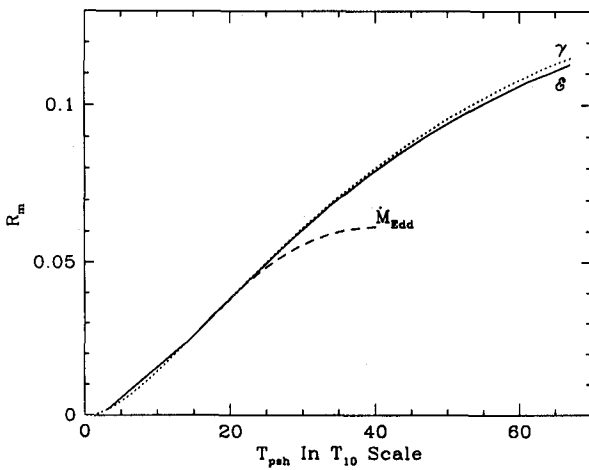


Fig. 3.8a

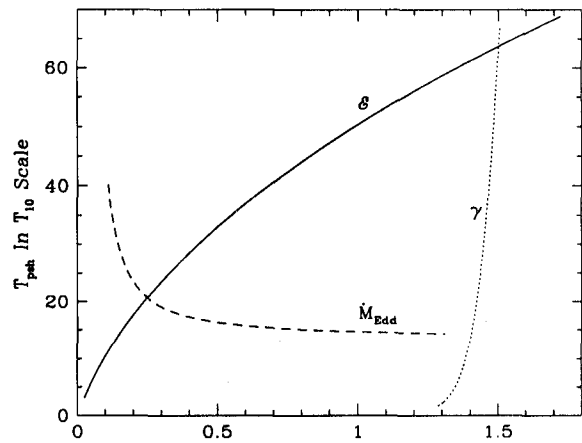


Fig 3.8b

Fig. 3.7-3.8(a-b):

Fig. 3.7: Variation of R_m with polytropic index γ of the inflow for a fixed value of specific energy $\mathcal{E} = 0.0001$ and accretion rate $\dot{M}_{in} = 0.2\dot{M}_{Edd}$. It is observed that R_m in general correlates with γ . See text for detail.

Fig. 3.8(a): Direct variation of R_m with post-shock proton temperature T_{psh} (scaled in the unit of T_{psh}^{10} and marked as T_{10} in the figure) for variation of specific energy \mathcal{E} (solid curve), accretion rate in terms of Eddington rate (dashed curve) and polytropic index γ (dotted curve) of the inflow.

Fig. 3.8(b) Dependence of post-shock proton temperature T_{psh} (scaled in the unit of T_{psh}^{10} and marked as T_{10} in the figure) with specific energy \mathcal{E} (solid curve), accretion rate in terms of Eddington rate (dashed curve) and polytropic index γ (dotted curve) of the inflow. While plotting \mathcal{E} is scaled as $\mathcal{E} \rightarrow 250.0 \times \mathcal{E}$.

The range of γ shown here is the range for which shock forms for the specified value of \mathcal{E} and \dot{M}_{in} . It is observed that $R_{\dot{m}}$ correlates with γ . we have found that the outflow temperature increases with increase in γ while M_{sh} and R_{comp} decrease. So here also the flow is essentially thermally driven and ‘weak shock’ solutions are preferred to obtain high outflows.

4.2.2.2 Temperature dependence of $R_{\dot{m}}$: a generic result for isothermal outflow

In *all* of the previous examples, where we have studied the dependences of $R_{\dot{m}}$ on various input parameters as well as shock parameters, it is observed that whether the mass outflow rate correlates or anti correlates with any of the members of $\{\mathcal{P}_s\}$ (our three parameter input set) or with any shock parameters (r_{sh} , M_{sh} or R_{comp} , for example), $R_{\dot{m}}$ *always* correlates with the outflow temperature which tells that isothermal outflow is essentially thermally driven *in general*. That means if shock forms, whatever be the initial flow conditions and whatever be the nature of the dependence of $R_{\dot{m}}$ on any of the inflow/shock parameters, hotter flow *always* produce more winds. Hence the post-shock temperature plays a crucial role in our model. Above mentioned fact is manifested in fig 3.8(a) and 3.8(b). In figure 3.8(a), we plot $R_{\dot{m}}$ directly with post shock proton temperature obtained for three different cases. The solid line marked with \mathcal{E} gives the temperature changes for varying the inflow specific energy while keeping accretion rate and polytropic index constant, the dotted line marked with \dot{M}_{Edd} is drawn for the case where the accretion rate (in the unit of Eddington rate) is varied for a constant values of energy and polytropic index and lastly, the dashed line marked with γ is obtained for variation of the polytropic index of inflow keeping energy and accretion rate constant. It is clear from the figure that $R_{\dot{m}}$ *always* increases with increase of post shock proton temperature (thus with the outflow temperature). In fig 3.8(b), we directly show the dependence of post shock proton temperature on \mathcal{E} , \dot{M}_{in} and γ of the inflow. The solid curve gives the variation with energy while the dotted and the dashed curve represent the variation with accretion rate and polytropic index of the inflow respectively. It is observed that while flow temperature increases with increase of \mathcal{E} and γ , decrease of \dot{M}_{in} (measured in the unit of Eddington rate and marked as \dot{M}_{Edd} in the figure) increases the flow temperature T_{psh} . Inference drawn by combining fig 3.8(a) and 3.8(b) tells us that while $R_{\dot{m}}$ correlates with \mathcal{E} and γ , it anticorrelates with the accretion rate, which again, is in one to one agreement

with the results obtained in §4.2.2.1a - §4.2.2.1c.

At this point, we must mention one limitation of this work. Our calculations presented here in this chapter, being a simple minded one, do not explicitly include various radiation losses and cooling processes combined effects of which may reduce the post shock proton temperature and the outflow temperature, in reality, could be lower than what we have obtained here and the amount of outflow would be less than what is obtained in our calculation. This deviation will be more important for the cases with high accretion rate. Nevertheless, cases for low accretion rate discussed here would not be affected that much and our preliminary investigation shows that even if we incorporate various losses, the overall profile of the various curves showing the dependence of $R_{\dot{m}}$ on different inflow parameters would be *exactly* the same, only the numerical value of $R_{\dot{m}}$ in some cases (especially for high accretion) might decrease. Detail computation of $R_{\dot{m}}$ including different loss processes are in progress and is expected to be presented in near future.

Concluding Remarks

Chapter 4

SUMMARY

We discuss the fundamental achievements in our work which may distinguish our model from the existing models dealing with accretion-powered extragalactic outflows and finally draw the conclusions by indicating the possibilities for further extensions of works presented in this thesis.

A number of unsolved issues regarding the origin and formation of astrophysical outflows emanating from sources powered by accreting compact objects have been successfully addressed in this thesis work as we believe. Fundamental achievements in this work which may distinguish our model from all other existing disk-wind models in the literature are illustrated below.

Using a set of hydrodynamic steady state conservation equations in pseudo-Newtonian framework, we have been able to explain the formation of outflows only from the knowledge of accretion parameters thus could successfully bridge a gap between the equations governing accretion and wind for infalling matter forming an accretion disk as well as for nearly freely falling Bondi type spherical/quasi-spherical accretion onto a Schwarzschild black hole. In doing so we essentially tracked a steady state flow from infinity and extracted outflows from the same by proposing suitable mechanisms for formation of a virtual surface from where the outflow happens to be launched. We want to emphasize at this point that generation of outflows as well as exact computation of its rate $R_{\dot{M}}$ and dependence of $R_{\dot{M}}$ on various physical quantities governing the flow have been investigated in our model only from the knowledge of accretion parameters which has never been done in any of the existing models (see Chapter 1.4 for a general outline of various disk-wind models).

We have already mentioned several times that (see Chapter 1.4) while self-similar models

are the valuable first steps, they can *never* be the full answer, and indeed any model which works equally well at all radii is quite unsatisfactory to prove its viability. Thus the preferred model (explaining the origin of outflows) *must* be one which is able to select the *specific* region of jet formation. In this context an extremely important achievement of our model is that it is *not* self-similar; outflows generate from a *specific* region location of which from the central accretor is *exactly* measurable self-consistently. Also to be noted that the jet/ outflow formation region in our model, for disk-outflow system as well as for Bondi type accretion, is located sufficiently close to the compact object (a few tens of r_g in general and sometimes even less), which, in principle, *should* happen for optimal extraction of maximum possible amount of gravitational energy available to be put onto the matter at the base of the outflow for providing maximum outward pressure (thermal plus ram) to let the wind get a stronger 'kick'. That this situation (e.g. launching of outflows from a reasonably close vicinity of the central accretor) genuinely happens in reality is proved beyond doubt by latest observation of M87 jet. Using latest VLBA observations with a global array of radio telescopes at a wavelength of 7mm at 43.237 GHz, Junor, Biretta & Livio (Junor, Biretta & Livio, 1999) have shown that collimation of M87 jet occurs at distance $\sim 30 - 100 r_g$ and continues out to $\sim 1000 r_g$ with a large opening angle $\sim 60^\circ$ on scales $< 0.04 pc$ near the centre (the broadest opening angle for any extragalactic jet ever detected). It has been strongly argued that the region in which the jet first formed, *can never be much larger than* $\sim 30 r_g$ which *firmly supports* the viability and consistency of our solution scheme for jet production. Figure 4.1 shows the step by step close up look at the jet of M87. The top left image is the 15 GHz VLA radio image (taken on February, 1989) of the large scale jet. The top right image is the optical image of the giant elliptical galaxy M87 taken with HST WFPC 2 (taken on February, 1998) revealing the bright optical jet. The bottom image is the pseudo-colour rendition of the nucleus of M87 at 43.237 GHz on 3rd March 1999.

The generality in application of our outflow model comes from the fact that our calculation is *not* restricted to any particular mass of the central compact object. As mass of the accretor (scaled in the unit of M_\odot) enters in our calculation through accretion rate \dot{M}_{Edd} , our solution scheme as well as general flow profile will be valid for systems harbouring compact object of *any* mass in general rather than being restricted to some specific cases; only the regions of parameter space responsible for outflow formation will get shifted and the numerical value of R_M might change due to its dependence on accretion rate.

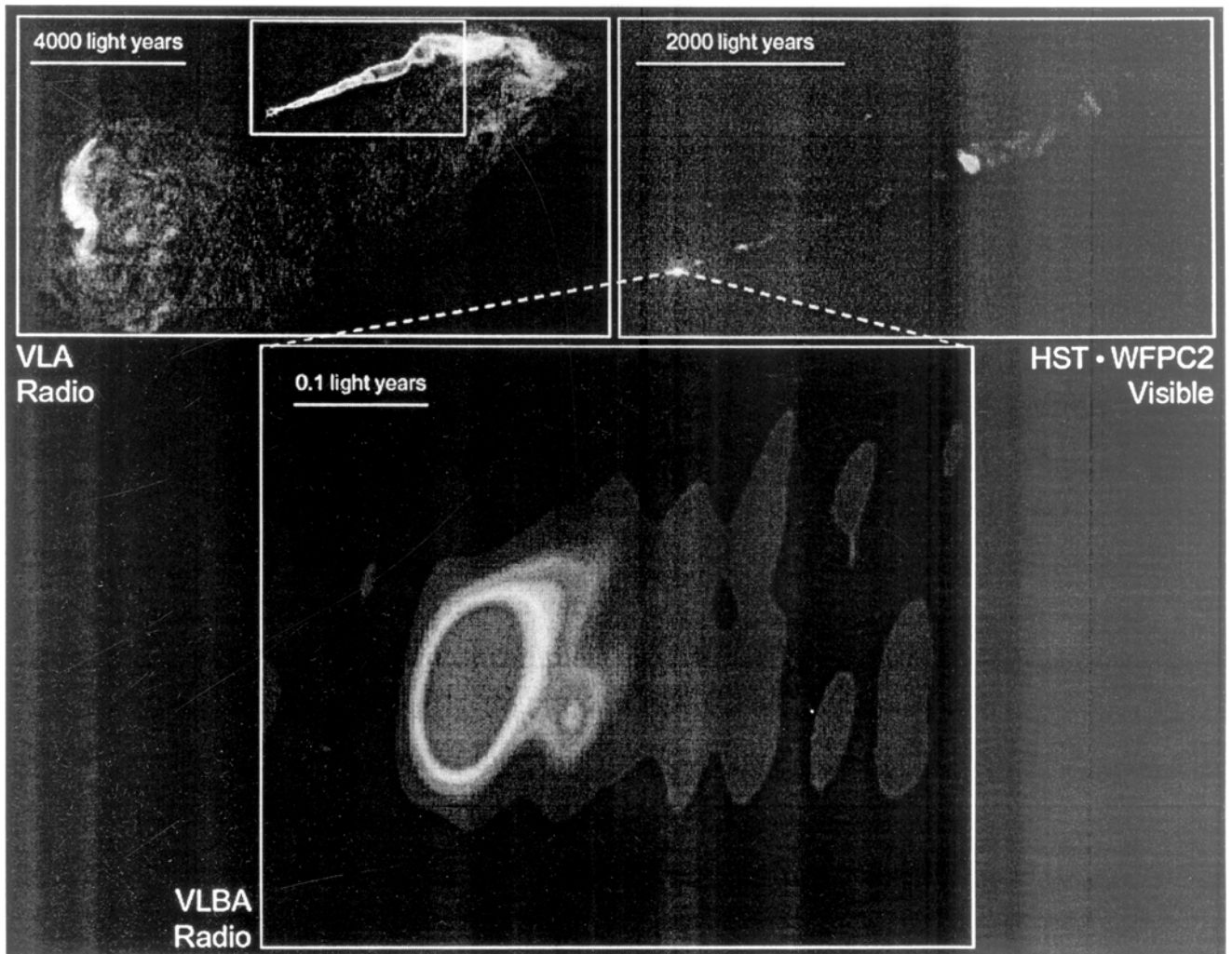


Fig. 4.1:

A Close-up look at the jet of M87. Picture taken from HST public archive, see text for detail.

Thus not only the jets from sources situated at the dynamical centres of active galaxies and QSOs, jet from stellar mass black hole powered microquasars would also be investigated in the frame work of our model. Also in §5 of Chapter 2.2 we have illustrated the fact that with a general knowledge of outflow rate, we can proceed to investigate several important phenomena of related interest which shows that our model is expected to possess an wide applicability in some other fields of investigation also.

Below we summarize the basic features and provide concluding remarks for two individual cases of our investigation, e.g., for disk-outflow system as well as for outflows from spherical accretion.

1 DISK-OUTFLOW SYSTEM

In this sector we have provided a new semi-analytical semi-numerical scheme which successfully computes the mass outflow rate from the advective accretion disks around galactic and extra-galactic black holes. Since the general physics of advective flows are similar around a neutron star, we believe that the conclusions may remain roughly similar provided the shock at X_{s3} forms, although the boundary layer of the neutron star, where half of the binding energy could be released, may be more luminous than that of a black hole and may thus affect the outflow rate. We have chosen a limited number of free parameters just sufficient to describe the inflow and only one extra parameter for the outflow and that is also for polytropic outflow, the isothermal outflow is described in terms of inflow parameters only without any need for a single other extra parameter. We find that the outflow rates can vary from a very few percentage of the inflow rate, to as much as the inflow rate (causing almost complete evacuation of the accretion disk) depending on the inflow parameters. For the first time, it became possible to use the exact transonic solutions for both the disks and the winds and combine them to form a self-consistent disk-outflow system.

The basic conclusions of this work are the followings:

- a) It is possible that most of the outflows are coming from the centrifugally supported boundary layer (CENBOL) of the accretion disks.
- b) The outflow rate generally increases with the proton temperature of CENBOL. In other words, winds are, at least partially, thermally driven. This is reflected more strongly when the outflow is isothermal.
- c) Even though specific angular momentum of the flow increases the size of the CENBOL, and one would have expected a higher mass flux in the wind, we find that the rate of the outflow is actually anti-correlated with the λ of the inflow. On the other hand, if the angular momentum of the outflow is reduced by hand, we find that the rate of the outflow is correlated with λ of the outflow. This suggests that the outflow is partially centrifugally driven as well.
- d) The ratio $R_{\dot{m}}$ is generally anti-correlated with the inflow accretion rate. That is, disks of lower luminosity would produce higher $R_{\dot{m}}$.
- e) Generally speaking, supersonic region of the inflow do not have pressure maxima. Thus, outflows emerge from the subsonic region of the inflow, whether the shock actu-

ally forms or not.

Here we assumed that the magnetic field is absent. Magnetized winds from the accretion disks have so far been considered in the context of a Keplerian disk (see §3 of Chapter 1.4 for detail) and *not* in the context of sub-Keplerian flows on which we concentrate here. Secondly, whereas the entire Keplerian disk was assumed to participate in wind formation (see §3 of Chapter 1.4 for detail), here we suggest that CENBOL is the major source of outflowing matter. It is not unreasonable to assume that CENBOL would still form when magnetic fields are present and we speculate that since the Alfvén speed is, by definition, higher compared to the sound speed, the acceleration and therefore the mass outflow would also be higher than what we computed here. Moreover, suitable introduction of toroidal magnetic field in our model with associated “hoop” stress, would lead to a better understanding of the “collimation problem” of the jet.

Would our solution be affected if radiation pressure is included? Our preliminary investigation with a Γ/r^2 force term (whose effect is to weaken gravity) suggests that for non-zero Γ in the inflow, the mass-loss rate changes significantly. This is because the shock location increases when Γ is increased. This in turn reduces the mass loss rate. On the other hand, when Γ is non-zero in the outflow, the effect is not very high, since the outflow rate is generally driven by thermal effect of the *disk* and not the wind. Similarly, we see a significant reduction of the outflow when the average specific angular momentum of the outflow is reduced. This is expected since the outflow is partially centrifugally driven. This effect is stronger when the outflow is isothermal.

2 OUTFLOWS FROM SPHERICAL ACCRETION

Although there have been many attempts in the literature to study the astrophysical outflows from the galactic and extra-galactic sources, till today, at the best of our knowledge, no such model is available which can compute the mass outflow rate from non-rotating accretion of this kind in terms of *only three* inflow parameters (and one extra parameter γ_0 for polytropic outflow) and is able to rigorously study the dependence of R_{in} on various physical parameters governing the accretion, which, as we believe, has been successfully performed in works presented Chapter 3. We take a spherical, steady, self-supported pair-plasma pressure supported shock surface around a Schwarzschild black hole as the ‘effective’ physical barrier from where the outflow could be generated. We then calculate

the location of this shock surface and compute the rate of the mass-outflow R_M generated from this surface in terms of *only three inflow parameters*, namely, the specific energy \mathcal{E} , mass accretion rate \dot{M}_{in} and the polytropic index γ (only one extra parameter γ_0 was used to study the polytropic outflow) and rigorously study the dependence of this rate on various physical parameters governing the inflow and on different shock parameters. We take polytropic accretion while the outflow is taken to be polytropic as well as isothermal also by properly justifying the validity of the isothermality assumption. We thus, also self-consistently construct a 'hybrid' inflow-outflow model which could successfully connect flows obeying two different equations of state (polytropic inflow-isothermal outflow). Using HST and ground based telescopes in Australia and Chile and invoking gravitational microlensing technique, recent observations (15th June, 1999: results embargoed until 12.30 PM (EST), 31st January, 2000) of adrift of two isolated black holes (having mass $6M_\odot$) among the stars in our galaxy (**HST PRESS RELEASE No: STScI - PR00 - 03**) indicates that accreting stellar mass black holes need not always require the sort of interaction in a binary system to form rather may also be produced in the collapse of isolated massive stars. This extremely crucial finding *indicates* that not only for SMBHs sitting at galactic centres accreting matter with mutually cancelled negligible angular momentum (see §1 of Chapter 3.), our model dealing with outflows from relativistic hadronic interaction supported shock surfaces, may find important applications in investigation of winds *also* from stellar mass black holes (isolated).

At this point, it is worth mentioning that the hot and dense pair plasma pressure supported shock surface around black holes, which is served here as the effective physical barrier around compact objects regarding the mass outflow, may be generated due to other physical effects as well (Chang & Ostriker, 1985, Babul, Ostriker and Meszaros, 1989, Park, 1990).

We can summarize the basic conclusions (common for polytropic as well as isothermal outflows) as follows:

(i) It is possible that outflows for quasi-spherical Bondi type accretion onto a Schwarzschild black hole are coming from the pair plasma pressure supported shock surface. The pair plasma pressure supported shock surface can serve as the 'effective' physical barrier around the black hole regarding the computation of mass outflow rate. The pair plasma pressure supported shock surface can serve as the 'effective' physical barrier around the

black hole regarding the computation of mass outflow rate. Also is possible to construct a 'hybrid' inflow outflow system (which could connect flows with two different equations of state) to investigate outflows and to compute $R_{dot{M}}$.

(ii) Generally speaking, as our model deals with high shock Mach number (low energy accretion) solutions, outflows in our work always generate from the supersonic branch of the inflow, i.e, shock is always located *inside* the sonic point.

(iii) Unlike the disk outflow system (Chapter 2.), here we found that the $R_{\dot{m}}$ never attains a very high value. This is because matter is ejected out due to the pressure of the relativistic plasma pairs which is *less enough* in comparison to the pressure generated due to the presence of significant angular momentum. However, in the present work we have dealt only high Mach number solution which means matter is accreting with sufficiently low energy. This is another possible reason to obtain a low mass loss rate. If, instead of high Mach number solution, we would use low Mach number solution, e.g, high energy accretion, the mass outflow would be considerably higher (this is obvious because it has already been established in present work that $R_{\dot{m}}$ increases with \mathcal{E}).

Other conclusions for individual cases are in order:

2.1 Polytropic Outflow

(i) The outflow rate monotonically increases with the specific energy of the inflow and nonlinearly increases with the Eddington rate of the infalling matter .

(ii) $R_{\dot{m}}$, in general, correlates with γ_o but anticorrelates with γ .

2.2 Isothermal Outflow

(i) Computation of $R_{\dot{m}}$ can be carried out in terms of only three inflow parameters $\{\mathcal{E} : \dot{M}_{in} : \gamma\}$ set of which we we call $\{\mathbf{P}_3\}$.

(ii) Outflow can vary anywhere from a very few fraction of percentage to a couple of percent depending on parameters of $\{\mathbf{P}_3\}$, thus an wide range of $R_{\dot{m}}$ has been investigated successfully.

(iii) Shock does not form always. Although for most of regions of the parameter space (spanned by \mathcal{E} , \dot{M}_{in} and γ) shock forms, shock does not form for all values of \mathcal{E} , \dot{M}_{in} and γ .

(iv) While $R_{\dot{m}}$ increases with increase in \mathcal{E} and γ , decrease in \dot{M}_{in} increases $R_{\dot{m}}$. In other words, low luminosity objects produce high outflow and the 'high energy - low accretion rate' solutions are the best choice to maximize $R_{\dot{m}}$.

(v) Isothermal outflow is thermally driven, hotter flow produces high outflow *always*.

(vi) Outflow could be obtained for both super Eddington as well as sub-Eddington accretion.

(vii) While constant accretion rate with variable energy solutions prefers 'weak shock', constant energy with variable accretion rate requires 'strong shock' to produce high outflow rate.

There are a number of possible improvements which could be made on this work. For instance, the effect of radiation pressure on both the inflow and the outflow could be taken into account. A preliminary investigation shows that the effect of radiation force, when included into the basic conservation equations (eqs. (1-2), (11-12) and (16-17)) decreases the value of $R_{\dot{m}}$. This is probably because introduction of any radiation term which is proportional to $\frac{1}{r^2}$, weakens gravity and pushes the shock location outwards, combined effect of which is the decrement of $R_{\dot{m}}$. Another possible improvement is to include the magnetic field to give the outflow an appropriate geometry. In our model, we assumed the outflow to be quasi-spherical as like the inflow. The introduction of magnetic field probably could collimate the outflow thus would help to investigate the structure of jet in greater detail. Lastly, we did not self-consistently compute γ_0 as a function of inflow parameters and γ_0 was supplied as a free parameter. In our future work, we will be presenting the self-consistent calculation of γ_0 to reduce the number of free parameters of the problem.

So far, we made the computation around Schwarzschild black hole. Our work could be extended to study mass outflow in Kerr space time as well. This is under preparation and will be presented elsewhere.

3 EPILOGUE

We have carried out our calculations for the Schwarzschild black hole using Paczyn'ski-Wiita pseudo-Newtonian potential. Now we would like to extend our calculations in fully general relativistic framework so that the parameter space for calculation gets modified and the mass-loss rate calculated in this way could be compared with our previous

results. Finally, we would like to carry out all of our calculations (done for Schwarzschild black hole) in Kerr space-time to bring the whole picture into focus.

It is to be noted that although the existence of astrophysical outflows and jets from the galactic and extragalactic sources are well known, their rates are not. Similarly, till date, there is no definitive model present in the literature which can handle the origin of this outflow in a self-consistent way. Hence we think that the formation and dynamics (acceleration and collimation) of these outflows are the open problems in present day theoretical astrophysics. Along with our present analysis of mass outflow in Schwarzschild geometry, if we can carry out our calculation in Kerr geometry as well, we strongly believe that these combined calculations definitely could shed some new light on the origin and energetics of the astrophysical jets.

BIBLIOGRAPHY

- Abramowicz, M. A. & Kato, S. 1989. *ApJ*. 336, 304.
- Abramowicz, M. A. & Chakrabarti, S. K. 1990. *ApJ*. 350, 281.
- Abramowicz, M. A. et al. (eds.) 1998. *Theory of Black Hole Accretion Disks*. Cambridge University Press.
- Abramowicz, M. A., Czerny, B., Lasota, J. P. & Szuszkiewicz, E. 1988. *ApJ*. 332, 644.
- Abramowicz, M. A., Jarosynsky, M. R. Sikora, M. 1978. *A & A*. 63, 221.
- Abramowicz, M. A., & Zurek, W. H. 1981. *ApJ*, 246, 314.
- Antonucci, R. 1993. *ARA&A*. 31, 473.
- Ardavan, H. 1979. *MNRAS*. 189, 397.
- Arai, K. & Hasimoto, M. 1992. *A & A*. 254, 191.
- Artomiva, I. V. Bjornsson, G. & Novikov. I. D. 1996, *ApJ*, 461. 565.
- Axford, W. I. 1981, *Ann. NY Acad. Sci.*, 375,297.
- Axford, W. I. 1981a, *Proc. 17th Int. Cosmic Ray Conf. (Paris)*, 12, 155.
- Axford, W. I., Leer, E., & Skadron, G., 1977, *15th Int. Cosmic Ray Conf. (Plovdiv)* Vol. 11, p. 132.
- Baade, W. & Minkowski, R. 1954. *ApJ*, 119, 215.
- Baan, W. A. Wood, P. A. D. & Haschick, A. D. 1982. *ApJ*. 260, L49.
- Babul, A., Ostriker, J. P. & Mészáros, P., 1989, *ApJ*, 347, 59.
- Baldwin, J. et al. 1977. *A & A*. 61, 165.
- Begelman, M. C. 1993. in *Astrophysical Jets*. (eds.) Burgarella, D., Livio, M. & O'Dea .Cambridge University Press.
- Begelman, M. C., Blandford, R. D. & Rees, M. J. 1984. *Rev. Mod. Phys.* 56, 255 (BBR84)
- Bell, A. R. 1978, *Mon. Not. Roy. Astron. Soc.* 182, 147.
- Bell, A. R. 1978a, *Mon. Not. Roy. Astron. Soc.* 182, 443
- Beskin, V. 1997. *Phys. Uspekhi*. 40, 659.
- Beskin, V. Pev, V. *Phys. Uspekhi*, 1993. 36, 529.
- Biretta, J. A. 1993. in *Astrophysical Jets*. (eds.) Burgarella, D., Livio, M. & O'Dea. p. 263. Cambridge University Press.
- Bisnovatyi-Kogan, G. 1998. in *Observational Evidence for Black Holes in the Universe*. ed. Chakrabarti, S. K. p. 1. Kluwer Academic: Holland.
- Blandford, R. D. 1976. *MNRAS*. 76, 465.
- Blandford, R. D. 1993. in *Active Galactic Nuclei*. ed. Courvoisier, T. J. L. & Mayor, M. p161. (Springer-Verlag).
- Blandford, R. D. 1999. in *Astrophysical Discs*. *ASP Conference Series*.
- Blandford, R. D. 2000. *Proc Discusson Meeting on Magnetic Activity in Stars, Discs and Quasars*. Ed. D. Lynden-Bell, E. R. Priest and N. O. Weiss. To appear in *Phil. Trans. Roy. Soc. A*
- Blandford, R. D. & Begelman, M. C. 1999. *MNRAS*. 303. L1.
- Blandford, R. D. & Payne, D. G. 1982. *MNRAS*. 199. 883. (BP82)
- Blandford, R. D. & Rees, M. J. 1974. *MNRAS*. 169, 395. (BR74)
- Blandford, R. D. & Znajek, R. L. 1977. *MNRAS*. 179, 433.
- Blandford, R. D., & Eichler, D. 1987, *Phys. Repts*. 154, 1.
- Blandford, R. D., & Ostriker, J. P., 1978, *ApJ*. 221, L29.
- Blondin, J. M. 1986. *ApJ*. 308, 755.
- Blumenthal, G. R. 1970. *Phys. Rev. D*. 1, 1596.
- Bondi, H. 1952, *MNRAS*. 112, 195.
- Bregman, J. N. 1990. *A & A Rev*. 2, 125.
- Bridle, A. H. & Perley, R. A. 1984. *ARA&A*. 22, 319.
- Buff, J. & McCray, R. 1974. *ApJ*. 189, 147.
- Burgarella, D., Livio, M. & O'Dea, C. P. (eds.) 1993. *Astrophysical Jets*. Cambridge University Press.

- Camenzind, M. 1986. *A & A.* 156, 137.
- Cannizo, J. K. 1992, *ApJ.* 385, 94.
- Castor, J. I., Abott, D. C. & Klein, R. I. 1975, *Ap.J.*, 195, 157.
- Celloti, A., Miller, J. C. & Sciama, D. W. 1999. *Class. Quant. Grav.* 16, A3.
- Chakrabarti, S. K. 1984a. *ApJ.* 288, 1.
- Chakrabarti, S. K. 1984b. *ApJ.* 288, 7.
- Chakrabarti, S. K. 1988. *J. Astrophys. Astron.* 9, 49.
- Chakrabarti, S. K. 1989. *ApJ.* 347, 365. (C98)
- Chakrabarti, S. K. 1989a. *PASJ.* 41, 1145.
- Chakrabarti, S. K. 1989b. *MNRAS.* 240, 7.
- Chakrabarti, S. K. 1990. *Theory of Transonic Astrophysical Flows.* World. Scientific.
- Chakrabarti, S. K. 1996. *ApJ.* 464, 664. (C96)
- Chakrabarti, S. K. 1996a. *Phys. Reports.* 266, 229.
- Chakrabarti, S. K. 1996b. *MNRAS.* 283, 325.
- Chakrabarti, S. K. 1997. *ApJ.* 484, 313. (C97)
- Chakrabarti, S. K. 1998. *Ind. Jour. Phys.* 72B(3), 183.
- Chakrabarti, S. K., 1999, *A & A* 351, 185.
- Chakrabarti, S. K., Jin, L. & Arnett, W. D. 1987. *ApJ.* 313, 674.
- Chakrabarti, S. K. & Bhaskaran, P. 1992. *MNRAS.* 225, 255.
- Chakrabarti, S. K. & Molteni, D. 1993. *ApJ.* 417, 671.
- Chakrabarti, S. K. & Molteni, D. 1995. *MNRAS.* 274, 80.
- Chakrabarti, S. K. & Titarchuk, L. G. 1995. 456, 623. (CT95)
- Chakrabarti, S. K. & Mukhopadhyay, B. 1999. *A & A.* 344, 105.
- Chakrabarti, S. K. & Manickam, S. G. 2000. *ApJ.* 531, L41.
- Chang, K. M. & Ostriker, J. P. 1985. *ApJ.* 288, 428.
- Clavel, J. et al. 1990. *MNRAS.* 246, 668.
- Colgate, S. A. & Li, H. 1998. in *Proc. VII Conf. and Lindau Workshop on Plasma Astrophysics and Space Physics.* Lindau. Germany.
- Contopoulos, J. 1995, *Ap.J.*, 446, 67.
- Contopoulos, J. 1995. *ApJ.* 450, 616.
- Contopoulos, J. 1996. *ApJ.* 460, 185.
- Contopoulos, J. & Lovelace, R. V. E. 1994. *ApJ.* 429, 139.
- Contopoulos, J. & Kazanas, D. 1995. *ApJ.* 441, 521.
- Cowie, L. L. Ostriker, J. P. & Stark, A. A. 1978. *ApJ.* 226, 1041.
- Cowsik, R. & Lee, M.A. 1981, *Proc. 17th Int. Cosmic Ray Conf. Paris.* (ed. C. Refter). Vol2, P.318.
- Cowsik, R. & Lee, M.A. 1982. *Proc. R. Soc. Lond. A.* 383, 409.
- Crary, D. J. et. all. 1996, *Ap.J.*, L71.
- Curtis, H. D. 1918. *Pub. Lick. Obs.* 13, 31.
- Daly, R.A. & Loeb, A. 1990, *Ap.J.*, 364, 451.
- Das, T. K., 1998. in *Observational Evidence for Black Holes in the Universe*, Ed. S. K. Chakrabarti (Kluwer Academic: Holland). p. 113.
- Das, T. K. 1999a, *Ind. Jour. Phys.* 73(B), 1,1.
- Das, T. K. 1999b, *MNRAS.* 308, 201.
- Das, T. K. 1999c, *Ind. Jour. Phys.* 73(B), 6, 899.
- Das, T. K. 2000. *MNRAS.* (In Press).
- Das, T. K. & Chakrabarti, S. K., 1999. *Class. Quantum Grav.* 16,3879.
- De-Young, S. D. 1991. *Science.* 252, 389.
- Ebisawa, K. et al. 1993. *ApJ.* 403, 684.

- Eckart, A. & Genzel, R. 1997, *MNRAS*, 284, 576.
- Edelson, R. A. 1992. *ApJ*. 401, 516.
- Eggum, G. E. 1988. *ApJ*. 330, 142.
- Eggum, G.E., Coroniti, F.V., Katz, J.I. 1985, *ApJ.*, 298, L41.
- Ellision, D. C. & Eichler, D., 1984. *ApJ*. 286, 691.
- Ellision, D. C., Eichler, D., 1985. *Phys. Rev. Letters*. 55 2735,
- Fabian, A. C. & Rees, M. J. 1995. *MNRAS*. 277, L55.
- Falcke, H. 1994. Ph. D. Thesis.
- Falcke, H. 1999. in *The Central Parsecs of the Galaxy*. ed. Falcke, et al. ASP. Conf. Series.
- Ferrari, A. 1998. *ARA&A*. 36, 539.
- Ferrari, A. Trussoni, E., Rosner, R. & Tsinganos, K. 1985, *ApJ*, 294, 397.
- Flammang, R. A. 1982. *MNRAS*. 199, 833.
- Flammang, R. A. 1984. *MNRAS*. 206, 589.
- Ford, H. C. et al. 1994. *ApJ*. 435. L27.
- Ford, H. C. et al. 1998. in *IAU Symp. 184. The Central Region of the Galaxy and Galaxies*. ed. Sofue. (Dordrecht:Kluwer)
- Frank, J. King, A. R. & Raine, D. J. 1992. *Accretion Power in Astrophysics* (2nd. ed; Cambridge; Cambridge University Press.)
- Fukue, J. 1982, *PASJ*, 34, 163.
- Fukue, J. 1987. *PASJ*. 39, 309.
- Fukue, J. 1989. *PASJ*. 41, 123.
- Fukue, J. & Okada, R. 1990. *PASJ*. 42, 249.
- Genzel, R. et. al. 1994. *Rep. Prog. Phys*. 57, 417.
- Goldreich, P. Goodman, J. & Narayan, R. 1986. *MNRAS*. 221, 339.
- Greenhill. L. J. et al. 1995a. *ApJ*. 440. 619.
- Greenhill. L. J. et al. 1995b. *A & A*. 394, 21.
- Ghez, A. M., Klein, B. L., Morris, M. & Becklin, E. E. 1998. *ApJ*. 509, 678.
- Guilbert, P. W. & Rees, M. J. 1994. *MNRAS*. 233, 475.
- Gundermann, E. 1965. Ph. D. Thesis. Harvard Univ. Cambridge. MA.
- Hardee, P. E., Bridle, A. H. & Zensus, J. A. (ed.) 1996. *Energy Transport in Radio Galaxies and Quasars*. A. S. P. Conf. Series 100.
- Harms, R. J. et al. 1994. *ApJ*. 435, L35.
- Hashimoto, M., Eriguchi, Y., Arai, K. & Muller, E. 1993. *A & A*. 268, 131.
- Hawley, J. F. & Blaes, O. M. 1987. *MNRAS*. 225, 677.
- Hawley, J. F., Smarr, L. L. & Wilson, J. R. 1984a. *ApJ*. 277, 296.
- Hawley, J. W., Smarr, L. L. & Wilson, J. R. 1984. *ApJ*. 457, 805
- Hawley, J. W., Smarr, L. L. & Wilson, J. R. 1985. *ApJ. Suppl.* 55, 221.
- Herrnstein, J. R. et al. 1999. *Nature*. 400, 539.
- Heyvaerts, J. 1999. *Proc. 19th Texas Symp. in Rel. Astrophys.* (in Press).
- Ho, L. C. 1998. in *Observational Evidence for Black Holes in the Universe*. ed. Chakrabarti, S. K. p. 157 Kluwer Academic: Holland.
- Hogan, C. J. & Applegate, J. H. 1987. *Nature*. 390, 236.
- Hook, I. M. et al. 1994. *MNRAS*. 268, 305.
- Hoshi, R. & Shibazaki, N. 1977. *Prog. Theor. Phys.* 7, 203.
- Hoyle, F. & Lyttleton, R. A. 1939. *Proc. Camb. Phil. Soc.* 35, 592.
- Huges, P. A. (ed.) 1991. *Beams & Jets in Astrophysics*. Cambridge University Press.
- Ichimaru, S. 1977. *ApJ*. 214, 840.
- Impy, C. D. & Naugebauer, G. 1988. *Astron. J.* 95, 307.
- Inoue, H. 1992. In *Frontiers of X-ray Astronomy*, ed. Tanaka, Y. & Kpyama, K. (Tokyo: Universal Press) 291.
- Iwasawa, K. et al. 1998. *MNRAS*. 295, L201.

- Jennison, R. C. & Dasgupta, M. K. 1953. *Nature*. 172, 996.
- Jin, L. Arnett, W. D. & Chakrabarti, S. K. 1989. *ApJ*. 336, 572.
- Junor, W., Biretta, J. A. & Livio, M. 1999. *Nature*. 401, 891.
- Königl, A. 1989, *ApJ.*, 342, 208.
- Kazanas, D., Ellison, D. C., 1986, *ApJ*. 304 178. (KE86)
- Kembhavi, A. K. & Narlikar, J. V. 1999. *Quasars & Active Galactic Nuclei*. Cambridge University Press.
- Kirk, J. G. & Duffy, P. 1999, *J. Phys. G25*. R163-R194.
- Koide, S., Shibata, K. & Kodoh, T. 1998. *ApJ*. 495, L63.
- Kormendy, J. & Richstone, D. 1995. *ARA&A*. 33, 581. (KR95)
- Krabbe, A., Genzel, R., Drapatz, S. & Rotacijs, V. 1991. *ApJ*. 382, L19.
- Kraft, R. 1963. in *Advances in Astron. & Astrophys.* ed. Kopal, Z. 2, 43.
- Landau, L. D. & Lifshitz, E. M. 1998. *Fluid Mechanics*. (2nd. ed. reprint with correction) Butterworth-Heinemann. Oxford.
- Lanza, A. 1992. *ApJ*. 389, 141.
- Lanzafame, G., Molteni, D., Chakrabarti, S. K., 1998, *MNRAS*, 299,799.
- Lauer, T. et al. 1992. *Astron. J.* 103, 703.
- Li, Y. Z. 1993. Ph. D. Thesis.
- Li, Z., Chi-Ueh, T. & Begelman. M. C. 1992. *ApJ*. 394, 459.
- Liang, E. P. J. & Thompson, K. A. 1980. *ApJ*. 240, 271.
- Lighman, A. P. & White, T. R. 1988. *ApJ*. 335, 57.
- Lightman, A. P. & Eardley, D. M. 1974. *ApJ*. 187, L1.
- Lin, D. N. C. & Papaloizou, J. C. B. 1996. *ARA&A*. 34. 703.
- Lin, D. N. C. & Shields, G. 1986. *ApJ*. 305, 28.
- Longair, M. S., Ryle, M. & Scheuer, P. A. G. 1973. *MNRAS*. 164, 243.
- Lovelace, R. V. E. 1976. *Nature*. 262, 649.
- Lovelace, R. V. E., Berk, H. L. & Contopoulos, J. 1991. *ApJ*. 379, 696.
- Lovelace, R. V. E., Ustyugova, G. V., Koldoba, A. V. 1999. in *IAU Proc. No. 194: Activity in Galaxies and Related Phenomena*.
- Lovelace, R. V. E., Wang, J. C. L. & Sulkanen, M. E. 1987. *ApJ*. 315, 504.
- Lu, J. F., Yu, K. N., Yuan, F. & Young, E. C. M. 1997. *A & A*. 321, 665.
- Lu, J. F. & Yuan, F. 1997a. *PASJ*. 49, 525.
- Lu, J. F. & Yuan, F. 1998. *MNRAS*. 295, 66.
- Lynden-Bell, D, 1969. *Nature*. 223, 690.
- Lynden-Bell, D. 1978. *Physica. Scripta*. 17, 185.
- Macdonald, D. & Thorne, K. S. 1982. *MNRAS*. 188. 345.
- Madejski, G. M. 1999. in *Theory of Black Hole Accretion Disks*. ed. Abramowicz, M. et al. Cambridge University Press.
- Madejski, G. M. et al. 1994. in *Multiwavelength Continuum Emission of AGN*. Proc. IAU Symp. 159. ed. Courvoisier, T. J. & Blecha, A. (Kluwar: Dordrecht).
- Malec, E. 1996. *Class. Quant. Grav*. 13, 1849.
- Malec, E. 1999. *Phys.Rev. D60*, 104043
- Malkan, M. 1982. *ApJ*. 254, 22.
- Margon, B. 1984. *ARA&A*. 22, 507.
- Marschar, A. P., Vestrand, W. T. & Scott, J. S. 1980. *ApJ*. 241, 1166.
- Matsumoto, R. et al. 1996. *ApJ*. 461, 115.
- McHardy, I. M. 1989. in *Two Topics in X-Ray Astronomy*. Proc. 23rd ESLAB symp. (European Space Agency, Munich)
- Meier, D. L. et al. 1997. *Nature*. 388, 350.
- Menten, K. M., Reid, M. J., Eckart, A. & Genzel, R. 1997. *ApJ*. 475, L111.
- Mestel, L. 1954. *MNRAS*. 114, 437.

- Mészáros, P. 1975. *A & A.* 44, 59.
- Mészáros, P. & Ostriker, J. P., 1983, *ApJ*, 273, L59.
- Mészáros, P. & Rees, M. J. 1997, *ApJ*. 482, L29.
- Meyer, F. & Meyer-Hofmeister, E. 1998. *A & A.* 104, L10.
- Michel, F. C. 1972, *Astr. & Space Sci.* 15, 153.
- Mirabel, I. F. & Rodríguez, L. F. 1998. *Nature*. 392, 673.
- Mirabel, I.F. & Rodríguez, L. F. 1994, *Nature* 371, 46.
- Miyoshi, M. 1998. in *Observational Evidence for Black Holes in the Universe*. ed. Chakrabarti, S. K. p. 141. Kluwer Academic: Holland.
- Miyoshi, M. et al 1994. *Nature*. 371, 395.
- Miyoshi, M. et al 1995. *Nature*. 373, 127.
- Moncrief, V. 1980. *ApJ*. 235, 1038.
- Molteni, D., Lanzafame, G. & Chakrabarti, S.K. 1994 *Ap.J.*, #25, 161.
- Molteni, D., Ryu., D. & Chakrabarti 1996, *Ap.J.*, 470, 460.
- Molteni, D., Sponholtz, H., Chakrabarti, S. K., 1996, *Ap.J.*, 457,805.
- Muchotrzeb, B. 1983. *Acta Astron.* 33, 79.
- Muchotrzeb, B. & Paczyński, B. 1982. *Acta. Astron.* 32, 1.
- Mukhopadhyay, B. 1998. in *Observational Evidence for Black Holes in the Universe*. ed. Chakrabarti, S. K. p. 105. Kluwer Academic: Holland.
- Mukhopadhyay, B. & Chakrabarti, S. K. 2000. *A & A.* 353, 1029.
- Mundell, C. G. et al. 1995. *MNRAS.* 272, 355.
- Murray, N. & Chiang, J. 1997. *ApJ.* 474, 91.
- Murray, N. & Chiang, J. 1998. *ApJ.* 494, 125.
- Mushotzsky, R. F., Done, C. & Pounds, K. A. 1993. *ARA&A.* 31, 717.
- Nandra, K. & Pounds, K. A. 1994. *MNRAS.* 268, 405.
- Nandra, K. et al. 1997. *ApJ.* 477, 602.
- Narayan, R. & Yi, I. 1994. *ApJ.* 428, L13.
- Narayan, R. et al. 1998. *ApJ.* 492, 55.
- Nitta, S. Takahashi, T. Tomimatsu, A. 1991. *Phys. Rev. D.* 44, 2295.
- Nobilli, L., Turolla, R. 1998. in *Astrophysical Jets-Open Problems*. 3rd. Torino Workshop. ed. Massaglia, S., Bodo. G. p. 31. Amsterdam. Gordon & Breach.
- Nobuta, K. & Hanwa, T. A. 1999. *ApJ.* 510, 614.
- Novikov, I. & Thorne, K. S. 1973. in *Black Holes*. ed. DeWitt, C. & DeWitt, B. Gordon & Breach. NY. p. 343.
- Oosterbroeck, T. et al. 1996. *A & A.* 309, 781.
- Ostriker, J. P. et al. 1976. *ApJ.* 208, L61.
- Ouyed, R. & Pudritz, R. E. 1997. *ApJ.* 484, 794.
- Ouyed, R. & Pudritz, R. E. 1997a. *ApJ.* 482, 712.
- Paczyński, B. & Muchotrzeb, B. 1982. *Acta Astron.* 32, 1.
- Paczyński, B. & Wiita, P. J. 1980, *A & A.* 88, 23. (PW80)
- Paczyński, B. & Bisnovatyi-Kogan, G. 1981. *Acta Astron.* 31, 283.
- Papadakis, I. E. A. 1993. *MNRAS.* 272, 161.
- Papadakis, I. E. A. 1995. *MNRAS.* 447, L17.
- Papaloizou, J. C. B. & Pringle, J. E. 1984. *MNRAS.* 208, 721.
- Park, M. G., 1990. *ApJ.* 354, 64.
- Park, M. G., 1990a. *ApJ.* 354, 83.
- Pearson, T. J. & Zensus, J. A. 1987 in *Superluminal Radio Sources*. ed. Zensus, J. A. & Pearson, T. J. p. 1. Cambridge University Press.
- Pedler, A. et al. 1993. *MNRAS.* 263, 471.

- Pelletier, G. & Pudritz, R. E. 1992. *ApJ*. 394, 117.
- Perola, G. C. et al. 1986. *ApJ*. 306, 508.
- Peterson, B. M. et al. 1991. *ApJ*. 368, 119.
- Phinney, E. S. 1982. in *Astrophysical Jets. 1st Torino Workshop*. ed. Ferrari, A. Pacholczyk, A. p. 201. Dordrecht:Reidel.
- Pietsch, W. et al. 1994. *A & A*. 284, 386.
- Plewa, J., Marti, M. J., Müller, e., Rozyczka, M., Sikora, M. 1997. in *Relativistic Jets in AGNs*. ed. Ostrowski, M. Sikora, M., Madejski, G. & Begelman, M. C. p. 104.
- Pounds, K. et al. 1990. *Nature*. 344, 132.
- Prendergast, K. H. & Burbidge, G. R. 1968. *ApJ*. 151, L83.
- Pringle, J. 1981. *ARA&A*. 19, 137.
- Protheroe, R. J., & Kazanas, D., 1983, *ApJ*, 256, 620. (PK83)
- Pudritz, R. E. & Norman, C. A. 1986. *ApJ*. 301, 571.
- Quateart, E., Narayan, R. & Reid, M. J. 1999. *ApJ*. 517, L101.
- Ramaty, R. & Lingenfelter, R. E. 1982. *Ann. Rev. Nuc. Phys.* 32, 235.
- Rees, M. J. 1971. *Nature*. 229, 312.
- Rees, M. J. 1984. *ARA&A*. 22, 471.
- Rees, M. J. 1997. in *Black Holes & Relativity: Chandrasekhar Memorial Conference*. ed. Wald, R.
- Rees, et al. 1982. *Nature*. 295, 17.
- Reynolds, C. S. & Begelman, M. C. 1997. *ApJ*. 488, 109.
- Robinson, E. L. 1976. *ARA&A*. 14, 119.
- Romanova, M. M. et al. 1997. *ApJ*. 482, 708.
- Rosso, F. & Peletier, G. 1994. *A & A*. 287, 325.
- Rydbeck, G. et al. 1993. *A & A*. 270, L13.
- Ryu, D., Chakrabarti, S.K., & Molteni, D. 1997, *ApJ*, 474, 378.
- Saikia, D. J. 1984. *MNRAS*. 208, 231.
- Saikia, D. J. 1998. in *Observational Evidence for Black Holes in the Universe*. ed. Chakrabarti, S. K. Kluwer Academic: Holland. p. 247.
- Salpeter, E. E. 1964. *ApJ*. 140, 796.
- Sauty, C. & Tsinganos, K. 1994. *A & A*. 287. 893.
- Scheuer, P. A. G. 1974. *MNRAS*. 166, 513.
- Shakura, N. I. & Sunyaev, R. A. 1973. *A & A*. 19, 137. (SS73)
- Shapiro, S. L. 1973a, *ApJ*. 180, 531.
- Shapiro, S. L. 1973b, *ApJ*. 185, 69.
- Shapiro, S. & Teukolski, S. 1983, *Black Holes, White Dwarfs, and Neutron Stars*. (Ny: Wiley)
- Shibata, K. & Uchida, Y. 1986. *PASJ*. 38, 631.
- Shibata, K. & Uchida, Y. 1990. *PASJ*. 42, 39.
- Shvartsman, V. F. 1971a, *Soviet. Astr.* 14, 662.
- Shvartsman, V. F. 1971b, *Soviet. Astr.* 15, 377.
- Smith, M. D., Smarr, L., Norman, M. L. & Wilson, J. R. 1983. *ApJ*. 264, 432.
- Softel, M. H. 1982. *A & A*. 116, 111.
- Sparks, W. B. et al. 1992. *Nature*. 355, 804.
- Spruit, H. C. 1987. *A & A*. 184, 173.
- Stone, J. M., Pringle, J. E. & Begelman, M. C. 1999. *MNRAS*. 310, 1002.
- Strohmayer, T. E., Zhang, J. H. Swank, Smale, A. 1996, *ApJ*, 469, L9.
- Sun, W. H. & Malkan, M. 1989. *ApJ*. 346, 68.
- Swada, K. Matsuda, J. & Hachisu, I. 1986. *MNRAS*. 219, 75.
- Tanaka, Y., 1995, *Nature*, 375,659.

- Tarafdar, S.P. 1988, *ApJ.*, 331, 932.
- Trussoni, E., Sauty, C. & Tsinganos, K. 1996. in *Solar and Astrophysical MHD Flows*. ed. Tsinganos, K. p. 383. Dordrecht:Kluwer.
- Uchida, Y. & Shibata, K. 1985. *PASJ.* 37, 515.
- Ueda, Y., Ebisawam K. & Done, C. 1994, *PASJ*, 46, 107.
- Ulrich, G. D., Maraschi, L. & Urray, C. M. 1997. *ARA&A*, 35, 445.
- Ustyugova, G. V. et al. 1995. *ApJ.* 439. L39.
- Van-Putten, M. 1996. *ApJ.* 467, L57.
- Vermulen, R. 1993. in *Astrphysical Jets*. ed. Burgarella, D. et al. p. 241. Cambridge University Press.
- Weaver, H. et al. 1965. *Nature*. 208, 29.
- Wiita, P. J. 1978a, *ApJ.* 221, 41.
- Wiita, P. J. 1978b, *ApJ.* 221, 436.
- Wiita, P. J. 1982, *ApJ.* 256, 666.
- Wiita, P. J. 1998. in *Black Holes, Gravitational Radiation and the Universe*, eds. B.R. Iyer & B. Bhawal p. 249. (Dordrecht: Kluwer).
- Wiita, P. J. 1998. in *Observational Evidence for Black Holes in the Universe*. ed. Chakrabarti, S. K. . p. 49. Kluwer Academic: Holland.
- Wilson, J. R. 1972, *ApJ.* 173, 431.
- Yokosawa, M. 1995. *PASJ.* 47, 605.
- Zel'dovich, Ya. B. & Novikov, I. D. 1964. *Sov. Phys. Dokl.* 158, 811.
- Zensus, J. A. 1997. *ARA&A*. 35, 607.